NASA

Technical Memorandum 83968

A Photochemical Study of the Kinetics of the Reactions of NH_2 with Phosphine, Ethylene, and Acetylene Using Flash Photolysis-Laser Induced Fluorescence

Salvatore R. Bosco

JULY 1982

National Aeronautics and
Space Administration

Goddard Space Flight Center
Greenbelt, Maryland 20771

THE CATHOLIC UNIVERSITY OF AMERICA

A PHOTOCHEMICAL STUDY OF THE KINETICS OF THE REACTIONS OF NH_2 WITH PHOSPHINE, ETHYLENE AND ACETYLENE USING FLASH PHOTOLYSIS - LASER INDUCED FLUORESCENCE

A DISSERTATION

submitted to the Faculty of the

School of Arts and Sciences

of the Catholic University of America

in Partial Fulfillment of the Requirements

For the Degree

Doctor of Philosophy

by

Salvatore Ronald Bosco

Washington, D.C.

1962

OF PO

This Dissertation was approved by Louis J. Stief, Ph.D. as Director, and by William A. Sanders, Ph.D., and John B. Hunt, Ph.D. as Readers.

Director

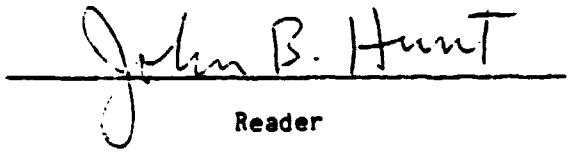

Reader

Reader

A PHOTOCHEMICAL STUDY OF THE KINETICS OF THE REACTIONS OF NH_2 WITH PHOSPHINE, ETHYLENE AND ACETYLENE USING FLASH PHOTOLYSIS - LASER INDUCED FLUORESCENCE

by

S. R. Bosco

Planetary modelers attempted to explain the abundance of ammonia in the Jovian atmosphere despite its ready photolysis. Modelers argued that thermal processes are inadequate to totally compensate for photochemical and chemical ammonia loss and considered ammonia coupling reactions with other atmospheric constituents to provide ammonia reservoirs. The rate constants for the potentially important reactions of NH_2 radicals with phosphine, acetylene and ethylene were measured to provide modelers data which were unavailable or over which there was controversy. Additionally, the coupling reaction with phosphine was studied because phosphine was thought to generate PH_2, a precursor of P_4 which was a possible source of coloration of the Great Red Spot.

The flash photolysis method for the production of NH_2 radicals and the laser-induced fluorescence method for radical detection were chosen because of the high sensitivity this technique affords especially under the temperature and pressure range at which the study was conducted. Care was taken to ensure that secondary reactions and reaction with photochemical products did not interfere with the results.

The result for $NH_2 + PH_3$ was $k = (1.52\pm0.16)\times10^{-12}e^{-(928\pm56)/T}$ cm^3 $molec^{-1}$ sec^{-1} over the range 218-456°K and was pressure independent. A BEBO/Activated Complex Theory calculation of the pre-exponential factor of a bent P-H-N activated complex was within a factor of 4 of the measured value. The result for $NH_2 + C_2H_4$ from 250-465°K and 5-100 torr total

pressure was $k = (3.41 \pm 0.12) \times 10^{-14} e^{-(1318 \pm 23)/T}$ cm^3 $molec^{-1}$ sec^{-1}. At 465°K and 5 torr, the ethylene reaction showed a drop in rate indicating a possible adduct forming channel. The $NH_2 + C_2H_2$ result from 241-463°K and 5-100 torr total pressure was found to be pressure dependent and the high pressure limit was $k = (1.11 \pm 0.36) \times 10^{-13} e^{-(1852 \pm 100)/T}$ cm^3 $molec^{-1}$ sec^{-1}. The rates of NH_2 with acetylene and ethylene were compared with those from other studies.

It was determined that the rates of reactions studied were too slow to be significant as ammonia reservoirs in the Jovian atmosphere. The results provide modelers with data relevant to the Jovian atmosphere upon which to base future models.

TABLE OF CONTENTS

ACKNOWLEDGMENTS

I would like to thank the United States Air Force for making this assignment possible and the personnel of AFIT for their fine personnel support. My sincere gratitude goes to Dr. Charles Nash for assisting me in preparing for this assignment and for encouraging me to pursue this work.

I would like to thank The Goddard Space Flight Center for extending me the opportunity to conduct this research at their facility and to all of the personnel assigned to the center who gave most generously of their time in assisting me in this project. I am especially grateful to Dr. Louis Stief for granting me the privilege of studying under his direction and for the many long hours of patient guidance he gave. I am indebted to Mr Bill Brobst and Dr. Dave Nava for their friendship and help in bearing with me through many long hours of experiments, several thesis drafts and, possibly, a few puns along the way. Dr. John Allen's suggestions especially concerning the use of the polarizing lens were invaluable to the completion of this work as were the advice of Drs. Regina Cody and Joe Nuth. I sincerely appreciate the assistance and helpful comments of my readers, Drs. William Sanders and John Hunt and I thank Drs. Joe Michael and Bruce Klemm for their suggestions in preparing parts of this manuscript.

Finally, and foremost is the gratitude and love I wish to express to my wife, Joann, for her patience and understanding in tolerating all of the difficult situations that graduate study brings while bearing the brunt of the load of raising our family during the past two years.

LIST OF TABLES

LIST OF FIGURES

CHAPTER I

INTRODUCTION

A. Planetary Aspects - The Jovian Atmosphere

1. Jupiter

About 4.5 billion years ago, a cloud of interstellar gas began to condense under gravitational attraction to form the sun, planets, and minor bodies that comprise our solar system. While no single mechanism for the formation of the solar syster is universally accepted, it is generally acknowledged that solar bodies all condensed from this solar nebula and, consequently, had the same initial composition.[1]

About 99.9% of the solar nebular mass formed the sun; of the remainder, nearly 70% became the planet Jupiter. The immensity of the Jovian mass takes on additional significance when one considers that, had Jupiter's mass been just a few times its current value, gravitational contraction would have continued to raise the planetary core temperature until self-sustaining nuclear reactions could ignite.[2] The sun and Jupiter would have become a binary star system with grave implications for life on earth.

Besides its immense size, Jupiter's unique coloration, turbulent atmosphere, and system of orbiting bodies have piqued man's curiosity as to its composition and structure. Using an early telescope, Galileo, in 1610

discovered the four major satellites of Jupiter. His correct interpretation of their motion as bodies circling a center other than earth became the foundation of the Copernican arguments leading to modern astronomy.[3] Subsequent telescopic observations led to the identification of unique colorations in Jupiter's atmosphere called bands and zones. The most distinct and long-lived of these was the Great Red Spot which was first observed by Robert Hooke in 1664.

Man's desire to know more about Jupiter and its atmosphere and the potential for applying this knowledge to terrestrial meteorology prompted several fly-bys of the planet by unmanned spacecraft. Pioneers 10 and 11 were the first terrestrial spacecraft to make close observations of Jupiter. More recently, Voyagers I and II, as part of their spectacular information gathering mission to the outer planets, have added immeasurably to our knowledge of Jupiter and its satellites. These close observations, together with earth-based measurements, have provided a more detailed picture of the planet's atmosphere than previously available, yet leave unanswered many questions as to the dynamic relationships of the constituents of Jupiter's atmosphere.

2. The Jovian Atmosphere

a. Structure

Models of Jupiter predict only the possible existence of a solid core or surface.[4] This core is described as being about the size of the earth and exists under a pressure of about 10^8 atmospheres (atm)[4] at about 30,000° K.[5] Above this core, pressures and temperatures decrease slowly

with increasing altitude in dense oceans of liquid helium and liquid metallic hydrogen. At about 70,000 km from the planetary center, where temperatures have dropped to below 1000° K, an ocean of liquid molecular hydrogen gives way to a gaseous atmosphere in which pressures decrease with increasing altitude from about 100 atm. to the high vacuum of space and temperatures fall to as low as 110° K before climbing gradually to about 850° K in the Jovian thermosphere.[6]

It is just below this inflection point in the temperature versus altitude profile that the visible Jovian cloud layers are found and it is in this region that some of the most significant photochemistry of Jupiter's atmosphere might occur. Cloud layer composition has never been verified by direct measurement, but rather has been inferred from models[7] based on the temperature-altitude profile of species whose presence on Jupiter has either been verified or which are consistent with solar-norm ratios. The uppermost cloud layer is white and is thought to be composed of ammonia crystals. Below this, a cloud layer, possibly of NH_4SH, varies in color from yellow to brown. The deepest layer, which is thought to be an aerosol of aqueous ammonia solution, is bluish. Temperatures in this layer reach about 300° K.

The Jovian atmosphere is undergoing dynamic vertical and horizontal motion. Cooler regions called bands and hotter ones called zones move across the face of the planet at horizontal velocities of up to 125 m/sec.[8] Adjacent bands may move at nearly equal velocities, but in opposite directions. Apparent vertical motions, driven by the hotter interior, could serve to mix the components of the atmospheric layers, further complicating Jovian meteorology.

b. Composition

Because of its enormous mass and consequent high gravitational field, Jupiter is presumed to have retained all of the elements in their original proportions (called the solar norm) that condensed to form the planet from the solar nebula.[9] If the mean molecular velocity of an element exceeds about 20% of a planetary escape velocity, that element will be lost to space in about 10^8 years.[10] The smaller planets, such as the Earth, with their weaker gravitational fields, lost their hydrogen and helium early in their history, whereas Jupiter retained these species.

While hydrogen and helium are the most abundant constituents of the Jovian atmosphere (comprising over 99% by mole fraction), several more photochemically interesting minor constituents, listed in Table 1, have been identified in recent years. The theoretical relative abundances predicted in Table 1 are based on an assumed solar norm composition. These predictions are applicable to the region just above the cloud layers where the temperature is about 150°K and the total pressure is around 10-100 torr.[11] This area constitutes the bottom of the Jovian stratosphere.

In current models, the methane concentration remains relatively high in a region from the cloud layers upwards for about 100 km. In contrast, the ammonia concentration falls off rapidly with increasing altitude mainly because of the lower NH_3 vapor pressure at the cold temperatures found in the lower stratosphere. For example, at about 100°K, the vapor pressure of ammonia is about 10^{-4} torr, while that of methane is about 100 torr.[12] The excess ammonia condenses out from the vapor when its concentration exceeds the saturation vapor pressure.

Table 1[11]

Composition Model of the Jovian Stratosphere

Species	Mole Fraction	Species	Mole Fraction
H_2	.90	C_2H_6	$3x10^{-5}$
He	.10	C_2H_2	$5x10^{-7}$
CH_4	$7x10^{-4}$	PH_3	$5x10^{-7}$
NH_3	$2x10^{-4}$	C_2H_4	$2x10^{-5}$

3. Modeling the Jovian Atmosphere

a. Description of a Planetary Model

Atmospheric models are based on the composition and chemical behavior of the constituent species and the indigenous meteorological conditions. Some models are concerned primarily with transport phenomena on a global scale; these are based on complex, three-dimensional models and, because of the large number of variables already involved, make it difficult to include parameters for the discrete chemical behavior of the constituents. In an alternative approach, a one-dimensional model has been employed in which only vertical diffusion is considered and which does include detailed chemical reaction information.[13]

Bulk transport for each of the i minor species included in this model can be described by the continuity equation[14]:

$$(1)\quad M(\partial f_i/\partial t) - \partial/\partial z\{K_i M(\partial f_i/\partial z)\} = P_i - L_i$$

where f_i is the mole fraction of any minor constituent i; P_i and L_i are the chemical production and loss rates, respectively; M is the bulk atmospheric density; z is the altitude, t is time, and K_i is the altitude dependent eddy diffusion coefficient for i in cm^2/sec. Most workers do not consider short term temporal effects such as diurnal variation in this model, and so $\partial f_i/\partial t = 0$.

i.The Eddy Diffusion Coefficient, K_i

Physical transport processes can involve mixing by turbulence or by molecular diffusion. Molecular diffusion is generally ignored in applying this model to the terrestrial stratosphere;[15] this factor is similarly dismissed here on the basis that, in the dense Jovian lower stratosphere, molecular diffusion would be even less important. One-dimensional vertical mixing is limited, therefore, to turbulent mixing called eddy diffusion. K_i is empirically determined based on the vertical distribution of a diffusing specie.[16]

ii. The Rate of Photochemical Production and Loss

The low temperatures of the upper Jovian troposphere and lower Jovian stratosphere make molecular reactions, which generally have significant activation energies, negligibly slow. Reactions involving radical species have low activation energies and may, therefore, be potentially important under these conditions. Explanations for the rate of production of radical species revolve around solar-radiation-induced photochemical reactions.

In general, when a molecule absorbs radiation, the absorption process obeys the Beer-Lambert Law, equation (2).

$$(2)\quad \ln(I/I_o) = -\epsilon c l$$

This law states that the logarithm of the fraction of light absorbed by a species is directly proportional to the concentration of the absorbing species, c and the length of the path of the light through the absorbing species, l. The proportionality constant ϵ, called the absorption coefficient, depends on the nature of the absorbing species and the temperature at which absorption occurs. If the absorption or attenuation of the radiation is altitude-dependent, then the differential form of the Beer-Lambert Law at a fixed wave number,

$$(3)\quad \partial I/\partial l = -I\epsilon c \quad [17]$$

is more appropriate.

To quantify the photochemical production process, the photodissociation coefficient, J (sec^{-1}), is defined by[18]:

$$(4)\quad J = \int_0^{\infty} \phi_{\bar{\nu}} I_{\bar{\nu}} \sigma \, d\bar{\nu}$$

where $I_{\bar{\nu}}$ is the intensity of radiation at a given wavenumber, $\bar{\nu}$, in quanta cm^{-2} sec^{-1}; σ, the absorption cross section, is ϵ expressed in units of cm^2 $molecules^{-1}$; $\phi_{\bar{\nu}}$ is the quantum yield for the process at $\bar{\nu}$, where the quantum yield refers to the number of molecules dissociated per photon absorbed. The rate of formation of radical species i by a photochemical process which enters equation (1) as P_i, is determined by multiplying J by the concentration of the species from which i is photochemically formed; similarly, if a species is consumed , it enters equation (1) as a loss term, L_i.

iii.The Rates of Chemical Kinetic Production and Loss

Chemical processes have been suggested to explain the rate of consumption of certain of the minor constituents of the upper Jovian troposphere and lower stratosphere via the reaction with photochemically produced radical species. In order to formulate an expression for the rate of a reaction, it is first necessary to have some idea of how the reaction occurs. Some reactions are complex; that is, they occur by a series of steps. Others, called elementary reactions, occur in a single step.

Whether elementary or complex, reactions can be categorized by their order and their molecularity. The order of a reaction is an experimentally determined quantity and is the sum of the exponents of all species appearing in a mathematical expression of the rate of the reaction called the rate law expression. Proof that a reaction is of a particular order consists of showing that it obeys the rate law expression characteristic of that order. The molecularity of a reaction is the number of distinguishable reactive particles which come together to form a complex that directly gives rise to the products. For an elementary reaction, the order and molecularity are the same.[19]

Chemical reactions can also be categorized either as metathetical or adduct forming. Metathetical reactions include those in which atom transfer occurs and can be described by the general equation:

(5) $A + BC \rightarrow AC + B$

The rate of this elementary reaction (which is identical with the rate of loss of A or BC, $L_A = -\partial[A]/\partial t$ or $L_{BC} = -\partial[BC]/\partial t$) is proportional to the

concentrations of both A and BC, written [A] and [BC]. This rate can be represented by the rate law expression:

$$(6)\ L_A = L_{BC} = k[A][BC]$$

where k is the constant of proportionality called the rate constant. The reaction in this case is second order and bimolecular.

If an adduct is formed as a result of the collision of A and B, a somewhat different treatment is required. Equations (7) through (9) describe a situation in which the excess vibrational energy in AB^* must be removed by collisional transfer to some third body, M, so that a stable product can form. Otherwise, the excited intermediate will decompose via vibration to give A and B back again.

$$(7)\ A + B \rightarrow AB^*$$

$$(8)\ AB^* + M \rightarrow AB + M^*$$

$$(9)\ AB^* \rightarrow A + B$$

Equations (7) through (9) describe the process whereby A and B are lost from the system and, therefore, equation (10) can be written:

$$(10)\ L_{AB^*} = k_8[AB^*][M] + k_9[AB^*] - k_7[A][B]$$

where the minus sign is used for the process by which AB^* is formed. Since AB^* is an unstable intermediate with a presumed short lifetime, its

concentration should become constant and hence the steady state treatment can be applied:[20]

$$(11)\quad L_{AB^*} = 0$$

Solving for $[AB^*]$,

$$(12)\quad [AB^*] = \frac{k_7[A][B]}{k_8[M] + k_9}$$

The rate of consumption of A (or B) can be described by:

$$(13)\quad \text{Rate} = L_A = L_B = k_8[AB^*][M]$$

and, substituting for $[AB^*]$ from (12),

$$(14)\quad \text{Rate} = L_A = L_B = \frac{k_8 k_7[A][B][M]}{k_8[M] + k_9}$$

In order to probe the possibility of adduct formation, it is necessary to examine the reaction rate over a range of pressures. At low pressures, where $k_8[M] \ll k_9$, equation (14) becomes:

$$(15)\quad L_A^\circ = L_B^\circ = \frac{k_8 k_7[A][B][M]}{k_9}$$

and the expression shows a third order kinetic rate law. When pressures are high and $k_8[M] \gg k_9$, equation (14) becomes:

$$(16)\quad L_A^{\infty} = L_B^{\infty} = k_7[A][B]$$

and second order kinetics apply.

In either the metathetical or adduct forming case, if A and B are consumed, the process enters equation (1) as an L_i term for A and/or B. Conversely, if a product is formed (eg., AC in the metathetical case or AB in the adduct case), it enters equation (1) as a P_i term for either AC or AB.

b. The Ammonia Paradox

The composition of a planetary atmosphere remains relatively constant with altitude unless disequilibrating loss or production processes such as photolysis or chemical reactions occur or an isotherm is reached at which condensation can occur. Models of the ammonia concentration in the Jovian atmosphere place its abundance at the solar norm, yet ammonia is presumed to be readily photolyzed by the ultraviolet component of solar radiation in the Jovian stratosphere to form hydrazine, N_2H_4, by[21]

$$(17)\quad NH_3 + h\nu \rightarrow NH_2 + H$$

followed by:

$$(18)\quad NH_2 + NH_2 + M \rightarrow N_2H_4 + M$$

where M is any third body molecule or atom which absorbs excess energy. In fact, Atreya et al.[21] argue that, during the course of about 60 million

years, all of the Jovian ammonia should have been converted to hydrazine by reaction (18) and subsequently, to nitrogen and hydrogen through N_2H_4 photolysis and N_2H_2 decomposition in the lower stratosphere and upper troposphere. In addition to the direct photolysis of hydrazine to give N_2H_2 and H_2, this can occur via the sequence:

$$(19)\ N_2H_4 + h\nu \rightarrow N_2H_3 + H$$

$$(20)\ H + N_2H_4 \rightarrow N_2H_3 + H_2$$

$$(21)\ H + N_2H_3 \rightarrow N_2H_2 + H_2$$

Both sequences may be followed by thermal decomposition of N_2H_2:

$$(22)\ N_2H_2 \xrightarrow{\Delta} N_2 + H_2$$

In view of the reactions described, it is significant to note that no molecular nitrogen has been detected on Jupiter.

Modelers have attempted to explain the anomalously high ammonia abundance in light of the potentially significant photochemical loss processes cited above. Atreya et al.[21] contend that:

$$(23)\ NH_2 + H + M \rightarrow NH_3 + M$$

accounts for the recycling of about 33% of the NH_2 back into NH_3, while Strobel[22] estimates that about 62% of the NH_2 radicals are so converted. It is evident that reaction (23) by itself cannot account completely for the

stabilization of the ammonia concentration.

In addition to photochemical processes, thermal regeneration of ammonia in the Jovian interior and rapid upward vertical transport processes may account for a significant part of the ammonia regeneration. Atreya et al.[21] in summarizing likely ammonia regeneration processes, includes one in which hydrazine produced by reaction (18) could condense out of the Jovian stratosphere and be transported downward to the hotter lower atmosphere. There, N_2H_4 can be thermally dissociated by:

$$(24)\quad N_2H_4 \rightleftharpoons 2NH_2$$

The subsequent reaction of NH_2 with hydrogen can regenerate ammonia at high temperature by:

$$(25)\quad NH_2 + H_2 \rightarrow NH_3 + H$$

In addition, if N_2 were available the complex reaction:

$$(26)\quad N_2 + 3H_2 = 2NH_3$$

can also occur at pressures of about 3000 atm. Ammonia produced would then, presumably, be transported upward to renew the cycle.

Both of these thermal mechanisms rely on the formation of hydrazine by reaction (18) and, therefore, any process which inhibits reaction (18) could limit the significance of these mechanisms in the ammonia regeneration scheme. In fact, however, there is currently no evidence to

either support or discredit the supposition that ammonia is generated in the interior of the Jovian atmosphere.

c. Possible Ammonia Reservoirs on Jupiter

Several models have been proposed which involve coupling reactions of the NH_2 radical with other minor species which are present in the Jovian atmosphere. These reactions could provide reservoirs for ammonia or help to explain the regeneration of ammonia in Jupiter's atmosphere.

Strobel,[23] for example, suggested that a coupling could exist between NH_2 and phosphine, PH_3, to regenerate NH_3 by:

$$(27)\quad NH_2 + PH_3 \rightarrow NH_3 + PH_2 \qquad \Delta H^\circ = -24 \text{ kcal/mole}^{24}$$

This particular reaction is significant for yet another potentially important reason. PH_2 radicals can disproportionate to give PH_3 and PH according to the mechanism proposed by Norrish and Oldershaw.[25] PH radicals combine to give P_2 and H_2, and P_2 can lead to P_4, red phosphorus. Prinn and Lewis[26] suggest that P_4 is the red chromophore which may be responsible for the characteristic color of Jupiter's Great Red Spot. If reaction (27) is fast enough, it might account for PH_2 in Jupiter's stratosphere thus providing a source for both P_4 formation and the regeneration of ammonia.

Other reactions that may be important in explaining the consumption or regeneration of ammonia are:

(28) $NH_2 + C_2H_2 \overset{(M)}{\rightarrow} NH_2C_2H_2$

or $\rightarrow NH_3 + C_2H$ $\Delta H^\circ_{298} = 22.6$ kcal/mole[24]

(29) $NH_2 + C_2H_4 \overset{(M)}{\rightarrow} NH_2C_2H_4$

or $\rightarrow NH_3 + C_2H_3$ $\Delta H^\circ_{298} = -5.1$ kcal/mole[24,12]

(30) $NH_2 + CH_4 \rightarrow NH_3 + CH_3$ $\Delta H^\circ_{298} = 1.5$ kcal/mole[24]

Reaction (28) is considered in light of the discovery that acetylene was found to scavenge PH_2 radicals.[27] NH_2 radicals might, therefore, be presumed to react in an analogous fashion.

Schurath et al.[28] examined the reaction products of the photolysis of a mixture of ethylene and ammonia by radiation of 206.2 nm. They concluded that ethylene is scavenged by NH_2 radicals and identified ethylenediamine as one of the products of reaction (29) and the subsequent reaction:

(31) $NH_2C_2H_4 + NH_2 \overset{(M)}{\rightarrow} C_2H_4(NH_2)_2$

In addition to the reaction of NH_2 with ethylene, Schurath et al. reported that hydrogen produced in the photolysis of NH_3 was quickly scavenged by C_2H_4 to give C_2H_5:

$$(32)\ H + C_2H_4 \overset{(M)}{\rightleftharpoons} C_2H_5$$

They further identified butylamine, ethylamine, and butane among the reaction products which they attributed to the reactions:

$$(33)\ NH_2C_2H_4 + C_2H_5 \overset{(M)}{\rightleftharpoons} C_4H_9NH_2$$

$$(34)\ NH_2 + C_2H_5 \overset{(M)}{\rightleftharpoons} NH_2C_2H_5$$

and $$(35)\ C_2H_5 + C_2H_5 \overset{(M)}{\rightleftharpoons} C_4H_{10}$$

The substantial methane concentration projected in the lower Jovian stratosphere and upper troposphere where NH_2 is formed and the thermochemical neutrality of reaction (30) require that reaction (30) also be considered.

B. NH_3 Photochemistry and NH_2 Reaction Kinetics

1. Introduction: The NH_3 Molecule

Ammonia and its photochemical transformation into the amidogen radical, NH_2, are central to all of the reactions involved in the ammonia paradox. The ammonia molecule has a trigonal pyramidal geometry. The H-N-H

bond angle is 107.8° and the NH equilibrium bond distance is 1.0173 Å.[29] The NH_2-H bond dissociation energy is 98.85 kcal/mole.[29]

Watanabe[30] measured the absorption spectrum of ammonia (Fig. 1) in the vacuum ultraviolet from 110 to 220 nm. He determined that, above 140 nm the absorption coefficient reaches a maximum of about 560 atm^{-1} cm^{-1}, base e, 0°C at about 195.0 nm and falls off to about 220 atm^{-1} cm^{-1}, base e, 0°C at around 205.0 nm. Absorption falls off further at longer wavelengths and ammonia is virtually transparent above 230 nm.

The absence of rotational fine structure in vibrational bands of the NH_3 absorption spectrum indicates rotational predissociation. Predissociation occurs when the discrete levels of one state overlap the continuum of a state in which dissociation occurs. Provided the restrictions of certain selection rules are met,[31] the molecule can cross over to the continuum and dissociate. If predissociation occurs faster than the vibrations occur, no vibrational structure is observed. If no rotational structure is observed, as in the ammonia case, then predissociation is similarly competitive with rotational time ($\sim 10^{-11}$ sec). Predissociation indicates a high primary quantum yield for the photolysis of ammonia. The primary quantum yield is defined as the number of molecules dissociated per photon absorbed.

Figure 1

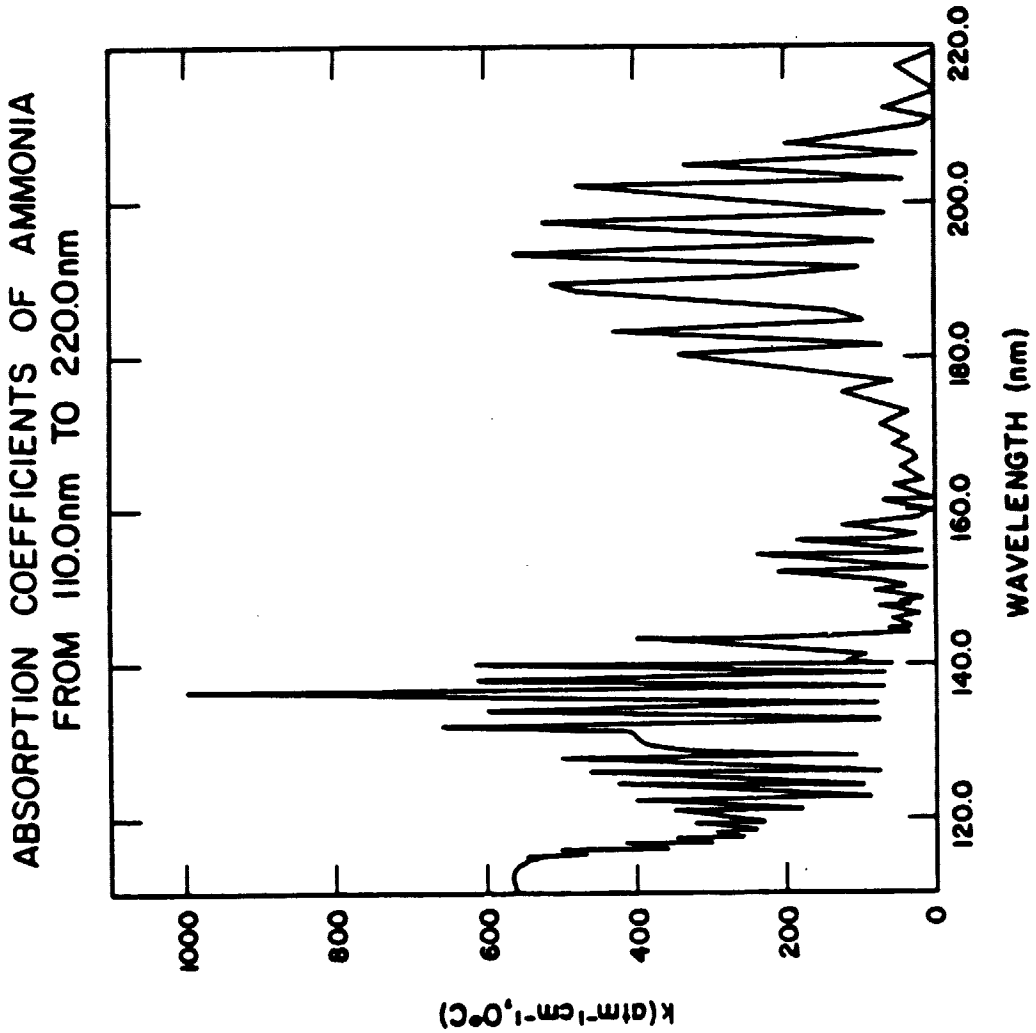

2. NH_3 Photochemistry

Ammonia is photolyzed by vacuum ultraviolet radiation to give NH_2, NH, H, and H_2 in various electronic states depending on wavelength. Okabe[32] has discussed the most important processes involved:

		Threshold Wavelength
(36)	$NH_3 + h\nu \rightarrow NH_2 (\tilde{X}\ ^2B_1) + H\ (^2S_{1/2})$	280.0 nm
(37)	$NH_3 + h\nu \rightarrow NH\ (a\ ^1\Delta) + H_2\ (^1\Sigma_g^+)$	224.0 nm
and (38)	$NH_3 + h\nu \rightarrow NH\ (\chi\ ^3\Sigma^-) + 2H\ (^2S_{1/2})$	147.0 nm

where the parenthetical symbols describe the spin value, angular momentum, and symmetry of the electronic state. The $\tilde{X}$ state is the ground electronic state.

Process (36) is the major primary photochemical pathway for NH_3 photolysis between 122.0 nm and 220.0 nm.[33] Photolysis energies of 101 kcal/mole or greater are required for this process to occur.[33] The primary quantum yield for process (36) was determined to be nearly unity at both the Hg 184.9 nm and I 206.2 nm lines.[34,35] Process (37) has a reported primary quantum yield of 0.005 and 0.04 at 206.2 nm and 184.9 nm respectively[32] and therefore, may be considered to be of minor importance at these wavelengths. Photolysis by radiation at wavelengths below 140.0 nm results in higher yields of NH due to processes (37) and (38).

The presence of methane in the Jovian stratosphere simplifies the photochemistry of ammonia. The high methane absorption coefficient for radiation below 160.0 nm[36] coupled with the significantly higher methane concentration, ensures that methane will absorb most of the solar radiation below 160.0 nm in the stratosphere of Jupiter. Thus, it is necessary to consider only the photochemistry of ammonia at wavelengths greater than 160.0 nm, since ammonia is more dense in the upper troposphere. It is then possible to consider the photochemistry of methane and ammonia separately as suggested by Atreya et al.[21]. Because methane shields ammonia from most of the radiation below 160.0 nm so effectively, it is evident from the foregoing discussion that the only primary process of importance in Jovian photochemistry is reaction (36). In this case, NH_2 is produced almost exclusively in its ground electronic state.[37]

3. The NH_2 Radical

a. General

The ground state for the planar NH_2 radical has an ($\tilde{X}\ ^2B_1$) electronic configuration. The N-H bond distance is 1.024 Å and the H-N-H bond angle is 103.4°[38] The bond dissociation energy for NH-H is $\leq$ 90 kcal/mole.[39]

The first excited state of NH_2 ($\tilde{A}\ ^2A_1$) lies 31.7 to 66.4 kcal/mole above the ground state.[40] Dressler and Ramsay[41] were the first to positively identify the fluorescent emission from NH_2 ($\tilde{A}\ ^2A_1$) produced by the flash photolysis of ammonia.

The NH_2 ($\tilde{A}\ ^2A_1$) fluorescent signal can be used in NH_2 kinetic

studies to monitor the relative NH_2 concentration over short time intervals. The NH_2 ($\tilde{A}\ ^2A_1$) radical has a short radiative lifetime (~ 8×10^{-6} sec)[42] indicating that an allowed transition to the ground state occurs. In order for this fluorescence monitoring of NH_2 ($\tilde{X} \rightarrow \tilde{A}$) to be useful, collisional quenching of the excited state must be understood. This can be discussed using the Stern-Volmer treatment.

b. Stern-Volmer Theory

If a molecule or radical, A, absorbs I_a quanta of radiation per second per cm^3 and undergoes a transition to an excited electronic state, A^*, by:

(39) $A + h\nu \rightarrow A^*$ $\qquad I_a\ (sec^{-1}\ cm^{-1})$

after which A^* may undergo fluorescence:

(40) $A^* \rightarrow A + h\nu$ $\qquad k_f\ (sec^{-1})$

self quenching:

(41) $A^* + A \rightarrow 2A$ $\qquad k_q(concentration^{-1}\ sec^{-1})$

or quenching by a non-absorbing foreign gas, M:

(42) $A^* + M \rightarrow A + M$ $\qquad k_m(concentration^{-1}\ sec^{-1})$

where k_f, k_q and k_m are the rate constants for equations (40), (41), and (42), respectively.

Assuming steady state conditions for the concentration of A^*,

$$(43)\quad \partial[A^*]/\partial t = 0 = I_a - k_f[A^*] - k_q[A^*][A] - k_m[A^*][M]$$

and $$(44)\quad I_a = (k_f + k_q[A] + k_m[M])\,[A^*]$$

From (44) and for $I_f = k_f[A^*]$

$$(45)\quad I_a = I_f(1 + (k_q/k_f)[A] + (k_m/k_f)[M])$$

Equation (45) shows that, in a given experiment, regardless of foreign gas if $k_f >>$ both k_m and k_q, $I_f = I_a$. If quenching is relatively fast as in the current case,

$$(46)\quad I_f = I_a$$

The Beer-Lambert Law for absorption by A is $I = I_o e^{-\epsilon[A]l}$. For weak absorption, we can expand the exponential term using $e^x = 1 - x + ...$ and, truncating the expansion after two terms, to give:

$$(47)\quad I/I_o = 1 - \epsilon[A]l$$

or $$(48)\quad 1 - I/Io = \epsilon[A]l$$

I_a is the radiation absorbed by A and is clearly proportional to $I_o - I$.

Then,

$$(49)\quad I_a = I_o \epsilon [A] l.$$

I_a is proportional to [A] by (49) and $I_a = I_f$ by (46). Then

$$(50)\quad [A] \propto I_f$$

Equation (50) states that the fluorescent intensity for the excited state, A^*, is proportional to the concentration of the ground state under the conditions of the above treatment. Since the NH_2 ($\tilde{X}\ ^2B_1$) → ($\tilde{A}\ ^2A_1$) transition occurs under conditions where absorption is relatively weak and the lifetime of the NH_2 ($\tilde{A}\ ^2A_1$) is short, the NH_2 ($\tilde{A}\ ^2A_1$) fluorescence signal is proportional to the concentration of the ground state NH_2 and can be used in time dependent (kinetic) measurements when the observed time is long compared to the emissive lifetime.

4. NH_2 In Kinetic Studies

Kroll[43] investigated the fluorescent spectrum of NH_2 ($\tilde{A}\ ^2A_1$) produced in a flowing system by the reaction of H atoms (produced in a microwave discharge) with hydrazine, N_2H_4. Fluorescent lines in the NH_2 spectrum were identified by setting a continuous wave dye laser to the approximate wavelength and scanning manually while looking for fluorescence. The absorption spectrum of NH_2 was photographed following the flash photolysis of NH_3. That portion of the absorption and corresponding fluorescent spectrum observed by Kroll relevant to the present study is

presented in Fig. 2. Fluorescence lines are grouped by common upper rotational state.

One of the first time-resolved laser induced fluorescence studies of the NH_2 radical was performed by Hancock et al.[44] NH_2 ($\tilde{A}\ ^2A_1$) fluorescence was used to monitor the NH_2 ($\tilde{X}\ ^2B_1$) concentration. An NH_2 ($\tilde{X}\ ^2B_1$) rovibronic transition caused by absorption of radiation at 570.3 nm was used to produce the electronically excited NH_2. Lesclaux et al.[45] used a continuous wave dye laser to monitor the NH_2 radical concentration by absorption of 597.73 nm radiation. In both studies NH_2 ($\tilde{X}\ ^2B_1$) radicals were produced by the flash photolysis of NH_3 and the resulting time resolved decays were used to measure the rate of consumption of NH_2 radicals in their reactions with various species. Hack et al.[46] produced NH_2 radicals in a flow tube by reacting ammonia with fluorine atoms produced in the microwave discharge of F_2. They monitored the NH_2 radical concentration by detection of fluorescent radiation when the NH_2 radicals were excited by 3kHz modulated 597.7 nm radiation. Work by Stief et al.[47] on the rate of reaction of NH_2 with NO utilized NH_2 fluorescence induced by the 570.3 nm line of a continuous wave dye laser to monitor the relative NH_2 concentration.

Figure 2

ABSORPTION AND FLUORESCENCE SPECTRUM OF NH_2

(Adapted from Kroll)[43]

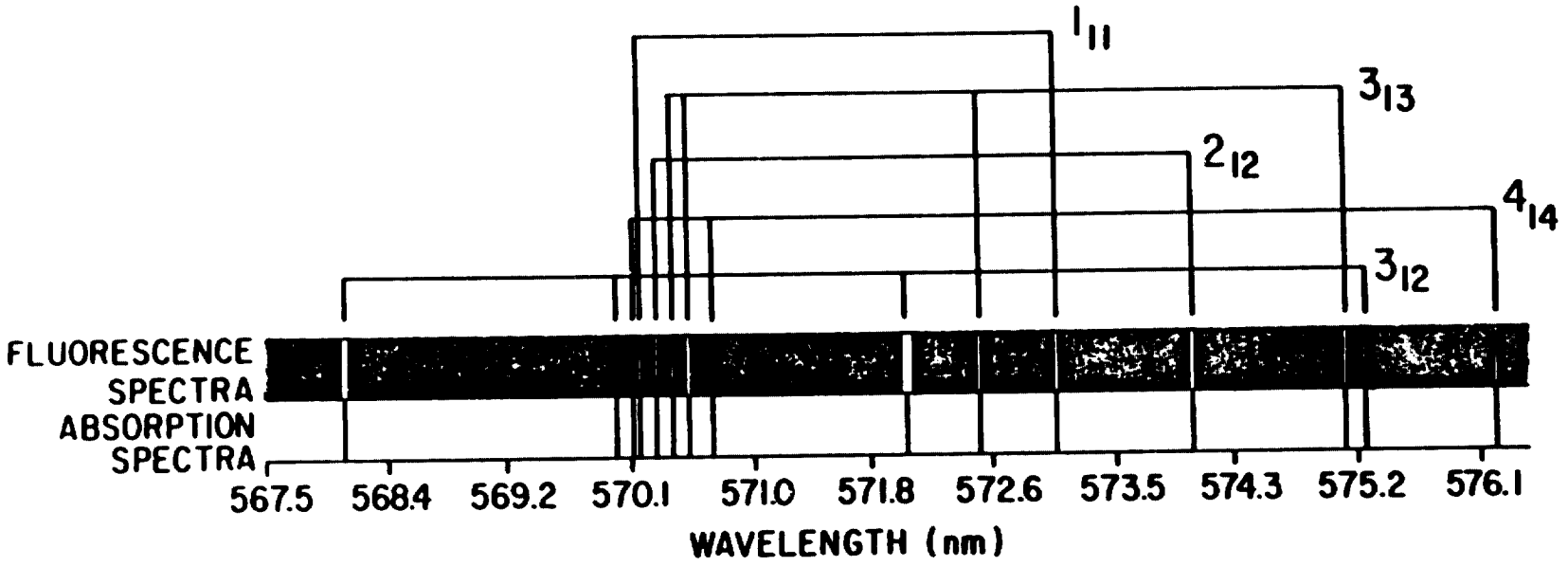

5. Previous Studies of Pertinent NH_2 Radical Reaction Rates

Data on the reaction rate constants of the NH_2 radical with other minor species present in the lower Jovian stratosphere and upper troposphere are sketchy. In some cases incompatible results have been presented.

Reaction (18):

$$(18)\ NH_2 + NH_2 + M \rightarrow N_2H_4 + M,$$

has been studied by several investigators;[48-50] however, the most comprehensive investigation, especially with regards to the pressure and temperature dependence of this reaction, was performed by Van Khe et al.[50] using the flash photolysis resonance absorption technique. No significant temperature effect was found at either the high or low pressure limits. At the high pressure limit, about 1000 torr, the apparent bimolecular rate constant is $k_{18}^{\infty} = (2.5 \pm 1.3) \times 10^{-11}$ cm^3 molecule^{-1} sec^{-1}; as the pressure approaches zero, the overall process becomes third order as shown by the general mechanism equation (15) and $k_{18}^{o} = (6.9 \pm 3.5) \times 10^{-30}$ cm^6 molecule^{-2} sec^{-1}.

The rate of reaction (23)

$$(23)\ NH_2 + H + M \rightarrow NH_3 + M$$

was studied by Gordon et al.[49] They found $k_{23}^{o} = 6.1 \times 10^{-30}$ cm^6 molecule^{-2} sec^{-1} at room temperature between 250 and 1000 torr. Reaction (23) appears

to approach a second order limit at higher than 1000 torr.

In a study of the rate of reactions of NH_2 radicals with various olefins using flash photolysis to produce the radical and detection by laser absorption, Lesclaux et al.[45] determined that, for $NH_2 + C_2H_4$, $k_{29} = 2.0 \times 10^{-13} e^{-(1.99 \pm .11) \times 1000/T}$ cm^3 $molecule^{-1}$ sec^{-1} at around 1 atm total pressure and between 300 and 500°K. In a later study, Khe and Lesclaux[51] obtained the same rate constant over a wider range of ethylene pressures from 10 - 100 torr and identified the possibility of a pressure dependence in the formation of an adduct, $NH_2C_2H_4$, at pressures below 10 torr at high temperature only. Because the rate constant was so small, they were not able to present the low pressure data within acceptable limits of uncertainty.

Hack et al.[46] studied reaction (29), at low total pressure (~1 torr) in a discharge flow-laser induced fluorescence experiment. In contrast to the results of Lesclaux et al. they found a higher rate, $k_{29} = (2.2 \pm 0.5) \times 10^{-15}$ cm^3 $molecule^{-1}$ sec^{-1} over the temperature range 295 - 505°K. The room temperature results of Hack et al. were nearly an order of magnitude above those of Lesclaux et al. and they were temperature independent. Although their experiments provide no direct evidence, Hack et al. also suggest that the adduct, $NH_2C_2H_4$, was formed as a product.

Both Hack et al. and Lesclaux et al. cited the results of Schurath et al.[28] to support their suggestion of adduct formation between NH_2 and C_2H_4. Schurath et al photolyzed ammonia using an I_2 discharge lamp at 206.2 nm in the presence of ethylene and performed a product analysis in experiments to determine the mechanism of reaction (29).

Only one measurement of the rate of reaction (28), $NH_2 + C_2H_2$, has been performed. Hack et al.[46] using the same procedure as in their study of

NH_2 and C_2H_4, found $k_{28} = 2.36 \times 10^{-8} T^{-2.7}$ cm^3 molecule^{-1} sec^{-1} over the temperature range 210 - 505°K and at a total pressure of about 1 torr.

In an attempt to measure the rate of reaction of NH_2 with methane, CH_4, only an upper limit could be established. Demissey[52] estimated $k_{30} << 4 \times 10^{-17}$ cm^3 molecule^{-1} sec^{-1} at 520°K.

No direct or indirect measurement of the rate of reaction (27), $NH_2 + PH_3$ has been performed. Buchanan et al.[53] performed a radiolysis of ammonia-phosphine mixtures and estimated that k_{27} should have an activation energy of not more than 2 or 3 kcal/mole. Using this estimated activation energy, they suggested that k_{27} is within one or two orders of magnitude of the rate of bimolecular collisions (~ 10^{-10} cm^3 molecule^{-1} sec^{-1} at 298°K).

C. Purpose of this Study

The primary purpose of this study is to provide reaction rate measurements for reactions of NH_2 with some of the other minor components of the Jovian lower stratosphere and upper troposphere. Particular emphasis is placed on those reactions for which there is no kinetic information or for which conflicting or incomplete rate measurements currently exist. These measurements will be made under temperature and pressure conditions which are as close as experimentally possible to those found in the region bounded by the upper troposphere and lower stratosphere of Jupiter.

Specifically, the rate of reaction (27), $NH_2 + PH_3$, will be measured. This is a potentially important reaction relating the photochemistry of ammonia and phosphine, and one for which no direct kinetic data are available. Since reaction (28), $NH_2 + C_2H_2$, has only been measured by Hack et al. and then only at 1 torr total pressure, additional

data are required to evaluate the importance of this reaction particularly at high pressures. If reaction (28) proceeds by adduct formation, then the rate of this reaction could be significantly higher at higher pressures than it is at the very low pressure of the Hack et al. study. The importance of determining the rate of reaction (28) is further enhanced by noting that acetylene is one of the products of the photolysis of both ethane and ethylene and, therefore, may be continuously generated in the upper Jovian troposphere.

Finally, there is an obvious need to resolve the apparent conflict between the results of Hack et al.[46] and Khe et al.[51] with regards to the rate of reaction (29), $NH_2 + C_2H_4$[46,51]. If reaction (29) were equally fast at all temperatures, as the results of Hack et al. indicate, it might prove to be a significant channel for removing NH_3 from the colder levels of the Jovian lower stratosphere. On the other hand, if the reaction does show a pressure dependence as indicated by Khe et al., this reaction may be of some significance in consuming ammonia in the upper troposphere where pressures are considerably higher (10^3 - 10^4 torr).

The overwhelming requirement compelling this study is the emphasis that modelers themselves have placed on the need to determine the rates of reactions which may help to explain the ammonia paradox in the Jovian atmosphere and for which either insufficient or unreliable data are currently available[21,22]. Accurate measurements made as close as possible to conditions found in the lower Jovian stratosphere and upper troposphere which meet modeler requests are the goal of this study.

CHAPTER 2

EXPERIMENTAL

A. Bimolecular Rate Constants and Other Kinetic Parameters

1. Reaction Rates

The goal of experiments in this study is to measure the rate of reactions (27), (28), and (29) over a range of temperatures and pressures. These measurements can then be used to develop mathematical expressions from which predictions can be made of the rates of these reactions under the wider range of temperatures and pressures indigenous to Jupiter's upper troposphere and lower stratosphere. As written, reactions (27), (28), and (29) describe elementary processes. The metathetical channels are therefore, according to Chapter 1, both bimolecular and of second order. The addition channels are termolecular and third order.

The rate of an elementary reaction can be determined by measuring the rate of production of a product or the rate of consumption of a reactant. The former method usually involves more difficulty because the products of an elementary reaction are very often reactive or the concentration of product cannot be followed readily (as in the case of ammonia in reaction (27)); then, measuring the rate of generation of a product is nearly impossible. In the case of the reactions being studied, the reaction products fall into one of the categories just mentioned and,

therefore, the method used to monitor the reaction rate will be to follow the rate of consumption of a reactant.

The rate of reaction of NH_2 radicals with either phosphine, acetylene, or ethylene may be expressed by the generalized equation:

$$(51)\quad NH_2 + X \rightarrow \text{products}$$

where X represents PH_3, C_2H_2, or C_2H_4 and will be termed the substrate. The rate of this reaction may be expressed as being proportional to the concentration of each of the reactants in equation (51), where the constant of proportionality is the rate constant, k. Thus, we can write:

$$(52)\quad \text{rate} = \frac{-d[NH_2]}{dt} = k_{bi}[NH_2][X]$$

where k_{bi} is the bimolecular rate constant and the bracketed terms represent the concentrations of NH_2 radicals and substrate, respectively. The equation may be further developed by dividing through by $[NH_2]$ to give:

$$(53)\quad \frac{-d[NH_2]}{dt}\,\frac{1}{[NH_2]} = k_{bi}[X]$$

Separating the variables and integrating (where the lim'ts are: $[NH_2]_o$ is the NH_2 concentration at time, t=0, and $[NH_2]$ is the NH_2 concentration at time, t) gives:

$$(54)\quad \int_{[NH_2]_o}^{[NH_2]} -d\ln[NH_2] = \int_{t=0}^{t=t} k_{bi}[X]dt$$

If [X] is so large that it is essentially invariant during the period over which the reaction is observed, [X] may be treated as a constant. All constant terms can be taken out of the integral to give:

$$(55)\quad -\int_{[NH_2]_o}^{[NH_2]} d\ln[NH_2] = k_{bi}[X]\int_{t=0}^{t=t} dt$$

Integration yields:

$$(56)\quad (\ln[NH_2] - \ln[NH_2]_o) = -k_{bi}[X]t$$

Taking the differential with respect to time gives the working form of the equation:

$$(57)\quad \frac{-d\ln[NH_2]}{dt} = k_{bi}[X]$$

In effect, the rate of the reaction is now reduced to dependence on only NH_2 concentration and the rate is said to be pseudo-first order.[54] Then (57) becomes:

$$(58)\quad \frac{-d\ln[NH_2]}{dt} = k_{pseudo}$$

and the study of the reaction rate is simplified considerably.

Reaction (51) may not be the only means by which NH_2 is consumed. If NH_2 radicals are produced, as will later be described in detail, in a relatively small volume near the center of the reaction cell, a concentration gradient is, therefore, set up in the reaction cell and a

mass flux established. The NH_2 radicals thus diffuse out from the volume in which they are produced. The rate of this non-reactive loss of NH_2 radicals due to diffusion may be accounted for by:

$$(59)\quad \frac{-d\ln[NH_2]}{dt} = k_d[NH_2]$$

where k_d is the rate constant for diffusion. (59) may be rearranged by dividing by $[NH_2]$ to give:

$$(60)\quad \frac{-d\ln[NH_2]}{dt} = k_d$$

Finally, combining the loss terms from (57) and (60) gives:

$$(61)\quad \frac{-d\ln[NH_2]}{dt} = k_{bi}[X] + k_d$$

which gives the overall rate of depletion of NH_2 by both elementary reaction (51) and by diffusional loss from the viewing zone. There may be, in addition to the above considerations, other processes that contribute to the consumption of NH_2 radicals. These processes could complicate the kinetic interpretation of the data, and will be discussed later with regards to each specific reaction studied.

2. The Temperature Dependence of Reaction Rates

Over 100 years ago, Hood[55] set down an empirical relationship identifying the temperature dependence of the reaction rate constant, k:

$$(62)\quad \log k = B - A'/T$$

where A' and B are constants and T is the temperature in degrees Kelvin, °K. Van't Hoff[56] first identified the temperature dependence of equilibrium constants and Arrhenius[57] extended his ideas to include an activation process to some intermediate configuration as a bridge for relating equilibrium constants to rate constants. The Arrhenius expression for the temperature dependence of the rate constant of a elementary reaction is given by:

$$(63)\quad k(T) = Ae^{-E_a/RT}$$

where E_a is the activation energy in calories/mole for the reaction (or the difference in energy between the reactants and the intermediate configuration). A is a constant called the pre-exponential factor having the same units as k(T). In classical collision theory, A represents the total number of collisions between reactants per unit time (including the proper geometric orientation) which lead to products. R is the ideal gas law constant, 1.987 cal $°K^{-1}$ $mole^{-1}$, and T is the temperature in °K.

Equation (63) may be expressed in another, more useful form:

$$(64)\quad \ln k = \ln A - E_a/RT$$

Since (64) is in the form of a straight line ($y = mx + b$), with ln k and 1/T as the variables, a graph of ln k versus 1/T should also be a straight line with slope of $-E_a/R$ and intercept of ln A. Whether or not a straight line is obtained in practice is one of the diagnostic tools of kinetics

because the Arrhenius equation is strictly applicable only to elementary reactions. Failure to obtain a straight line may indicate that the reaction under study involves more than one elementary reaction.[58]

3. Summary

Experimentally, this study is directed towards measuring the rate constants, activation energies, and Arrhenius parameters for reactions (27), (28), and (29) so that rate expressions for these reactions can be developed which are applicable to the range of temperatures and pressures found in the upper Jovian troposphere and lower stratosphere. In the following sections, the techniques and instrumentation used in making these measurements are described.

B. Experimental Techniques

The kinetic measurements made in this study utilized the flash photolysis technique to produce NH_2 radicals coupled with detection of NH_2 radicals by laser induced fluorescence. This method was selected because it combines several advantages over some other potentially feasible methods considered under the constraints required by this study. Huie and Herron[59] recently reviewed flow techniques and flash photolysis techniques and discussed their application to direct measurement of the rates of fast atom or radical reactions. Various detection methods can be used in conjunction with these techniques.

Flow techniques involve flowing the reacting species down a tube at such a rate as to achieve a plug flow and to measure the change of

concentration of a particular reactive species as a function of distance which is equivalent to time. Flow techniques have been used with a variety of detection methods such as mass spectrometry and electron spin resonance (ESR); also, optical absorption and fluorescence techniques have been used to good advantage in flow reactions. Mass spectrometry generally has a limited sensitivity to detection of transient species such as free radicals because of the losses incurred in wall collisions and also because of the difficulty of introducing these species into the mass spectrometer ionization chamber. There is a further problem of potential ambiguities in the fragmentation patterns of parent molecular species. ESR is useful only in detecting paramagnetic species such as radicals, and its sensitivity is usually much lower than the other detection methods referred to above.[60] Therefore, only the high sensitivity methods for detection of NH_2 radicals, absorption and fluorescence, will be considered here.

Howard[60] points out that the flow discharge technique has produced more gas phase kinetic data at 300°K than any other method. Since reaction progress can be frozen at a fixed observation point in a flow tube experiment, there is no constraint on detection speed of response. The flow tube technique has the further advantage of permitting the production of two labile reactants in isolation from one another, permitting the direct measurement, for example, of radical-radical reaction rates.

The requirement of maintaining a laminar flow with its high radial diffusion and low axial diffusion, and the high surface to volume ratio of the flow apparatus, impose certain limitations on the use of the flow technique in studying the kinetics of radical reactions.[59] In the plug flow approximation, radial diffusion is assumed to be rapid. At higher pressures, diffusion becomes slow compared to axial transport and, since

the flow velocity exhibits a parabolic radial profile for laminar flows, species, including radicals, will have a lower axial velocity at the walls than near the center of the tube. This limits the pressure range over which flow studies can be made. A more serious problem related to residence time at the walls is the possible occurrence of heterogeneous (wall) reactions. The high surface to volume ratio of most flow systems exacerbates this problem and could lead to derived rate constants which are too high. While coating the flow tube walls is a common practice in order to reduce heterogeneous reactions, the possibility of interfering wall reactions cannot be ruled out. This problem could be significant especially for slow reactions such as those being examined here.

The flash photolysis technique for producing a large amount of a transient species such as an atom or radical in a short time has both advantages and disadvantages.[60] Since the flash photolysis experiment is conducted in real time, fast time response detectors (as low as a microsecond) may be required. In addition, the need to selectively photolyze the source species but not the substrate places constraints on the variety of systems that can be studied using this technique. Flash photolysis systems are not, however, limited by the total pressures that can be employed; Howard[60] gives a range of 5 torr up to several atmospheres for flash systems (versus a range of 1-10 torr for flow systems). In addition, since higher concentrations of reactant species may be used, it is often possible to measure smaller rate constants than can be measured using the flow technique. The low surface area to volume ratios of reaction vessels used in flash photolysis experiments minimize the contributions due to wall reactions. Finally, the flash photolysis technique has available to it several diagnostic procedures with which to

analyze for the occurrence of secondary reactions.[61]

Rapid detection methods must be employed to monitor radicals produced by the flash photolysis technique and strong light sources are required to produce sufficient radiation at a specific wavelength so that a weakly absorbing species such as a radical can be observed. Therefore, laser absorption and laser induced fluorescence are the only methods that will be discussed here. Lasers provide a coherent, monochromatic source of radiation; dye lasers are easily tuned over a range of wavelengths in order to excite a specific molecular transition or absorption line. In absorption systems, the radical signal is the difference between the incident light intensity, I_o, or background, and the light intensity after passing through the sample, I. Absorption, based on the Beer Lambert Law, is high for high concentrations and therefore, at high pressures of absorber, $(I_o - I)$ is large and the signal to background, $(I_o - I)/I_o$ is large. The absorption system shows a much lower sensitivity at low pressures where the signal is a small difference between two large quantities and where the ratio of signal to background is small. With fluorescence methods, since the fluorescence signal can occur at a longer wavelength than that of the excitation radiation, there is little or no background interference from the excitation radiation.

The flash photolysis technique for producing NH_2 radicals was selected over the flow discharge technique because of the need to study reactions over a range of pressures corresponding as closely as possible to those found in the upper Jovian troposphere and lower stratosphere (5-100 torr). In addition, the flash photolysis method is more sensitive for studying slow reactions, and wall reactions are less significant than in the flow systems. The laser induced fluorescence method was selected for

NH_2 radical detection because it is more sensitive than absorption at the relatively low pressures at which this study was performed.

C. Flash Photolysis

1. General

The flash photolysis device, the development of which was pioneered by Norrish and Porter,[62] provides a method for producing over a very short time span a large amount of energy to be used in generating a transient species such as an atom or radical. While early devices were capable of discharging energies of up to 10^4 joules in a few milliseconds, refinements in instrumentation made possible sophisticated devices capable of high flash energies and much shorter flash duration.[63]

A flash lamp consists of a pair of electrodes which are fitted into a chamber and across which a charge is dissipated. The charge is provided by a D.C. power supply and stored temporarily by a capacitor that is connected in parallel to the electrodes. The energy provided by a flash lamp is given by:

$$(65)\quad E = 1/2\ CV^2$$

where E is the energy dissipated in joules, C is the total capacitance of the system in farads, and V is the voltage applied across the capacitor. Equation (66)

$$(66)\quad t = (LC)^{1/2}$$

's used to determine the flash duration, t, in seconds from the system inductance, L, and the total capacitance, C.

2. Equipment

The flash lamp used in this study consists of a polytetrafluoroethylene (Teflon™) cylinder housing two tungsten carbide tipped electrodes. The cylinder is pressurized with commercial (Goddard Space Flight Center) grade nitrogen of about 99.99% purity. The electrodes are connected to a 4.5 microfarad (mf), 20 kv model ESC 248C capacitor system manufactured by Tobe Deutschmann of Germany.

The capacitor spontaneously discharges when the voltage across the electrodes in the flash lamp reaches a critical value called the breakdown voltage. Operationally, breakdown is achieved by first fixing the nitrogen gas pressure within the lamp at a specific value by balancing the nitrogen flow into the lamp against its removal by a Welch model 1400 mechanical pump. At this pressure, the voltage across the electrodes is allowed to build up until it exceeds the breakdown voltage. The capacitors discharge and the process of charging is repeated. By selecting the rate of capacitor charging and the lamp gas pressure, the desired rate of flashing is obtained. Typical flashing rates are 2 to 4 seconds between flashes.

Using equation (65), output energies of 20 to 144 joules per flash are calculated for typical charging voltages of 3 to 8 kv. The discharging time for equipment used in these experiments has been calculated[64] to be ~1 microsecond using equation (66). The light plasma generated by the discharge capacitor decays more slowly.

The flash energy is dissipated through the nitrogen gas and the

resulting atomic nitrogen spectrum for a similar lamp is provided in Fig. 3. Only a small fraction of the energy dissipated is converted to vacuum ultraviolet radiation.

3. Limiting the Flash Lamp Output

Since the flash lamp output (Fig. 3) spans such a broad spectral range, it was necessary to filter the lamp to minimize the photolysis of phosphine, ethylene, or acetylene while still providing sufficient spectral radiation for strong absorption by ammonia.

The absorption spectrum of ammonia in the vacuum ultraviolet is shown in Fig. 4.[65] In the region from 170.0 nm to 210.0 nm, ammonia absorbs strongly and NH_2 is produced almost exclusively in its ground electronic state, ($\tilde{X}\ ^2B_1$). Excited NH_2 radicals ($\tilde{A}\ ^2A_1$) are produced only at wavelengths below 164.0 nm and then, with a quantum yield of less than .001[66]. Primary processes:

$$(36)\quad NH_3 \xrightarrow{h\nu} NH_2\ (\tilde{X}\ ^2B_1) + H\ (^2S_{1/2})$$

$$(37)\quad NH_3 \xrightarrow{h\nu} NH\ (a\ ^1\Delta) + H_2\ (^1\Sigma_g^+)$$

and $$(38)\quad NH_3 \xrightarrow{h\nu} NH\ (\tilde{X}\ ^3\Sigma^-) + 2H\ (^2S_{1/2})$$

occur in the near and vacuum ultraviolet and, based on the discussion in

Figure 3

N_2 FLASH LAMP OUTPUT

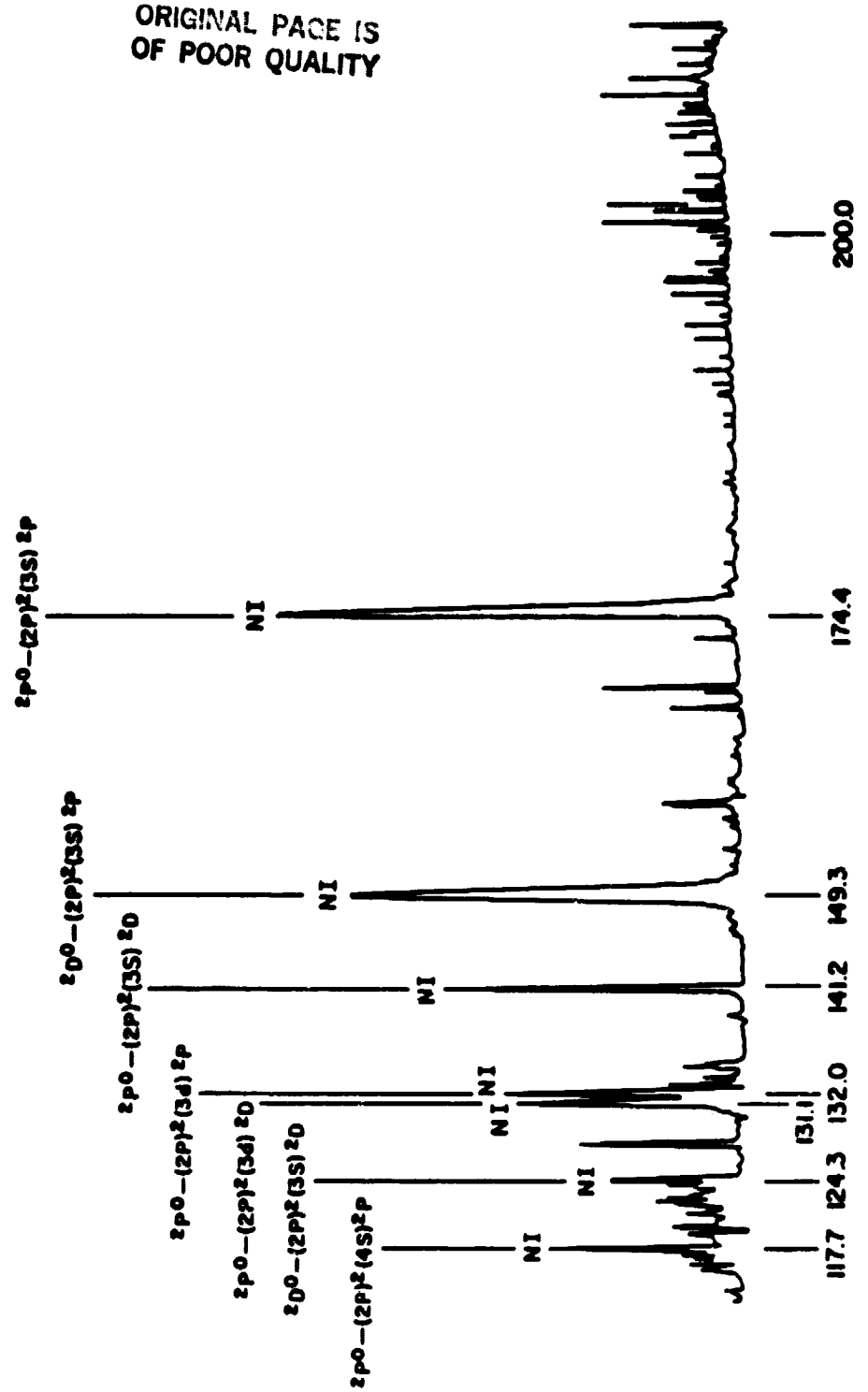

Figure 4

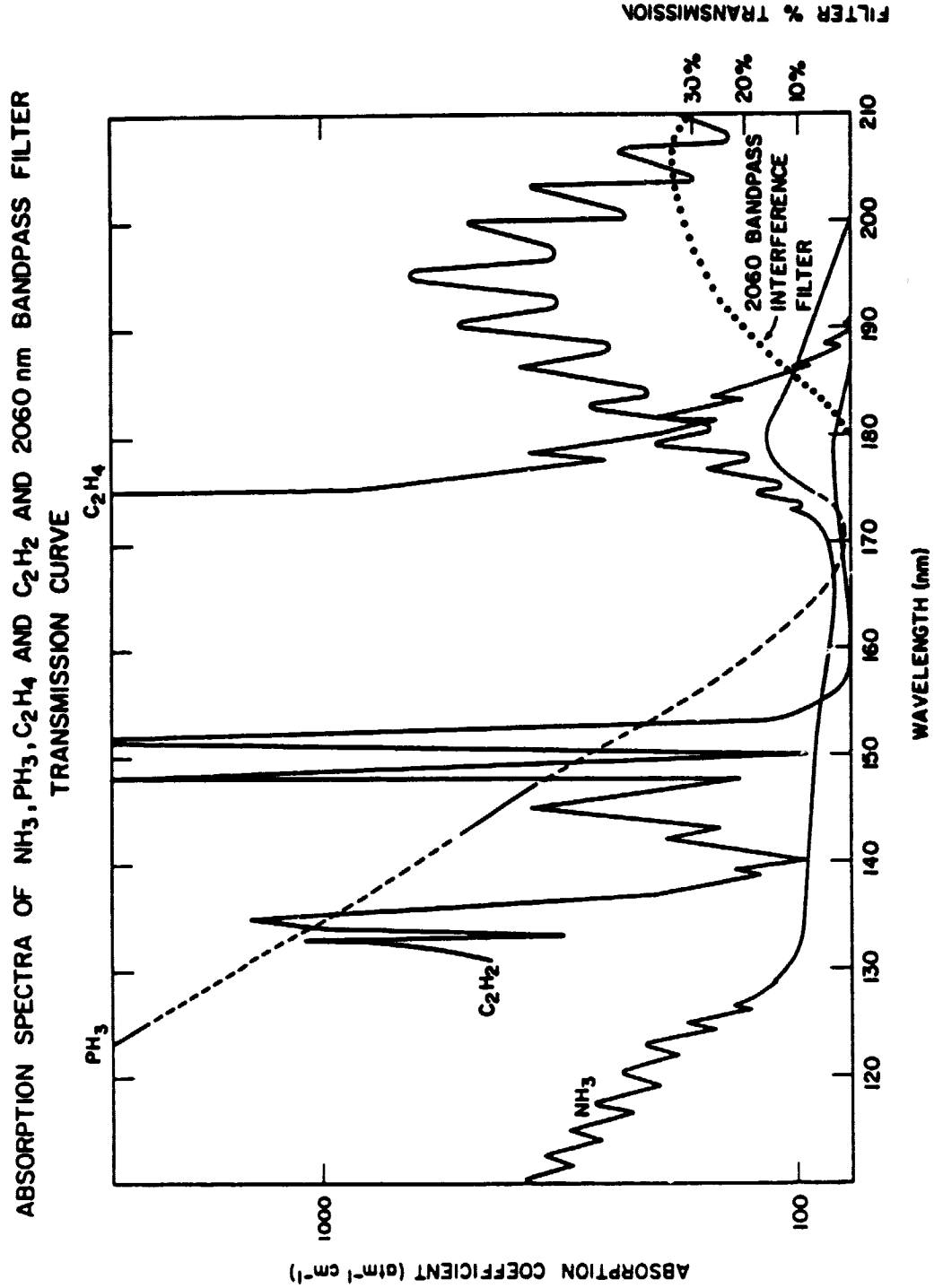

Chapter 1, section D. 3., are the only reported photoinduced reactions which need to be considered here.[66]

In most of the experiments conducted, an Acton Research Corp. 206.0 nm bandpass filter with 35% peak transmittance and a full width at half maximum (FWHM) of 40.0 nm, skewed towards higher wavelengths was placed over the flash lamp. This filter passed radiation in a spectral region where ammonia absorbed strongly while blocking radiation which would have resulted in the production of NH radicals and electronically excited NH_2 radicals. The filter bandpass is also shown in Fig. 4.

The 206.0 nm bandpass filter not only precluded the formation of undesirable ammonia photochemistry products, but also minimized any photolysis of any of the substrate gases. This is shown clearly in Fig. 4. Acetylene absorbs strongly in the region 155.0 nm; however, absorption drops off rapidly at higher wavelengths so that above 195.0 nm, the C_2H_2 absorption coefficient is less than 1 $atm^{-1}cm^{-1}$ (base e, 298°K). Ethylene absorbs strongly up to about 175.0 nm, but its absorption coefficient also drops off to less than 1 $atm^{-1}cm^{-1}$ (base e, 298°K) above 195.0 nm. Phosphine absorption falls off at higher wavelengths until it is below 1 $atm^{-1}cm^{-1}$ (base e, 298°K) at about 202.0 nm.

In some of the early experiments involving ammonia and phosphine, a 175.0 nm Ditric Optics Inc. interference filter with a skewed frequency width at half maximum of -13.0 nm and +25.0 nm was used.

D. Laser Induced Fluorescence

1. Historical

Lasers have previously been used to study NH_2 radical chemistry. In some early work, Atkinson[67] demonstrated the advantages of intracavity absorption of a dye laser output as a means for detecting free radicals such as NH_2 and HCO. Atkinson noted the convenience and sensitivity dye lasers afford in their ease of tuning to a particular resonant frequency and pointed out the potential applications of the method to kinetic problems. Kroll[68] used a continuous wave dye laser to produce upper electronic state NH_2 from ground state NH_2 radicals and used the resulting NH_2 fluorescent emission in spectroscopic studies of the NH_2 radical. Hancock et al.[44] first applied the resonance fluorescence technique to the NH_2 radical in their measurement of the rate constant for the reaction of NH_2 with NO. Since then, several studies have been published in which laser induced fluorescence was used to measure the rate constant for the reaction of NH_2 with NO_2, NO, and with unsaturated hydrocarbons.[46,47]

2. General

As discussed in an earlier section, the NH_2 radical is produced by the flash lamp almost exclusively in its ground electronic state. By the Beer Lambert law, a certain fraction of the NH_2 radicals can be made to absorb resonant radiation, radiation which corresponds to the energy difference for a transition between the ground electronic state and the

upper electronic state. The NH_2 radicals can emit this absorbed radiation by fluorescence, since the upper and lower states are of the same multiplicity (a spin allowed transition).[69] Based on the Stern Volmer argument presented in Chapter 1, the intensity of the fluorescence is then proportional to the number density of NH_2 radicals originally formed. More intense radiation sources will cause a stronger fluorescent signal until the transition becomes saturated.

Lasers provide a much more intense source of monochromatic radiation ($\sim 1 \times 10^{19}$ quanta cm^{-2} sec^{-1} for a typical 150 milliwatt output of the dye laser used) than is available using atomic resonance lamps (10^{11} to 10^{12} quanta cm^{-2} sec^{-1} from the 116.5 and 123.6 nm Kr resonance lines at a distance of 2 cm from a spherically shaped Kr lamp)[70]. Consequently, the use of lasers has grown in recent years as a means of producing resonant transitions and correspondingly stronger fluorescent emission.

3. Apparatus

A continuous wave dye laser is actually a system of two lasers that are operated in tandem. A pump laser is required to provide a monochromatic source of radiation which, when fed into a second cavity, causes a dye to lase over an appropriate band of wavelengths. The output of the dye laser depends on the dye used and the pump laser wavelength(s). Specific wavelengths can be selected from within the characteristic wavelength band of the dye laser output using a coarse tuning wedge and a fine tuning etalon in the laser to discriminate between wavelengths as close together

as 0.05 nm.[71]

A Spectra-Physics model 170 argon ion laser was used at about 5-6 watts output power to pump a Spectra-Physics model 375 continuous wave dye laser. A 1.5×10^{-3} M solution of Eastman Kodak Rhodamine 6G tetrafluoroborate in ethylene glycol was used as the dye. With Rhodamine 6G, dye laser output power of greater than 100 milliwatts can be obtained with a pump laser input of 4 watts over the range 565.0 nm to 652.5 nm.[72] A peak output power of about 150 mw can be achieved at 590.0 nm. The Rhodamine dye exhibits superior stability and longevity compared to other dyes that fluoresce at these wavelengths.

4. Laser Tuning

Prior to each experiment the dye laser was tuned to a wavelength corresponding to a strong NH_2 ($\tilde{X}\ ^2B_1$) absorption. This was accomplished using a small, fast flow discharge system illustrated in Fig. 5. The dye laser beam was deflected by a mirror so that it passed through a concave lens and was focused through the center of a glass tube. The far end of the tube was attached to a Wood's Horn to trap light scattered by the walls. The exterior of the tuning tube was coated black except for a small circular viewing area at right angles to the incident beam. The front of the tube was a 2 mm thick quartz window sealed in place with black wax.

A mixture of about 10% ammonia in helium was flowed through the cross tube at about 1 torr total pressure using a high speed mechanical pump. An electrodeless microwave discharge attached to the inlet arm was used to dissociate a fraction of the ammonia into NH_2, NH, and H. These

Figure 5

LASER TUNING APPARATUS

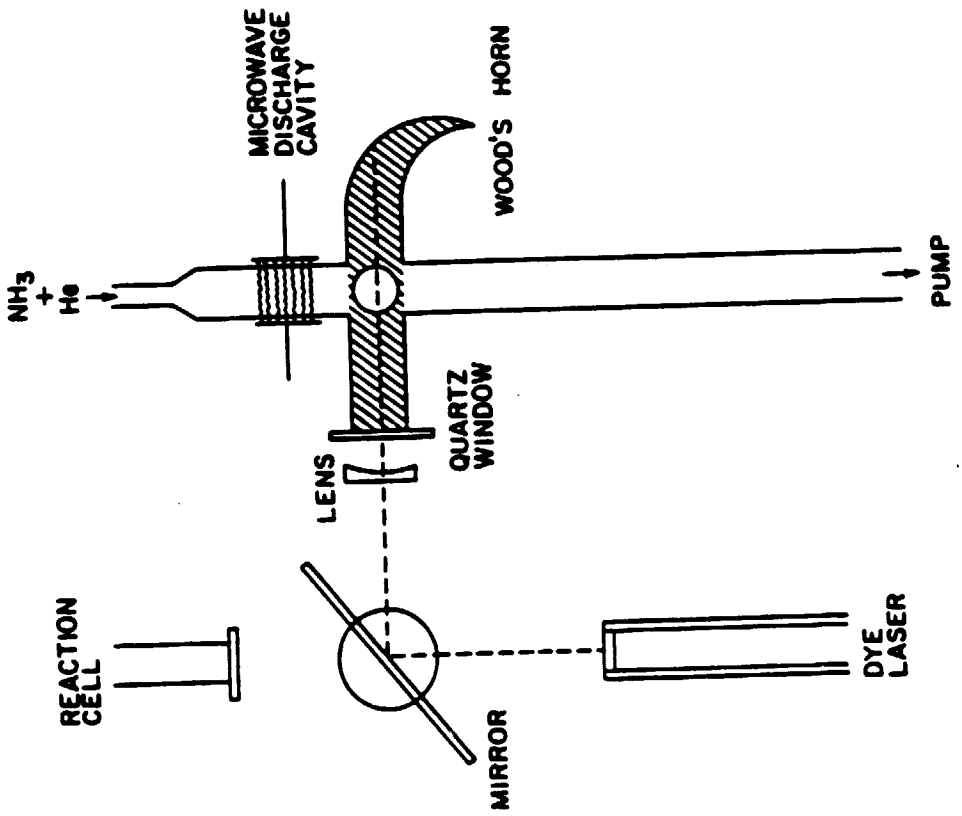

fragments then passed through the laser beam.

The tuning procedure was essentially the same as that described by Kroll[68] and Halpern et al[73]. Initial laser tuning was effected using the laser tuning wedge to adjust the dye laser output to around 568.0 nm or 570.0 nm. This wavelength was verified visually using a Jobin-Yvon hand held monochromator with a 0.25 mm slit. The monochromator read to within ±0.5 nm when the 577.0 nm and 579.1 nm lines of mercury from a common fluorescent light were measured. Next, the dye laser was scanned over a narrow range of wavelengths using the fine tuning etalon until a fluorescence was visually observed as a sharp orange line against the yellow laser background scatter in the tuning cell window. Fine tuning was completed with the etalon until the brightest fluorescence was obtained. The tuning procedure was performed periodically as a check of the dye laser output. The time resolved detection and measurement of the intensity of the NH_2 fluorescence was used to follow the rate of reaction of the NH_2 radical with phosphine, ethylene, and acetylene.

E. Detection of the Fluorescence Signal

1. The NH_2 Fluorescence Signal

NH_2 radical fluorescence resulting from absorptions at 570.3 nm and 568.2 nm are shown in Fig. 1. The manifold of fluorescence lines corresponding to absorption of 568.2 nm radiation occurs at 568.2 nm, 570.0 nm, 572.0 nm and 575.3 nm. Fluorescence lines at 570.3 nm and 574.2 nm correspond to absorption of 570.3 nm radiation.

The fluorescence resulting from the absorption of 568.2 nm or 570.3 nm radiation by NH_2 radicals was used to monitor the relative NH_2 ground state radical concentration. As already discussed (Chap. 1, sect. B.3.b), the strength of the fluorescent signal can then be used to determine the relative NH_2 concentration as a function of time. As NH_2 radicals are consumed, the number of scattered fluorescence photons detected per unit time decreases, and this provides the means for determining rate constants.

2. Detection and Analysis Apparatus

Fig. 6 provides a schematic of the equipment used in the production, detection, and analysis of the NH_2 fluorescence signal. The fluorescent radiation passed from the reaction cell, through a blackened honeycomb collimator that reduced wall-scattered light and then through a 577.7 nm Ditric Optics interference filter with a bandpass of 9.8±3.0 nm FWHM. This filter preferentially transmitted the longer wavelength NH_2 fluorescence lines, and restricted the detection of scattered laser light (568.2 nm or 570.3 nm). The use of this filter, therefore, significantly increased the NH_2 fluorescence signal to background ratio.

A very significant further increase in the NH_2 fluorescence signal to background ratio was achieved using a Melles-Griot polarized window which was placed in the optical train between the 577.7 nm filter and the photomultiplier. Since the emitted laser radiation was polarized, reflectively scattered laser radiation was also polarized. The NH_2 fluorescence radiation was isotropically scattered. Thus, while the

Fig. 6 Legend

DL- Dye Laser

RC- Reaction Cell

FL- Flash lamp

TP- Trap

P- Pump

PM- Photomultiplier

PD- Photodiode

PA- Power Amplifier

HVC- High Voltage Capacitor

HVPS- High Voltage Power Supply

LVD- Low Voltage Descriminator

MCA- Multichannel Analyzer

TTY- Teletype

OLC- On-line Computer

PS- Power Supply (for laser)

REACTION RATE DETECTION AND ANALYSIS EQUIPMENT

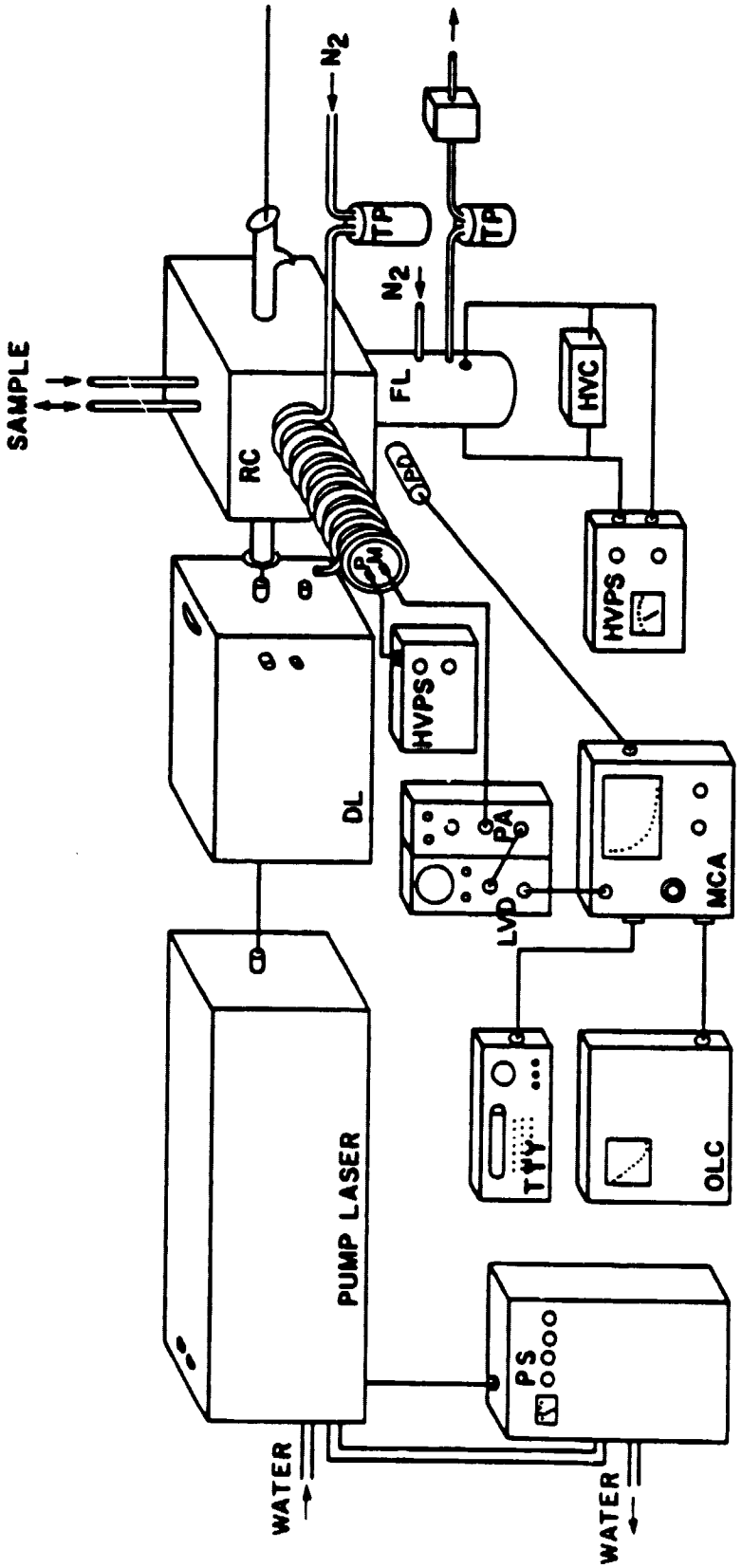

Figure 6

polarizing window reduced the overall signal by about 65% (manufacturer's specifications), reflectively scattered laser light was almost completely blocked and the signal to background noise ratio increased by at least an order of magnitude. The cause of some of the scattered light observed was never identified, but possible candidates include molecular Rayleigh scattering, small (<.5 micron diameter) particles in gas samples used, and reaction product which may have condensed to form an aerosol.

Scattered fluorescent light from electronically excited NH_2 radicals in the reaction cell was detected by a photomultiplier tube mounted at right angles to both the laser beam and the flash lamp. The signal was detected by an EMR 541E 01-14 photomultiplier tube with a spectral response between about 280.0 nm and 850.0 nm. Since the tube was sensitive to thermal noise, it was necessary to maintain it at -20°C to -30°C by blowing cooled dry nitrogen gas through a copper tube coiled around the photomultiplier housing.

The signal was fed from the photomultiplier through a preamplifier and into an Ortec model 454 amplifier. It then passed into an Ortec model 436 low voltage discriminator, which discriminated against low intensity pulses and shaped the pulse, and finally was fed into a Northern Scientific Co. NS 436 Multichannel Analyzer (MCA).

Memory in the MCA consisted of 1024 channels which were divided into either sixteen-64 channel memory units or eight-128 channel units. An interval time base ($1-1x10^{-5}$ sec) could be selected for each memory unit to fit experimental conditions. An EG & G model 568B photodiode detected the light from the flash lamp; a pulse from the photodiode passed through a discriminator and was used to trigger the MCA sweep. The MCA collected

photon counts i. the first data channel for the selected time base duration and then switched to the next channel etc., in sequence until all the channels in a memory unit had been used. The MCA then reset to the ready mode until next reactivated by a trigger pulse from the photodiode. This multiscaling mode of the MCA was used to accumulate photon counts from repetitive flashes until about 1000 counts had been accumulated in the first data channel. While the signal to background was, on the average, greater than 3:1, in practice, signal to background ratios ranged from about 1:1 to 30:1.

F. Data Collection and Analysis, Reporting Uncertainties and Error Analysis

1. Data Collection

Data Collected in the MCA could be viewed on a cathode ray tube as they were accumulated. Table 2 is an example of the photon counts collected by channel (with a time base of 1.5×10^{-3} sec per channel) during an experiment measuring the rate of NH_2 radical dissipation by diffusion. The first channel gives the number of flashes used in the experiment; channel 2 is normally omitted so that scattered photons from the flash lamp flash, which has a small, but finite duration, are not be counted. Channel 3 is the first data channel used in analysis. Fig. 7 displays these data.

After experiments were completed, data were transferred, to an RDA 6200 LP miniprocessor for analysis or, when desired, transmitted to a

Table 2

NH_2 Fluorescence Photon Count

Channels	Photon Counts									
1-10	00036	07570	02466	01798	01666	01276	01102	01030	00941	00842
11-20	00759	00689	00624	00588	00512	00494	00465	00478	00443	00378
21-30	00359	00400	00339	00346	00311	00315	00250	00292	00299	00275
31-40	00251	00232	00252	00266	00215	00252	00216	00238	00201	00201
41-50	00187	00199	00167	00185	00202	00169	00167	00169	00169	00134
51-60	00151	00168	00181	00172	00195	00148	00131	00179	00171	00163
61-70	00165	00151	00156	00165						

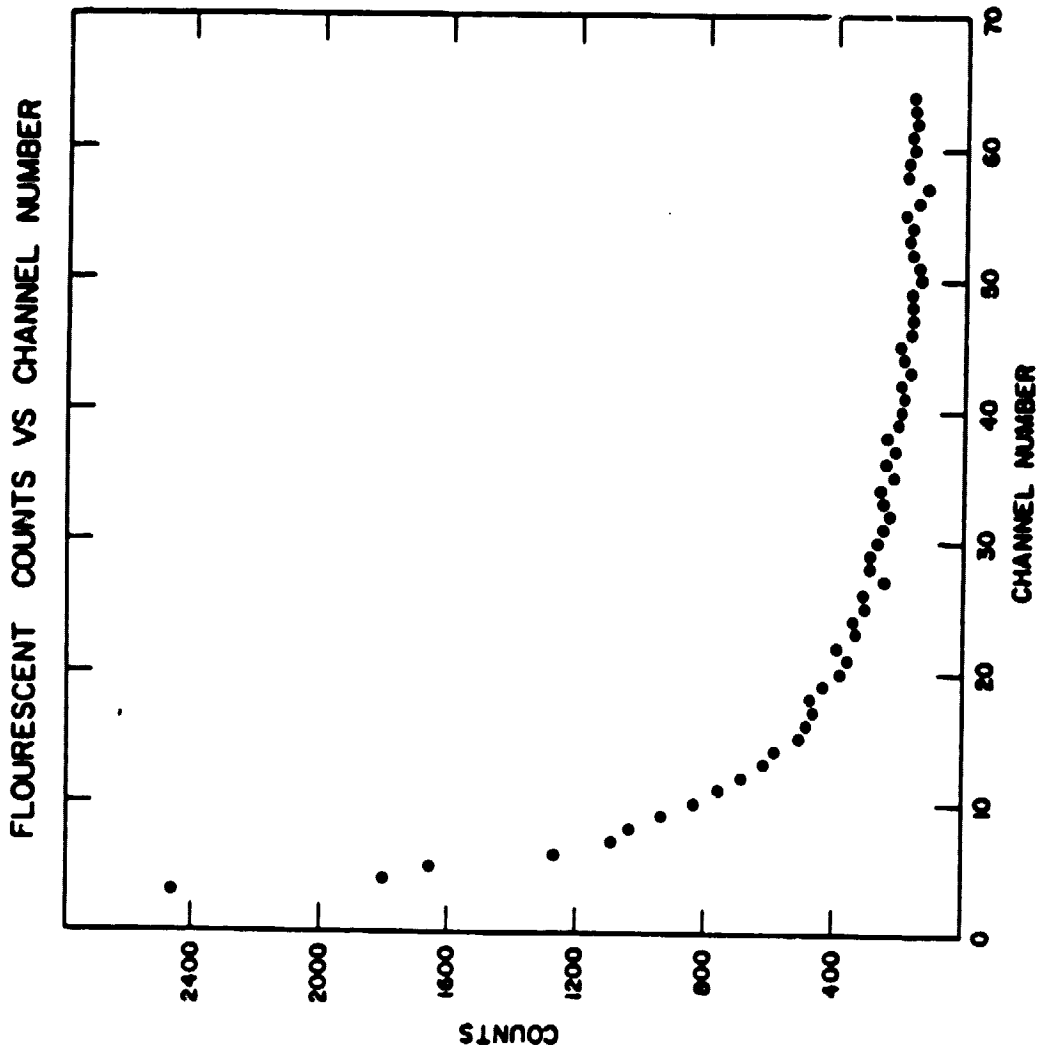

Figure 7

teletype terminal for page copy.

2. Data Representation and Analysis

Continuing with the discussion of the previous section on the use of the NH_2 fluorescence signal, the photon count due only to NH_2 fluorescence is proportional to the NH_2 radical concentration at any time, t. The quantity:

$$d\ln(NH_2 \text{ fluorescence counts})/dt = d\ln(\text{gross counts} - \text{background counts})/dt$$

can be substituted for $d\ln[NH_2]/dt$ in equation (61) to give:

$$(67)\quad \frac{d\ln(\text{gross counts} - \text{background counts})}{dt} = k_{bi}[X] + k_d$$

If a plot of ln (gross counts - background counts) = net counts versus time is linear, the slope of that line is the first order decay constant, called here k_{obs} and equation (67) can be rewritten:

$$(68)\quad k_{obs} = k_{bi}[X] + k_d$$

When k_{obs} is measured, at a given total pressure, in the special case where [X] = 0, then $k_{obs} = k_d$. k_{bi} is determined by measuring k_{obs} for some [X] at the same total pressure, temperature, and ammonia concentration as was used to determine k_d. Since k_d is proportional to temperature, total pressure, and ammonia concentration, it will be the same in both cases.

Then, by rearranging equation (68), k_{bi} may be readily derived:

$$(69)\quad k_{bi} = (k_{obs} - k_d)/[X]$$

Experimentally, as shown in Fig. 7, time bases for the MCA were selected so that signal decay was observed to decrease to the background level within about 1/4 to 1/2 of the available channels. An in-house computer program developed by Mr. Edward Rothe provided data analysis: A simple average of the counts in the last ten channels was used to determine the background count, N_B, and this value was subtracted from the total number of counts, N, in each data channel, starting with channel 3. An example of a $\ln(N-N_B)$ vs time graph based on the data in Table 2 is presented in Fig. 8.

3. Reporting Uncertainties

Based on counting statistics, the standard deviation in the photon count, N, is given by $\pm N^{1/2}$.[61] Since standard deviations are cumulative for the difference of two quantities, $\pm(N^{1/2} + N_B^{1/2})$ represents the standard deviation of the counts in any one data channel attributed to fluorescence. Using these formulae and the data from Table 2 as an example, the calculated fluorescence count for the first usable data channel (channel 3) was 2304±62 while that for channel 25, two decay lifetimes later, was 149±30, a rise of from 3% in the standard deviation of the former quantity to 20% in the latter. This effect is apparent in the increased scatter observed in Fig. 8 with increasing time (channel number) and was minimized both by using the tighter, initial portion of the decay and by analyzing

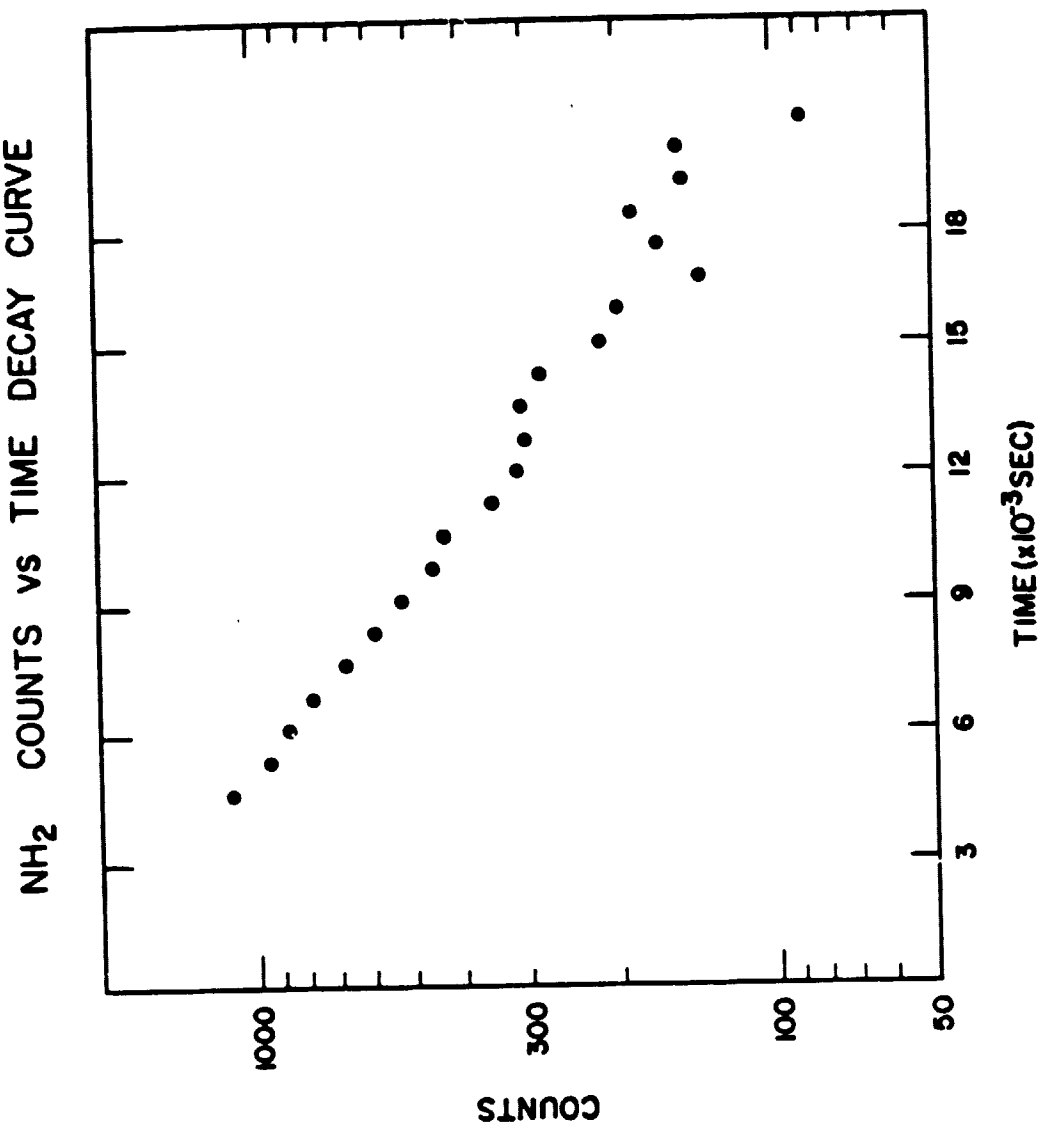

Figure 8

each experiment using several different start and stop channels giving equal weight to each analysis.

The forgoing mathematical treatment of uncertainty was one of the factors which influenced the method selected for data analysis in this study. When k_d is about 10% or less of k_{obs} for a reaction and therefore does not significantly increase the uncertainty, equation (69) is normally used to calculate k_{bi} for each experimental run.[61] If, however, k_d is greater than about 10% of k_{obs}, the increased influence on the uncertainty can be reduced by using a graphical method to calculate k_{bi} for a series of experimental runs. This series of experiments was performed using sets of samples varying only in the concentration of X. Values of k_{obs} were plotted against their corresponding X concentrations. The resulting straight line has k_{bi} as its slope and k_d as its intercept.

As with values of k_{obs} and k_{bi} discussed above, values of the Arrhenius pre-exponential factor and activation energy are reported with one standard deviation, $\pm\sigma$. The standard deviation in each of these quantities can be derived from the uncertainty in the slope and intercept of the line used to generate these results (equations (64) and (68)).

The standard deviation in the slope of a line, σ_{slope}, whose equation is of the form $y = mx + b$, where m is the slope and b is the y intercept is given by:[74]

$$(70)\quad \sigma_{slope} = s^2/\left(\sum_{i=1}^{n} X_i^2 - \left(\sum_{i=1}^{n} X_i\right)^2/N\right)$$

where

$$(71)\quad S^2 = \frac{1}{n-2}\;\frac{\sum_{i=1}^{n} Y_i^2 - \left(\sum_{i=1}^{n} Y_i\right)^2/N - \left(\sum_{i=1}^{n} X_i Y_i - \sum_{i=1}^{n} X_i \sum_{i=1}^{n} Y_i\right)/N}{\sum_{i=1}^{n} X_i^2 - \left(\sum_{i=1}^{n} X_i\right)^2/N}$$

X and Y are the variables, N is the number of measurements and S^2 is the

variance of a single measurement.

The standard deviation of the intercept, σ_{int}, is given by:

$$(72)\ \sigma_{int} = \{s^2 \sum_{i=1}^{n} X_i^2 / (N \sum_{i=1}^{n} X_i^2 - (\sum_{i=1}^{n} X_i)^2)\}^{1/2}$$

4. Other Sources of Error

In addition to the random error inherent in determining k_{obs}, there were subjective errors resulting from the necessity of choosing start and stop channels used in determining k_{obs}. These errors, however, were minimized by averaging the slopes obtained by using several start and stop channels for each k_{obs} reported.

Attention was paid to sources of systematic error such as the measurement of absolute pressure using the MKS Baratron.[61] The manufacturer claims an accuracy to within ~0.08%; therefore, in preparing a mixture composed of three gases, a cumulative error of ~0.32% results.

The stability of premixed samples was tested. No change in the rate constant for the reaction of NH_2 with substrate was observed for samples as much as two weeks old. Usually, however, experiments were conducted with samples that were either freshly made or, at most, one or two days old.

G. The Reaction Cell

A cut-away side view of the reaction cell is presented in Fig. 9. The cell consists of a 348 cm^3 cylindrical chamber placed within another, larger chamber. The reaction cell was made from a machined block of brass. One wall was detachable, being compression sealed to the rest with an

ORIGINAL PAGE IS
OF POOR QUALITY

Figure 9

THE REACTION CELL

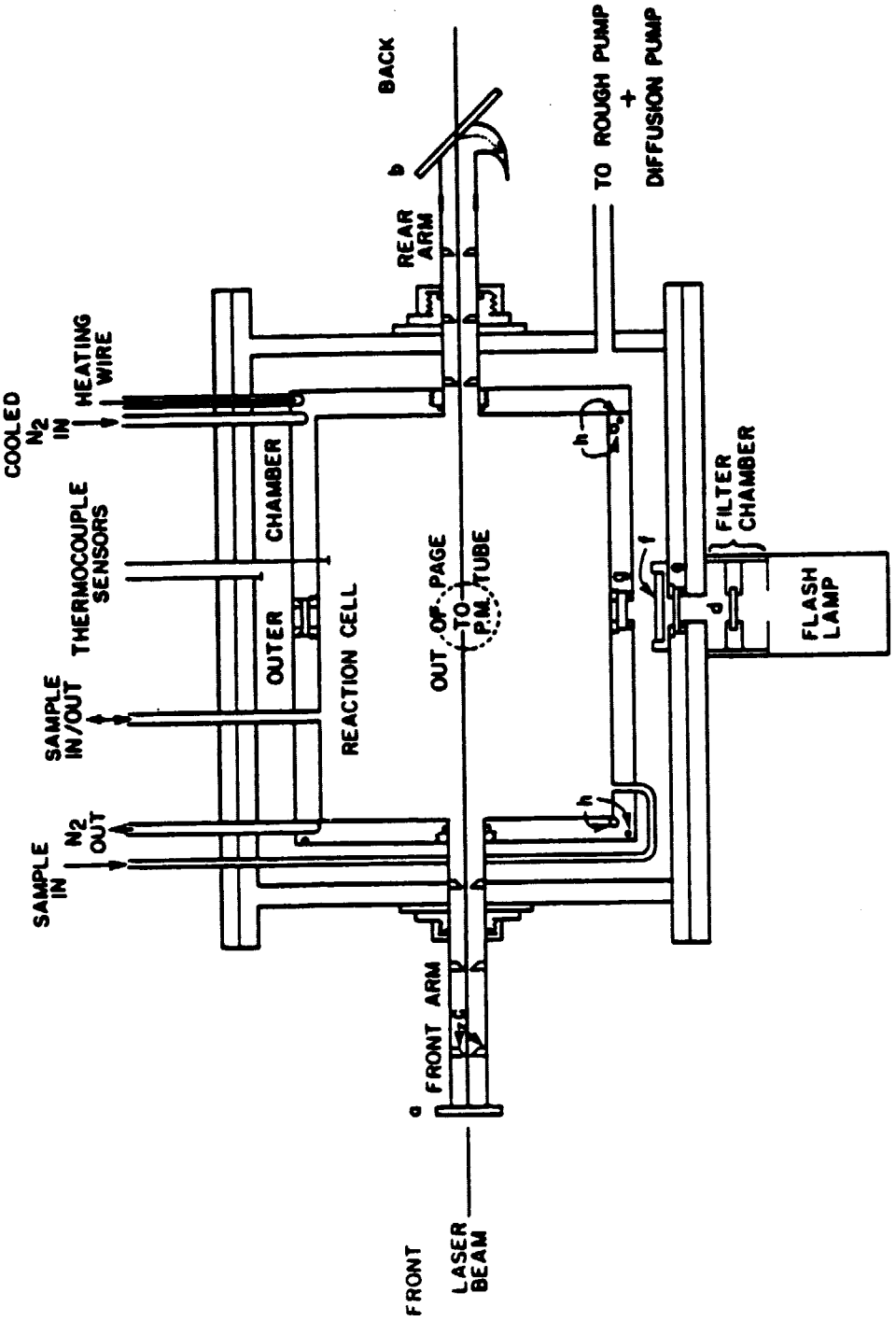

o-ring. The outer chamber was constructed of 1/2 inch thick flat brass plates brazed together.

Four stainless steel tubes comprising two inlet-outlet sets passed through holes cut in the top of the outer chamber and were connected to the reaction cell. These tubes acted as supports to suspend the reaction cell in the outer chamber so as to thermally isolate it from the outer chamber walls. Two of the tubes passed through the reaction cell walls and provided a path by which reaction gas mixtures were introduced into and removed from the reaction cell. The other two tubes connected to one set of continuous and independent channels drilled entirely within the reaction cell walls. To cool the cell for low temperature experiments, dry nitrogen gas was flowed first through a copper coil set in a Dewar of liquid nitrogen and then through the set of channels connected to the other set of inlet-outlet tubes. Temperature control was accomplished by throttling the rate of flow of cooled gas. The cell was heated by resistive heating when current passed through a fiberglass-insulated nichrome wire which ran through a second set of channels drilled in the reaction cell walls. Both sets of channels were configured so as to respectively cool or heat the cell as uniformly as possible. Cell temperature was monitored by two thermocouples using Dorian Thermocouple Indicators. One thermocouple was placed inside the reaction cell in the gas stream to measure reaction mixture temperature. The other was attached to the outside of the reaction cell wall and was used to measure the approximate cell temperature when the reaction cell was evacuated. The thermocouple indicators were calibrated against the known temperature of liquid nitrogen and the boiling and freezing points of water and found to be within $\pm 0.6°K$ between $77°K$ and $373°K$ using similar thermocouples.

Low pressures of about 2×10^{-5} torr were maintained in the outer chamber using a Varian HSA-2a diffusion pump with a cold trap and forepumped by a Welch model 1400 mechanical pump. This helped to stabilize the temperature in the reaction area by insulating the reaction cell from the outer chamber walls. It also prevented absorption of the flash lamp output in the outer chamber. The reaction cell was directly connected to the gas handling system by the set of inlet-outlet sample tubes shown in Fig. 9. Pumping of the reaction cell was provided by the same system which was used for the gas handling system.

Temperatures were limited by the requirement to maintain pressure or vacuum with the o ring compression seals of the optical ports. That range was extended by the use of silicone o-rings to provide a routine operating range of from about 210°K to 480°K.

Holes of 1.04 inch diameter were cut in the front and back of the reaction cell and outer chamber to provide access for stainless steel tubes or arms through which the dye laser beam could be directed into and out of the reaction cell. Quartz windows, a and b in Fig. 9, were sealed to the ends of the arms using black wax. The window on the front arm was perpendicular to the incident laser beam while the rear window was attached at the Brewster angle to deflect back-scattered laser light into a Wood's Horn light trap. The light trap was constructed of a glass to Kovar seal with the Kovar silver soldered to the stainless steel arm via a copper reduction fitting. Both the front and rear arms were each fited with three circular aluminum collimators, c in Fig. 9, painted black and machined so as to minimize light scattered from the leading edge surfaces. Finally, the arms were sealed to the reaction cell and outer chambers with machined brass retaining rings compression sealed with silicone o-rings.

Light from the flash lamp (sect. C above) was collimated when it passed through a filter chamber just beneath the entire cell assembly. A 2 mm thick MgF_2 (or, in some early experiments, LiF) window, d in Fig. 9, in the filter chamber transmitted most of the flash lamp output; it protected the 2mm thick suprasil (LiF in early experiments) window at the bottom of the outer chamber, e, by trapping Teflon™ and electrode fragments broken off from the lamp during flashing. Ready access to the filter chamber made periodic cleaning of the MgF_2 filter possible and precluded having to dissemble the reaction cell to clean the bottom windows.

A port in the side of the reaction cell (perpendicular to the arms and the filter chamber and facing out of the page as viewed in Fig. 9) was covered by a 1.5 inch focal length quartz lens. This lens focused the fluorescence through a 2 mm thick quartz window set in the outer chamber wall and onto the photocathode of the photomultiplier tube. The opposite wall of the reaction cell (into the page in Fig. 9) was covered with a honeycomb-shaped baffle, painted black, which prevented light which might have been scattered off the reaction cell walls from being directed onto the photomultiplier. Finally, the entire inner surface of the reaction cell was coated with blackened Teflon™ to reduce the possibility of both wall reactions as well as light scattering.

After the light from the flash lamp was filtered by passing through a suprasil window set into the bottom of the outer chamber by another brass retaining ring and o ring compression seal, it passed through the 206.0 nm bandpass interference filter (f in Fig. 9) This filtered light passed through a 2 mm thick LiF window, g, set in the bottem of the reaction cell by a brass retaining ring and o ring compression seal.

H. The Gas Handling System

The gas handling system, used in the preparation and storage of all gas samples and mixtures, is depicted in Fig. 10. The system is constructed primarily of glass and stainless steel with a few short pieces of copper tubing near the exhaust pump trap. Metal-to-metal permanent seals were made with soft silver solder, while readily detachable connections were achieved using Cajon Ultra-torr fittings (static o ring compression seals).

Components of the gas handling system can be categorized under the broad headings of storage area, pumping devices and pressure measuring devices. Gas mixtures were stored in five two-liter glass bulbs, S_1 through S_5, a 12-liter bulb, L_1, or in two-22 liter bulbs, L_2 and L_3. L_1 was generally reserved for diffusion mixtures. Purified gases were stored in detachable bulbs or in S_4 or S_5, and S_6 was reserved for use in distillations.

The gas handling system was sequentially pumped by two independent systems. A Welch model 1402 mechanical pump with a 100 liter/min capacity was normally used as a roughing pump to bring the system pressure down to about 0.5 torr. The line to this pump was trapped by a Dewar containing liquid nitrogen to prevent backstreaming of pump oil and material that might be dissolved in the pump oil. In order to achieve high vacuum, a Varian NRC 3340 Group II Air Operated Pumping System was used. The system consisted of a diffusion pump, cold trap, and a gate valve. The gate valve was solenoid controlled and air operated and it served as an automatic device to protect against inadvertent overpressurization of the pump during periods of unattended service. The diffusion pump was rated by the manufacturer at 285 liter/sec capacity. A Welch model 1402 mechanical pump

Fig. 10 Legend

T-Teflon Stopcock

H-Hoke Bellows-sealed Valve

Q- Quartz Window

DP-Diffusion Pump

PG-Penning Gauge

NV-Nupro Metering Valve

RP1, RP2-Welch Model 1402 Pump

V Veeco Bellows-sealed Vacuum Valve

Ø Circle-sealed Valve

B-Baratron

ThG-Thermocouple Gauge

SVO-Servo Metering Valve

LNC-Liquid Nitrogen Supply Controller

W+T-Wallace and Tiernan Pressure Gauge

ORIGINAL PAGE IS
OF POOR QUALITY

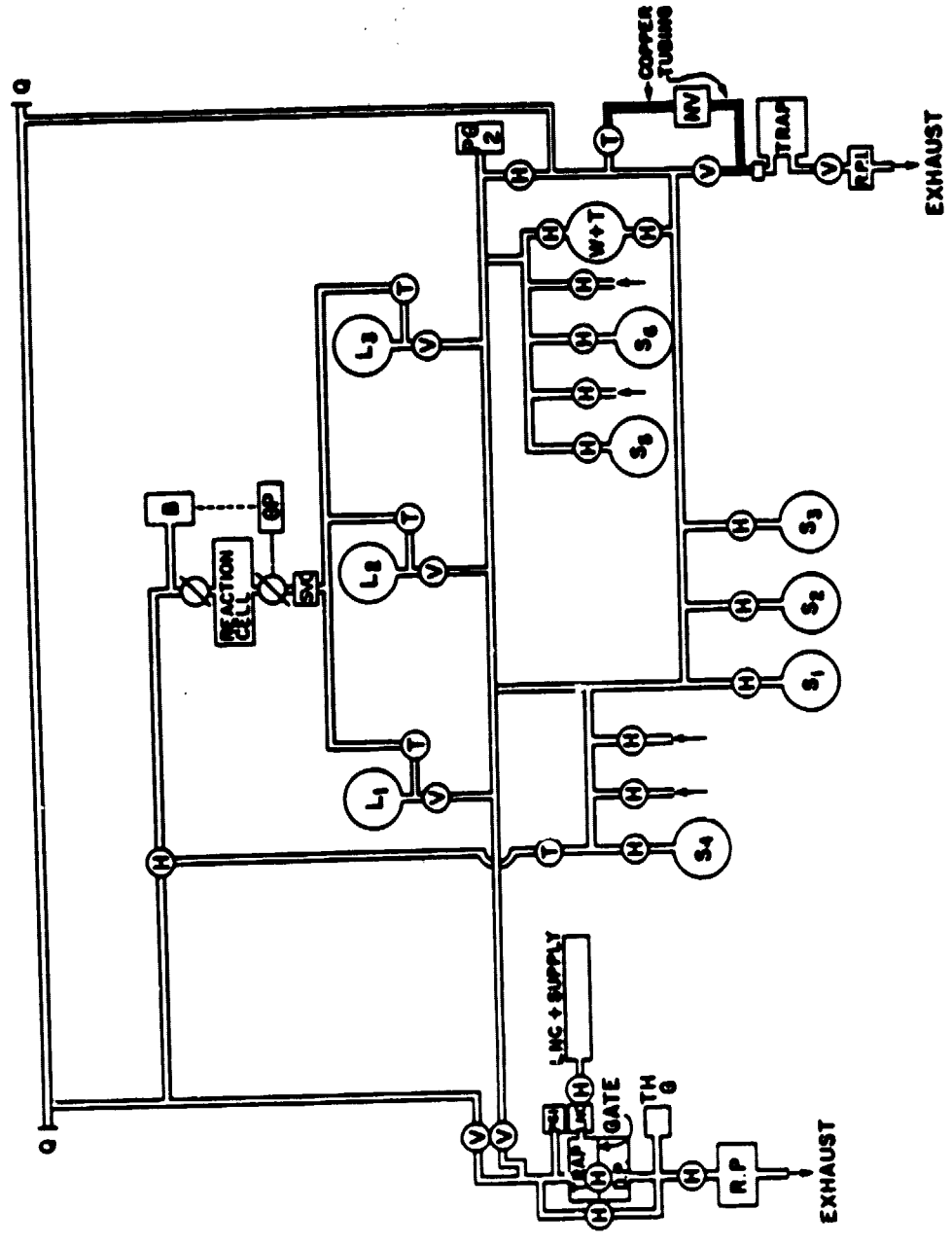

Figure 10

provided foreline pumping for the diffusion pump. The diffusion pump was capable of routinely pumping the entire gas handling system and reaction cell to a vacuum of better than $1x10^{-6}$ torr.

Pressures in the output line of the diffusion pump were read using either a Veeco Thermocouple Gauge and TG-7 Thermocouple Gauge Controller or a Penning GPH-001 Discharge Vacuum Gauge tube and a GPH-320 Penning Gauge Control Unit. The Thermocouple Gauge was sensitive only to about 1 millitorr; the Penning Gauge was used to read pressures as low as $1x10^{-7}$ torr. Both devices were used to monitor the vacuum pumping system.

I. The Preparation and Handling of Gas Mixtures

1. Preparation and Handling of Reagent Gases

All reacting gases were purified upon introduction into the gas handling system by a series of three freeze, pump, and thaw cycles designed to remove any noncondensable material that might have been introduced with the reagent gases. Most reagent gases were further purified by bulb-to-bulb distillation in which the first third of the distillate was discarded, the middle third retained for use and the final third also discarded. Distillation temperatures were chosen using vapor pressure data provided by Stull[75] such that at the distillation temperature used, the reagent gas had a vapor pressure of about 1-3 torr.

Ammonia (Ideal Gas Products Co., 99.999%) was distilled from an isopentane (2-methylbutane) bath maintained at about -105°C with liquid nitrogen. Water, nitrogen and hydrogen, the only significant impurities

originally present in the sample,[76] were not detected in a subsequent mass spectral analysis. In agreement with the observations of Lenzi et al., ammonia was found to be readily adsorbed onto glass surfaces.[42] Care had to be taken, therefore, whenever introducing ammonia into the system to ensure that the ammonia had come to equilibrium with the wall surfaces before taking pressure readings.

Phosphine (Ideal Gas Products, 99.998%) was distilled from an isopentane-liquid nitrogen slush bath at about -150°C. Hydrogen and nitrogen originally present as impurities[77] were not detected by mass spectral analysis subsequent to distillation.

Ethylene (Airco, 99.5%) was not distilled after the three freeze-pump-thaw cycles. Mass spectral analysis showed ethane as the only remaining impurity (<.05%). The ethane could not be removed by distillation because the vapor pressures of ethane and ethylene are nearly identical.[75] The presence of ethane as a contaminant was not considered to be a serious problem because the reaction of NH_2 with ethane had been shown to be much slower ($\sim 3.5 \times 10^{-18}$ cm^3 $molecule^{-1}$ sec^{-1}) than the reaction currently under study.[52]

Acetylene (Matheson, 99.6%) was introduced into the gas handling system through a trap cooled to -100°C using isopentane and liquid nitrogen. The purpose of the trap was to remove most of the acetone in which the acetylene is shipped.[78] The sample was purified as described earlier in this section and distilled from an isopentane-liquid nitrogen slush bath at about -140°C. None of the original contaminants, nitrogen, oxygen, and acetone[78] were detected in a subsequent mass spectral analysis.

2. Gas Mixtures

After purification, gases were mixed to provide samples of varying desired composition. Ammonia was generally introduced into one of the storage bulbs first; the substrate was added next, and finally the mix was brought to the final total pressure by adding Argon (Scientific Gas Co., 99.9999%) which was used without further purification. The Argon added helps to reduce the sharp temperature rise that might have accompanied the absorption of the large flash energies by the reactant in a very short time.[79] Also, the addition of buffer gas reduces diffusion times. All pressures were read on the MKS Baratron to .001 torr.

J. Experimental Procedure

The experimental procedure was essentially the same whether experiments were conducted in the flowing mode or in the static mode. A premixed sample was introduced into the reaction cell, and the dye laser tuned to 568.2 nm (or 570.3 nm). The laser beam was then directed through the cell as shown in Fig. 6. The nitrogen pressure in the flash lamp was set at a suitable flash energy and flash repetition rate and the sample was flashed until at least 1000 counts had accumulated in the first data channel of the MCA.

The flowing mode, in which a sample was flowed through the reaction cell at a rate such that the reacting gases were theoretically replenished in the reaction cell once every 3-5 flashes, was used to probe the occurrence of reactions of NH_2 with products. A change in the rate of reaction measured between the static and flowing modes would indicate the

possibility of an interfering NH_2-product reaction.

Experimentally, gas flow was controlled by throttling through a Nupro metering valve (Fig. 10) which had been calibrated for various total forepressures. The Baratron was offset by the total pressure desired and a Granville-Phillips Automatic Pressure Controller converted the difference between the actual pressure and the offset pressure into a voltage which opened (or shut) the servo metering valve so as to minimize this difference and maintain the preset pressure. Extensive use of the flowing mode was precluded in the ethylene and acetylene experiments because of the large amounts of these gases that would have been required. In phosphine experiments, pressures below about 20 torr could not be accurately controlled using the existing flow apparatus.

In static mode experiments, samples were replaced between experiments except when the experiment took a large number of flashes to accumulate significant signal. In the latter case, then samples were replaced at intervals during the experiment in order to minimize any interference from product buildup. As a substitute for flowing mode experiments, an experiment was periodically conducted in which a sample was flashed a given number of times. A second experiment was conducted under the same conditions except that the mixture was replaced periodically until the approximately same number of flashes had accumulated. If no change in the rate constant was observed between these single fill and multiple fill experiments, no reaction with product was indicated.

In order to probe reaction parameters, conditions such as flash energy, concentration of reactants, total pressure and temperature were varied for each reaction studied. The results of these experiments are provided in the following chapters.

CHAPTER 3

RATES OF REACTIONS OF NH_2 WITH ACETYLENE AND ETHYLENE

A. The Effect of Filters on Flash Lamp Output

1. Effective Flash Energy

Experiments were conducted to determine the impact of the window and filter combinations used in limiting the wavelengths put out by the flash lamp. This information is necessary so that the effective flash energy at which an experiment is conducted can be quoted and to provide an estimate of the initial NH_2 radical concentration in order to evaluate the potential impact of secondary reactions.

Experiments were conducted for each of three window and filter combinations for which the filter specifications are given in chapter 2 and the window characteristics are given by Okabe[80]. The 2 mm thick windows were set in the bottom of the outer chamber in the optical train of the flash lamp and the filters were placed in the outer chamber directly over these windows. A 15 torr total pressure mixture containing 0.600 torr of ammonia in argon was flashed in the static mode at 298°K. The relative flash lamp output was determined by extrapolating a plot of fluorescence counts less background vs time to t=0 and dividing the 'initial count' by the total number of flashes used. This 'initial count per flash', ICPF, was taken to be a measure of the photon flux reaching the cell since, as was shown in Chapter 2, the fluorescent radiation is proportional to the incident radiation absorbed. The ratio of ICPFs from

one set of experiments to the next was used to quantify the relative effectiveness of each filter and window system. Table 3 gives the results of these experiments.

Table 3

Relative Effective Flash Lamp Energy

Window Material	Filter	% Energy Transmitted
LiF	none	100
LiF	175.0 nm	43
Suprasil	206.0 nm	11

Table 4 gives the effective flash energy output corresponding to a given applied charging voltage. Values in the 'LiF only' column are calculated using equation (65) where C=4.5 microfarads.

$$(65)\quad E = 1/2\ CV^2$$

Values in the other two columns are calculated by applying the appropriate

relative effectiveness factors from Table 3. These flash energies are used in the appropriate columns of the data tables to be presented.

Table 4

Effective Flash Energy

Applied Voltage (kilovolts)	LiF only (J)	LiF/175.0 nm filter (J)	Suprasil/206.0 filter (J)
2.5	14.1	6.0	1.5
3.0	20.3	8.7	2.2
4.0	36.0	15.5	4.0
5.0	56.3	24.2	6.2
6.0	81.0	34.8	8.9
7.0	110.3	47.4	12.1
8.0	144.0	61.9	15.8
9.0	182.3	78.4	20.0
10.0	225.0	96.8	24.8

In a second set of experiments, k_{obs} was measured at 298°K for a 15 torr total pressure reaction mixture consisting of 0.600 torr of ammonia and 1.250 torr of ethylene in argon. k_d was measured for a mixture at the same temperature, total pressure and ammonia concentration, but containing no ethylene. A plot of $(k_{obs} - k_d)$ vs effective flash energy for the same set of window and filter combinations as were used in the previous experiments is presented in Fig. 11. Values of $(k_{obs} - k_d)$ are relatively constant with increasing effective flash energy up to about 20 joules. Above this energy, an increase in $(k_{obs} - k_d)$ with increasing flash energy is noted.

This flash energy effect is characteristic of systems in which secondary reactions have become significant and in which the quantity $(k_{obs} - k_d)$ no longer reflects the rate of the elementary reaction under study. Here, in particular, the reaction of NH_2 radicals with ethylene could be affected by increased H atom production from the photolysis of ammonia when using higher energy flashes. H atoms are scavenged by C_2H_4 in reaction (32):

$$(32)\quad H + C_2H_4 \overset{M}{\rightarrow} C_2H_5 \qquad k_{32}^{\infty} = 1.13\times10^{-12}\ cm^3\ molecule^{-1}\ sec^{-1}$$ [81]

and C_2H_5 radicals can react with NH_2 radicals by (34)

$$(34)\quad NH_2 + C_2H_5 \overset{M}{\rightarrow} NH_2C_2H_5 \qquad k_{34} = 4.2\times10^{-11}\ cm^3\ molec^{-1}\ sec^{-1}$$ [82]

Equation (61) would then need to be modified to include this new NH_2 loss factor to give:

ORIGINAL PAGE IS
OF POOR QUALITY

Figure 11

EFFECT OF FLASH ENERGY ON OBSERVED FIRST ORDER RATE CONSTANTS

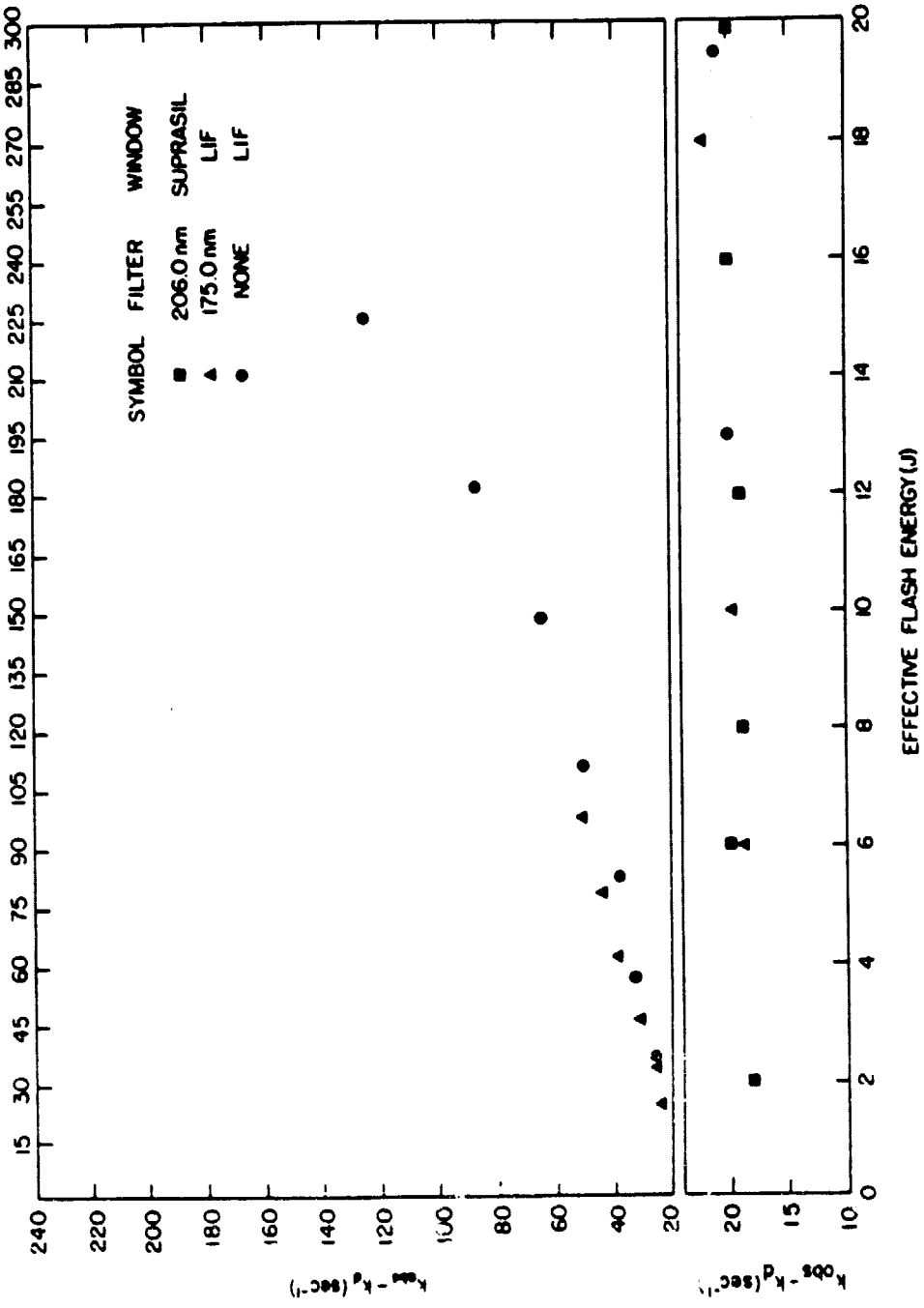

$$(73)\ \text{rate} = \frac{-d\ln[NH_2]}{dt} = k_{27}[X] + k_{34}[Y]$$

where X is the substrate C_2H_4 and Y is the substrate C_2H_5. Clearly, an increase in the production of H atoms will result in an increase in $[C_2H_5]$ and thereby increase the rate of consumption of NH_2 radicals due to reaction (34). Therefore, in order for the rate measurement to reflect only reaction (29), reaction conditions must be tailored so as to minimize the effect of (34) by keeping H atom production as low as possible.

2. NH_2 Radical Production

The effect of secondary reactions such as (34) can be determined if the rate constant for the reaction is known and if the NH_2 radical concentration can be determined. In order to estimate the NH_2 radical production under the present conditions, it would have been necessary to measure the absolute photon flux under each set of optical conditions used. Klemm and Stief[64] had calculated that the photon flux from the flash lamp passing through just a LiF window and incident on a smaller cell was about 10^{12} photons cm^{-2}. Their results were based on a measurement of the C_2H_2 produced by C_2H_4 photolysis in the reaction:

$$(74)\ C_2H_4 + h\nu \rightarrow C_2H_2 + H_2$$

The results of Klemm et al. cannot be directly applied to give an absolute photon flux for each of the window/filter conditions used here

unless the flash lamp output is uniform over the range 105.0 nm to about 210.0 nm and the absorption coefficient and quantum yield of NH_3 are known over the same wavelength range. Qualitatively, however, it can be reasoned that the restricting filter bandwidths and windows pass less radiation than does the LiF window alone and lead to the conclusion that the photon flux is certainly reduced from the Klemm et al. value. In addition, the larger cell volume and the increased distance between the current cell and the flash lamp should further reduce the photon flux. These considerations and the relative flash lamp outputs tabulated in Table 3 lead to placing a crude upper limit of about 10^{11} photons cm^{-2} on the photon flux using the suprasil/206.0 nm window/filter combination. NH_3 photoylsis proceeds with a quantum yield of unity[66] under the optical conditions used in these experiments. If the average ammonia absorption coefficient over the bandpass of the 206.0 nm filter is about 100 atm^{-1} cm^{-1}, the initial NH_2 concentration, $[NH_2]_o$, is conservatively estimated to be $\sim 2 \times 10^{10}$ molecules cm^{-3} for a typical 1 torr ammonia partial pressure.

B. The Rate of Reaction of NH_2 with Ethylene

1. Experimental Considerations

a. Secondary Reactions

In studying the rate of reaction of NH_2 with ethylene, it was necessary to ensure that measurements were conducted under conditions such that potential secondary reactions in which NH_2 was consumed were unimportant.

The following reactions must be considered when a mixture of ammonia and ethylene are flashed under the optical conditions described in chapter 2:

(17) $NH_3 + h\nu \rightarrow NH_2 + H$

(75) NH_2 diffusion

(18) $NH_2 + NH_2 + M \rightarrow N_2H_4 + M$

$k_{18} = 6.9 \times 10^{-30}$ cm^6 molec^{-2} sec^{-1} 50

(23) $NH_2 + H + M \rightarrow NH_3 + M$ $k_{23} = 6.1 \times 10^{-30}$ cm^6 molec^{-2} sec^{-1} 49

(29) $NH_2 + C_2H_4 \rightarrow$ products

(32) $C_2H_4 + H + M \rightarrow C_2H_5 + M$ $k_{32} = 1.1 \times 10^{-12}$ cm^3 molec^{-1} sec^{-1} 81

(34) $NH_2 + C_2H_5 \rightarrow$ products $k_{34} = 4.2 \times 10^{-11}$ cm^3 molec^{-1} sec^{-1} 82

(76) $C_2H_5 + C_2H_5 + M \rightarrow C_4H_{10} + M$

$k_{76} = 2.1 \times 10^{-11}$ cm^3 molec^{-1} sec^{-1} 83

The rate constants, where temperature variant, are for 298°K.

For a typical flash lamp output, the initial NH_2 and H concentrations are estimated to be about 2×10^{10} molecules cm^{-3} (based on the arguments in the previous section). At 298°K and 25 torr total pressure, in a mixture of which one torr was C_2H_4, 0.5 torr was ammonia

and the remainder argon, reaction (32) would be about 10^6 times as fast as reaction (23). It is therefore assumed that most of the hydrogen atoms produced by the photolysis of ammonia will react rapidly with C_2H_4 to produce C_2H_5 and that reaction (23) can be neglected. Based on the rates of (34) and (76), only about half of the C_2H_5 will be consumed by reaction (34). Under these conditions, the pseudo-first order contributions to the consumption of NH_2 by reactions (18) and (34) are calculated to be 0.1 sec^{-1} and about o.4 sec^{-1}, respectively. By using sufficiently large ethylene concentrations, k_{obs} from (29) can be made large compared to the pseudo-first order contribution due to (18). k_{75} measured in this study was found to be ~19 sec^{-1} at 298°K and 25 torr total pressure. Under these conditions reaction (75) will therefore be the only other significant process (exclusive of reaction(29)) by which NH_2 radicals are consumed.

An increase in pressure could cause the contribution to the consumption of NH_2 due to reaction (18) to increase. Care was taken therefore, to avoid high pressures. Total pressures were limited to ~100 torr, however, mainly because higher pressures than these resulted in severe quenching of the fluorescence signal. This limitation coincidentally avoided any significant contribution due to reaction (18). The use of very low pressures did create a minor problem in that diffusion increased, and therefore the theoretical uncertainty in k_{bi} which, based on the statistical treatment in chapter 2 was shown to be $\pm\{(k_{obs})^{1/2} + (k_d)^{1/2}\}$, also increased.

In order to ensure that secondary reactions such as (34) and (18) did not contribute significantly to the pseudo-first order rate constant, the flashing energy was routinely varied by at least a factor of 4 and by as much as an order of magnitude. An increase in k_{obs} with increasing

flash energy could indicate an increase in the production of H and NH_2 (and subsequently lead to an increase in C_2H_5 production due to reaction (32). This situation would result in an increase in the rate of NH_2 consumption due to secondary reactions. Those few experiments in which k_{obs} appeared to show an increase with increasing flash energy beyond experimental error were omitted.

Since radical-radical reactions have little or no activation energy[84], their rates are for the most part temperature independent. The effect of secondary reactions such as (34) should be more significant at lower temperatures where reactions such as (29), which have larger activation energies and therefore greater temperature dependence, are slower.

Experimental conditions limited the range of variation of ethylene concentration. For example, the very slow rate of reaction (29) precluded conducting experiments below 250 °K because of the large concentrations of ethylene that would have been required to give a satisfactorily high pseudo-first order rate constant. Attempts to use partial pressures of ethylene greater than ~8 torr resulted in a substantial loss of signal, presumably due to quenching of the NH_2 fluorescence.

b. Analysis for Reaction with Products

In order to investigate possible reactions of NH_2 radicals with any of the products of the initial reaction of NH_2 with ethylene, two types of experiments were conducted. In one, the rate of reaction in the flowing mode was compared to that in the static mode. Diffusion mixtures and reaction mixtures were flowed through the reaction cell at a volume

rate of flow which could have replaced the reaction mix every 3 or 4 flashes had a plug flow been established. Since, however, the sample inlet and outlet tubes were so narrow (1/8 inch inner diameter) and the cell volume so large (~300 cm^3), it is most likely that only a turbulent flow was established and the cell contents were not completely swept out and replaced with the regularity cited.

Flow experiments were conducted at 15 torr total pressure and at 298°K. The (first order) diffusion from flowing runs was 25±2 sec^{-1}. This compared with static runs under the same conditions which also gave 25±2 sec^{-1}. Reaction mixtures containing 2.813 torr of ethylene run in the flowing mode gave k_{obs} = 61 sec^{-1} and static runs under the same conditions gave 65±3 sec^{-1}. The bimolecular rate constant calculated by direct application of equation (77):

$$(77) \quad k_{obs} = k_{bi}[C_2H_4] + k_d$$

gave 3.95×10^{-16} cm^3 $molecule^{-1}$ sec^{-1}, nearly identical to the results obtained using the static mode (3.99×10^{-16} cm^3 $molecule^{-1}$ sec^{-1}).

In a second set of experiments conducted at 298°K, 15 torr total pressure and 12.1 J flash lamp output energy, a comparison was made of the reaction rate constants for varying numbers of flashes per filling. k_{obs} values for three such experiments were: k_{obs} = 28 sec-1 (125 flashes in 1 fill), 28 sec-1 (125 flashes in 5 fills), and 27 sec-1 (140 flashes in 2 fills). These experiments indicate there is no detectable reaction with products.

In order to ensure that no fluorescence due to any species other than laser excited NH_2 radicals was detected, experiments were conducted

in which a mixture of ethylene and argon was flashed with the laser passing through the mixture. No photon count above background was detected. In addition, a reaction mix containing ethylene, ammonia and argon was flashed with the laser blocked and, again, there was no photon count detected above background. This second experiment ensured that no fluorescence was detected due to any species created by the flash lamp.

2. Ethylene Results

All of the experiments were carried out under pseudo-first order conditions where $[C_2H_4] > [NH_2]$. The initial ethylene concentration was never less than $\sim 1.5 \times 10^{16}$ molecules cm^{-3}; the initial NH_2 concentration was calculated to be about 2×10^{10} molecules cm^{-3}. The decay of NH_2 radicals may then be represented by:

$$(78) \quad \frac{-d\ln[NH_2]}{dt} = k_{obs}$$

Integrating (78) from t=0 to some other time, t, gives:

$$(79) \quad \ln [NH_2] = -k_{obs}\, t + \ln [NH_2]_o$$

wnere $[NH_2]_o$ is the initial NH_2 radical concentration and $[NH_2]$ is the NH_2 radical concentration at time, t.

Fluorescence counts have been shown to be proportional to the NH_2 radical concentration. Net counts (gross counts less background, wnere background is the average of photon counts in the last ten channels) in a typical experiment are plotted against time in Fig. 12 for each

Legend for Fig. 12

Temperature (°K)	P_{total} (torr)	$[C_2H_4]$ (mtorr)	Flash Energy (J)	$[NH_3]$ (mtorr)
250	25	2235	8.9	1118
298	15	1250	15.8	600
373	25	2054	6.2	749
465	35	719	12.1	841

note: the graph of data at 298°K is displaced downward by an order of magnitude for clarity of presentation.

C-2

Figure 12

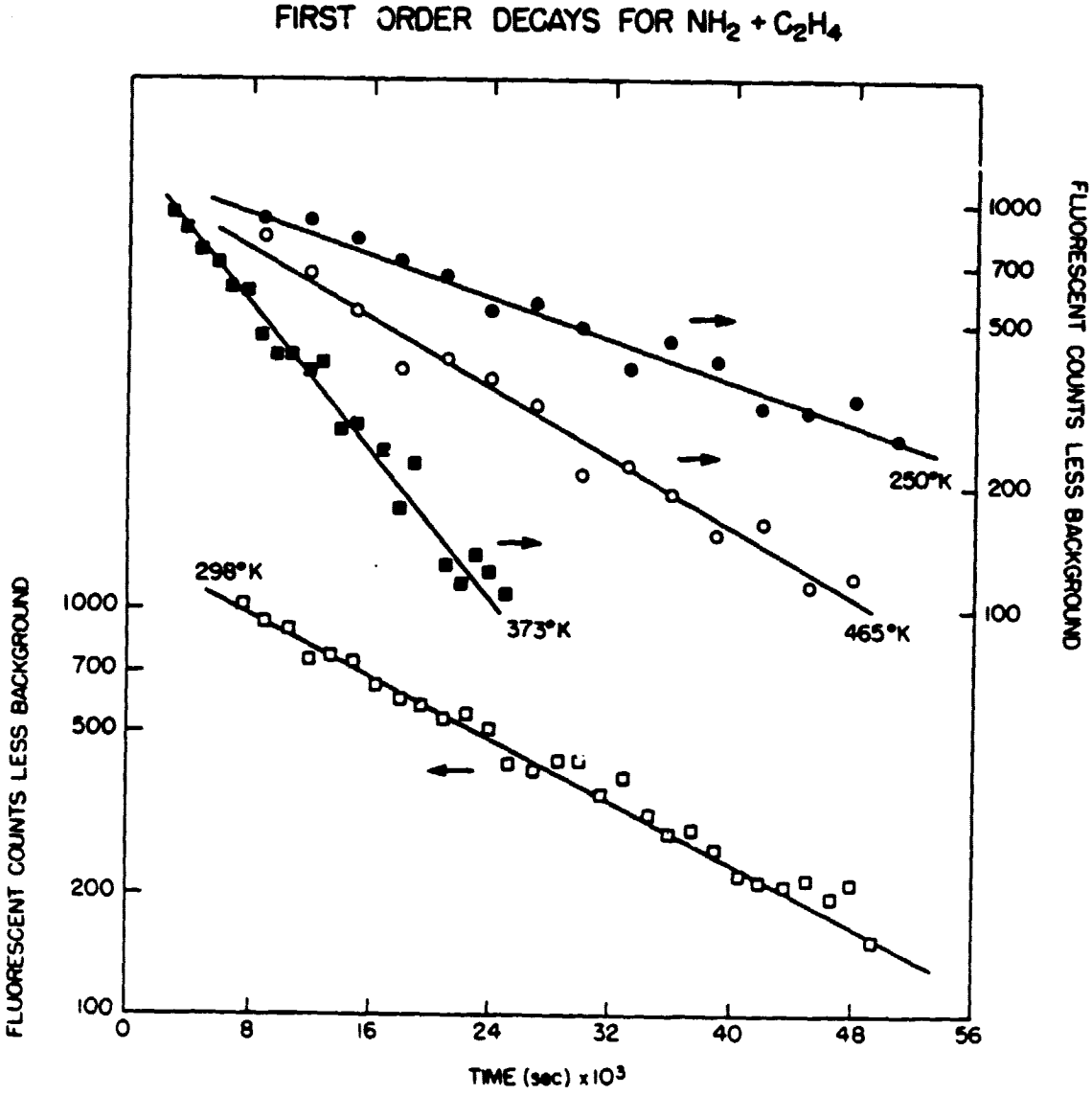

temperature studied. The linearity of these plots indicates that the decays represent a first order process. Since scatter and some possible curvature was noted in later portions of the decays (not shown), only the linear, initial portions of the decays were used.

Values of k_{obs} were calculated from the slopes of plots of ln (net counts) vs time, such as shown in Fig. 12. Analysis was conducted by an on-line linear least squares computer program using the RDA miniprocessor described earlier. A complete data table containing values of k_{obs} for corresponding conditions of temperature, total pressure, ammonia and ethylene concentrations, and flash energy is presented in Appendix I. Values of k_{obs} reported for each experiment are the average values for the analysis conducted under several different start and stop channels.

The observed pseudo-first order decay constant is represented by equation (77):

$$(77)\quad k_{obs} = k_{bi}[C_2H_4] + k_d$$

A plot of k_{obs} vs $[C_2H_4]$ yields a straight line with slope equal to k_{bi} and an intercept of k_d since reaction (29) is the only elementary reaction contributing to the consumption of NH_2 radicals. Fig. 13 shows a typical plot of k_{obs} vs $[C_2H_4]$. Experiments in which data points have identical k_{obs} values for a given ethylene concentration are represented by a circle circumscribed around the plotted point. Table 5 is a summary of k_{bi} values obtained for each of the experiments listed in Appendix I (a set consisted of a group of experiments performed at a fixed temperature, total pressure and ammonia concentration and varying only in ethylene concentration and flash energy). Uncertainties quoted are at the one standard deviation

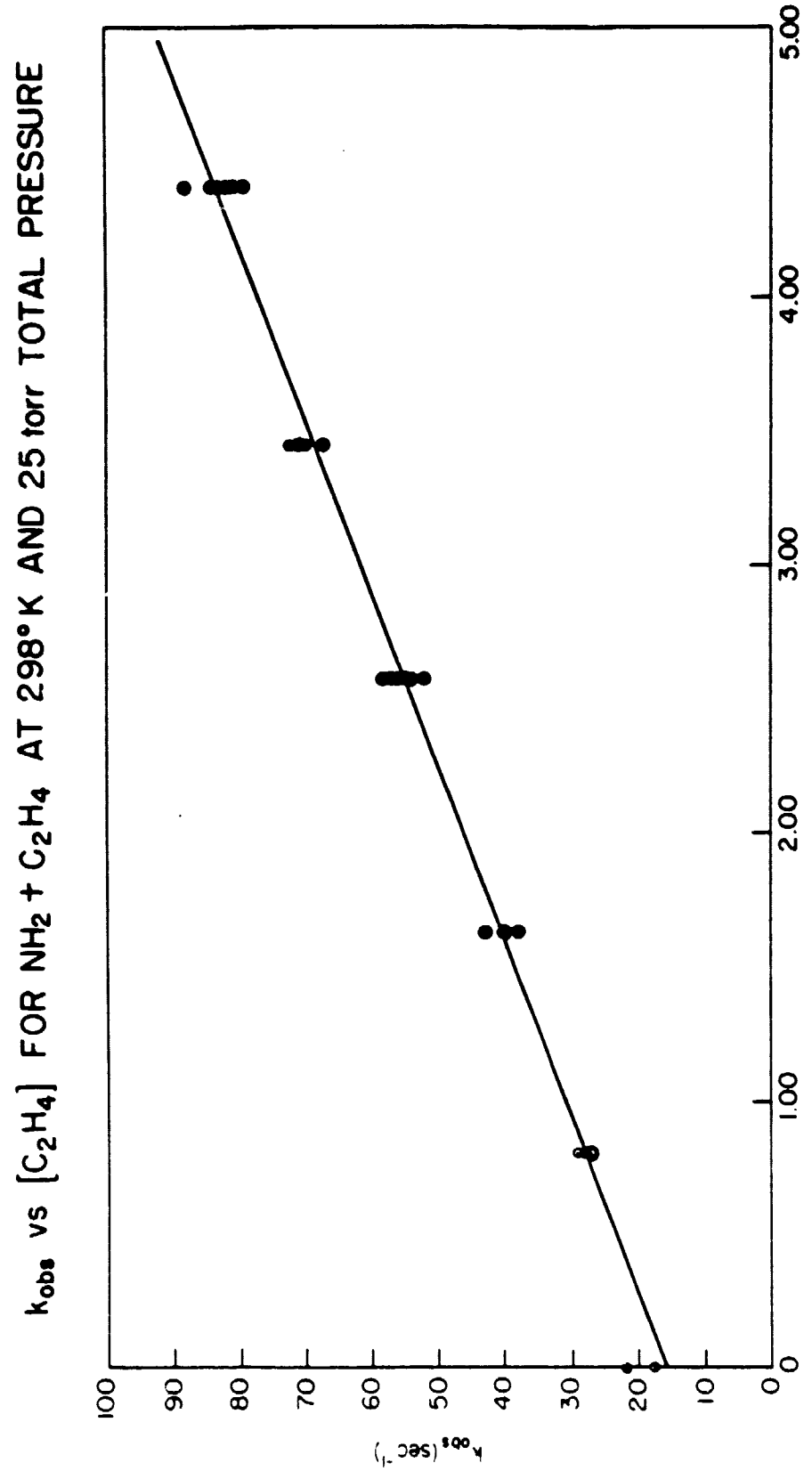

Figure 13

Table 5

Summary of k_{bi} Results for NH_2 + Ethylene

Temperature (°K)	P_{total} (torr)	$[NH_3]$ (mtorr)	# of Experiments	k_{bi} ($\times 10^{16}$) (cm^3 $molecule^{-1}$ sec^{-1})
250	10	475	21	1.91±0.16
	25	1192	28	1.49±0.10
		1118	32	1.54±0.16
	50	2235	21	2.08±0.09
298	10	400	23	4.85±0.35
	15	600	25	4.78±0.16
			41	4.42±0.15
	25	1000	24	4.30±0.15
			20	2.58±0.09
		1463	26	3.35±0.14
		938	37	4.58±0.08
	35	1400	23	4.29±0.15
	50	1000	29	3.01±0.24
	100	666	16	3.50±0.27

373	5	500	12	10.17±0.30
	10	500	18	11.93±1.40
	25	1249	23	9.78±0.38
		799	16	8.64±0.26
		749	30	11.95±2.66
	35	1118	11	9.34±0.54
465	25	651	13	16.4±0.7
	25	603	19	24.8±1.0
		1001	28	19.1±4.1
	35	841	26	18.3±0.5
460	5	327	14	11.6±0.4

level and are based on the treatment presented in chapter 2. The 5 torr total pressure experiments performed at 460°K are treated separately and will be discussed later.

The average value of k_{bi} for each temperature studied is presented in Table 6. (The high temperature set does not include the 5 torr experiments.)

Table 6

Arrhenius Plot Data for NH_2 + Ethylene

Temperature (°K)	# of Experiments	k_{bi} ($\times 10^{16}$) (cm^3 $molecule^{-1}$ sec^{-1})
250	102	1.76±0.29
298	268	3.99±0.77
373	110	10.3±1.4
465	86	19.7±3.6

Values of ln k_{bi} at each temperature are plotted against 1000/T in the Arrhenius plot of Fig. 14. The calculated intercept is -31.0104±0.0725 cm^3 $molecule^{-1}$ sec^{-1} and the slope is 1318±23 $degrees^{-1}$. The temperature dependent rate constant for reaction (29) is therefore:

$$k_{29} = (3.41\pm0.12)\times10^{-14}\ e^{-(1318\pm23)/T}\ cm^3\ molecule^{-1}\ sec^{-1}$$

Since the slope represents $-E_a/R$, the activation energy for this reaction is E_a = 2.619±0.046 kcal/mole.

No change in the rate constant was noted for a change in the total pressure except at the very highest temperature, and then, only at the lowest pressure examined, 5 torr.

3. Discussion

In an ab initio calculation of the energetics of the addition of NH_2 to C_2H_4, Shih et al.[85] predicted that the addition process is exothermic by 17±2 kcal/mole (In chapter 1, the abstraction channel was shown to be exothermic by 5.1 kcal/mole.) They also predict an activation energy of ~35-40 kcal/mole for the addition channel to account for the relative unreactivity of NH_2 towards addition to olefins. This value stands in contrast to the lower activation energy value of 2.6 kcal/mole presented here. The small pre-exponential factor determined from the experimental results of this study appears to account for the slow rate of this reaction.

The results presented here are in good agreement with those predicted by Benson.[86] Benson states that addition of a radical to a

Figure 14

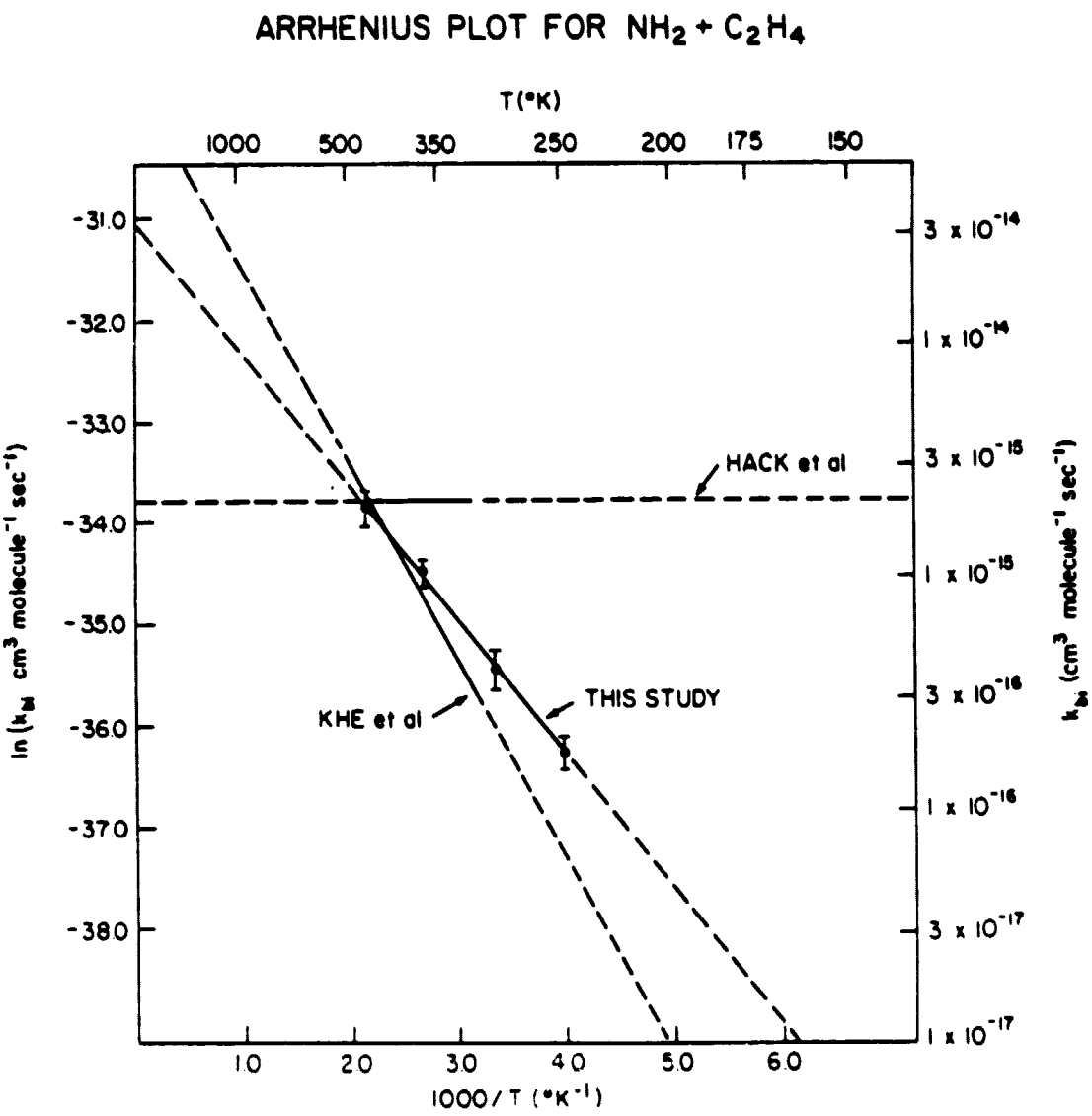

stable unsaturated species generally requires a small activation energy when the reaction is exothermic. Benson hypothesizes that the activation energy results from the crossover of an electronic state of the reactants with a different state of the products. Both NH_2 and C_2H_4 need to rehybridize their molecular orbitals in forming the adduct and Benson points out that such a change should occur at relatively close range, implying the same type of tight transition state as is found in abstraction reactions.

The small pre-exponential factor found in this study (3.4×10^{-14}) is even lower than that found by Khe et al. (4×10^{-13}) and is far smaller than that which would be predicted by Benson.[87] The value found here is consistent with a low steric factor which might be expected for the reaction of NH_2 and ethylene.

The experiments of Hack et al.[46] (also shown in Fig. 14) stand in contrast to those in this study and to those of Khe et al.[51] (also shown in Fig. 14). Hack et al. predict the formation of an adduct based solely on an assumption that NH_2 reacts with unsaturated olefins in analogy to the reactions of the isoelectronic OH with C_2H_2. Hack et al. find that the rate of reaction (29) is temperature invariant indicating that they are measuring the rate of a process that has no activation energy, such as a radical-radical reaction. In addition, adduct formation should be evidenced by a pressure dependence in the bimolecular reaction rate constant (as shown in equation 16). The experiments of Hack et al., however, were performed over too small a pressure range (0.4 torr to 1.0 torr) to show any pressure effect; however, their results should have been lower than those found here at higher pressures if the high pressure limit is greater than 1 torr. This is suggested by the data presented here, but

only at 465°K. Finally, it should be noted that, as has been mentioned previously, it is impossible to eliminate the potential interference due to wall reactions in a flow system.

Hack et al. prepared NH_2 in a glass flow tube by the reaction:

$$(78)\ NH_3 + F \rightarrow NH_2 + HF$$

where F atoms were generated by the microwave discharge of F_2. The same microwave discharge used to produce F atoms could also have produced O atoms if all of the O_2 present as an impurity in F_2 was not removed prior to use. In addition, the heterogeneous reaction of F atoms with the SiO_2 of the flow tube walls or with possible water adsorbed on the walls could also lead to the production of O atoms. Then the occurrence of the homogeneous reaction:[88]

$$(79)\ NH_2 + O \rightarrow NH + OH \qquad k_{79} = 3.5\times10^{-12}\ cm^3\ molec^{-1}\ sec^{-1}$$

$$\rightarrow HNO + H$$

must be considered here as a possible candidate to explain the difference between the Hack et al. results and those reported here. This problem was avoided in the present study by the method of generation of NH_2.

As shown in Fig. 14, the results of Khe et al.[51] agree closely with those found in this study. The increased sensitivity of the laser fluorescence method over that of laser absorption used by Khe et al. should indicate a higher level of confidence in the results presented here, especially at the lower pressures under which the bulk of this study

was conducted.

The possibility of a pressure dependence in reaction (29) as reported by Khe et al. was investigated.[51] At 5 torr total pressure and 460°K, the bimolecular rate constant dropped from $(1.97\pm0.26)\times10^{-15}$ to $(1.16\pm0.04)\times10^{-15}$ or, about 60% in good agreement with the approximately 50% drop reported by Khe et al. If an adduct was formed by the reaction channel:

$$(29)\ NH_2 + C_2H_4 + M \rightarrow NH_2C_2H_4 + M$$

an increase in pressure of the third body gas, M, would help to stabilize the adduct by removal of excess energy through collisional transfer. The reaction would be bimolecular at the high pressure limit and exhibit a termolecular rate constant behavior as the total pressure approaches zero according to the discussion in chapter 2. The bimolecular rate constant measured here represents the high pressure limit for reaction (29).

C. The Rate of Reaction of NH_2 with Acetylene

1. Experimental Considerations

Sketchy information makes a complete evaluation of the importance ndary reactions of the $NH_2 + C_2H_2$ system difficult. Reactions (17), 3), and (23) which were already evaluated with regards to their NH_2 + ethylene may be dismissed as relatively unimportant or rtance can be reduced here based on the same arguments. In

(80) $C_2H_2 + H \rightarrow C_2H_3$

$k_{80}^{\infty} = (4.26 \pm 0.20) \times 10^{-13}$ cm^3 molecule^{-1} sec^{-1} [89]

and (81) $NH_2 + C_2H_3 \rightarrow$ products

need to be considered here.

Since, from similar arguments as presented earlier, reaction (80) is ~10^5 times as fast as reaction (23) at around 25 torr total pressure, (80) is assumed to be the major consumptive process for H atoms and there should be a one-to-one correspondance between [H] produced and [C_2H_3].

The rate of reaction (81) has not been measured. The bond additivity method of Benson[90] was used to calculate heats of reaction from heats of formation. Based on values of ΔH_f° provided in Benson[91] the addition channel for reaction (81) is found to be endothermic. The abstraction channel for (81) is about as exothermic as is the corresponding reaction of NH_2 with C_2H_5 (ΔH_f° ~ -72 kcal/mole vs ΔH_f° ~ -71 kcal/mole, respectively). Therefore, reaction (81) is determined to be about as fast as reaction (34).

All other factors, such as $[NH_2]_o$, being approximately equal, reactions (18) and (81) could provide the only significant contribution to k_{obs} from secondary reactions. As was pointed out in section B above, however, contributions due to secondary reactions may be indicated by an increase in rate constant with increase in flash energy. Flash energy was continuously varied by a factor of at least 4 and by as much as 10 for all reaction sets and no significant change in the rate constant was noted. Additionally, any significant contribution due to reaction (18) should be evident by an increase in k_{bi} with increasing pressure and the

rate of (18) should be temperature independent. While there is a small increase in k_{bi} with increase in pressure noted at higher temperatures, no similar increase is noted at lower temperatures and therefore, there is no evidence of any contribution to k_{obs} due to reaction (18).

Values of k_d measured agree to within about 10% with the intercepts calculated from graphs such as in Fig. 16 except at the highest pressures measured and then, only for the highest temperature runs. This disagreement is also noted for the high pressure, high temperature runs conducted in the NH_2 + ethylene experiments. A possible small contribution to k_{obs} by a pressure dependent reaction may be hinted at here.

As with the ethylene experiments, an investigation of the reaction of NH_2 radicals with reaction products was conducted using both the flowing mode and the method of multiple reaction cell fills described previously. No indication of any significant change in rate constant was noted when using these diagnostic tools and, therefore no reaction with products is suspected.

A reaction mixture of acetylene and ammonia in argon was flashed with the laser blocked to determine if photons from any species other than laser excited NH_2 were being collected by the photomultiplier. In another experiment, a mixture of only acetylene in argon was flashed with the laser tuned to 568.2 nm to determine if fluorescence from either excited acetylene or from a possible acetylene photofragment was being collected by the photomultiplier. In neither experiment was any photon count above normal background detected.

2. Results

As with the ethylene experiments, all of the experiments in this section were carried out under pseudo-first order conditions where $[C_2H_2]_o \gg [NH_2]_o$. The acetylene initial concentration was always greater than or equal to 0.799 torr (2.6×10^{16} molecule cm^{-3}), a factor of about 10^5 larger than $[NH_2]_o$.

Figure 15 shows typical pseudo-first order decays for NH_2 in the presence of acetylene. The linearity of these plots demonstrates that the graph is representative of a first order process. Appendix II contains a complete compilation of values of k_{obs} calculated from the slopes of plots such as in Fig. 15 for each variation of temperature, total pressure, ammonia and acetylene concentration and flash energy at which measurements were made. The value of k_{obs} for a given entry is the average value for analysis of that experiment under several different start and stop channel conditions.

A modified version of equation (68):

$$(82)\quad k_{obs} = k_{bi}[C_2H_2] + k_d$$

can be used to obtain the bimolecular rate constant for reaction (28).

$$(28)\quad NH_2 + C_2H_2 \rightarrow \text{products}$$

Legend for Fig. 15

Temperature (°K)	P_{total} (torr)	$[C_2H_2]$ (mtorr)	Flash Energy (J)	$[NH_3]$ (mtorr)
298	10	1045	15.8	500
373	25	1349	8.9	1237
455	10	819	15.8	393

note: 455°K line is displaced downward by one order of magnitude

Figure 15

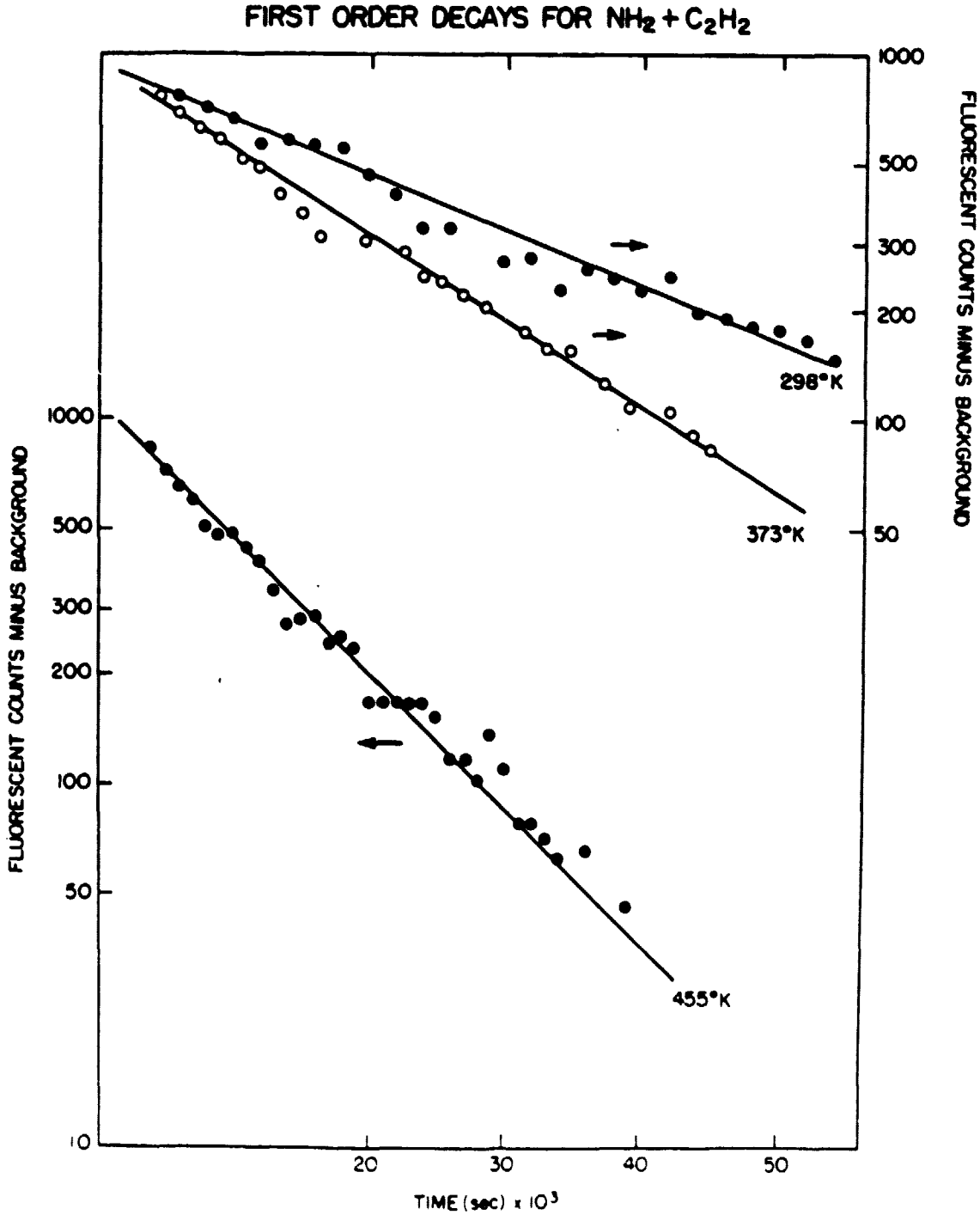

A plot of measured values of k_{obs} vs $[C_2H_2]$ yields a straight line whose slope is k_{bi} and whose intercept is k_d. A typical plot for a set of k_{obs} vs $[C_2H_2]$ data at 465°K, 25 torr total pressure, and 1.000 torr of ammonia is presented in Fig. 16. Table 7 summarizes k_{bi} values obtained from a similar graphical analysis for each set of experiments listed in Appendix II.

Unlike the ethylene results, the reaction of NH_2 with acetylene shows a clearly defined increase in rate with increase in pressure at both 373°K and 459°K. In Fig. 17, k_{bi} for reaction (28) is plotted against total pressure for each temperature studied. 459°K is the average temperature for the highest temperature experiment sets from Appendix II. In using the average temperature only about 1% error is introduced. The lower two temperatures show no pressure effect; at 373°K, there is a significant (50%) increase in k_{bi} from 5 to 100 torr and on the 459°K curve, a 100% increase in k_{bi} is noted for the same pressure range.

In Table 8, average values for k_{bi} are presented at 241°K and at 298°K. Values for k_{bi} at 373°K and 459°K represent only the high pressure experiments where it appears that k_{bi} is approaching a limiting value. At neither of the high temperatures was it experimentally possible to conduct higher total pressure experiments because of quenching which caused a loss of NH_2 fluorescence signal. The data in Table 8 are graphed in Fig. 18 in an Arrhenius plot. This plot was initially thought to be slightly curved, but a straight line can be drawn through the data points within the uncertainties. While it cannot be proven that the reaction rate constant has reached the high pressure limit, it appears from the graph to be approaching it. The data from Table 8 were used to derive an expression for the rate constant of reaction (28) near the high pressure limit:

Table 7

Summary of k_{bi} Results for NH_2 + Acetylene

Temperature (°K)	P_{total} (torr)	$[NH_3]$ (mtorr)	# of Experiments	k_{bi} ($\times 10^{16}$) (cm^3 $molecule^{-1}$ sec^{-1})
241	25	1005	17	0.559±0.071
298	10	500	19	2.00±0.13
	25	1000	16	2.18±0.09
		957	20	1.68±0.11
		1000	5*	2.24±0.22
		600	5*	2.02±0.36
	50	800	13	1.64±0.11
373	5	320	14	4.67±0.20
	10	479	17	4.99±0.26
	25	1237	21	5.31±0.28
	50	799	8	7.17±0.36
	100	795	11	7.06±0.20
460	5	260	13	12.5±0.8
455	10	393	29	10.3±0.5
463	25	1004	18	16.3±0.4
448		1000	11	14.8±0.5
463	50	805	13	20.6±0.6
454	100	819	12	21.0±0.9

*Flowing mode experiments

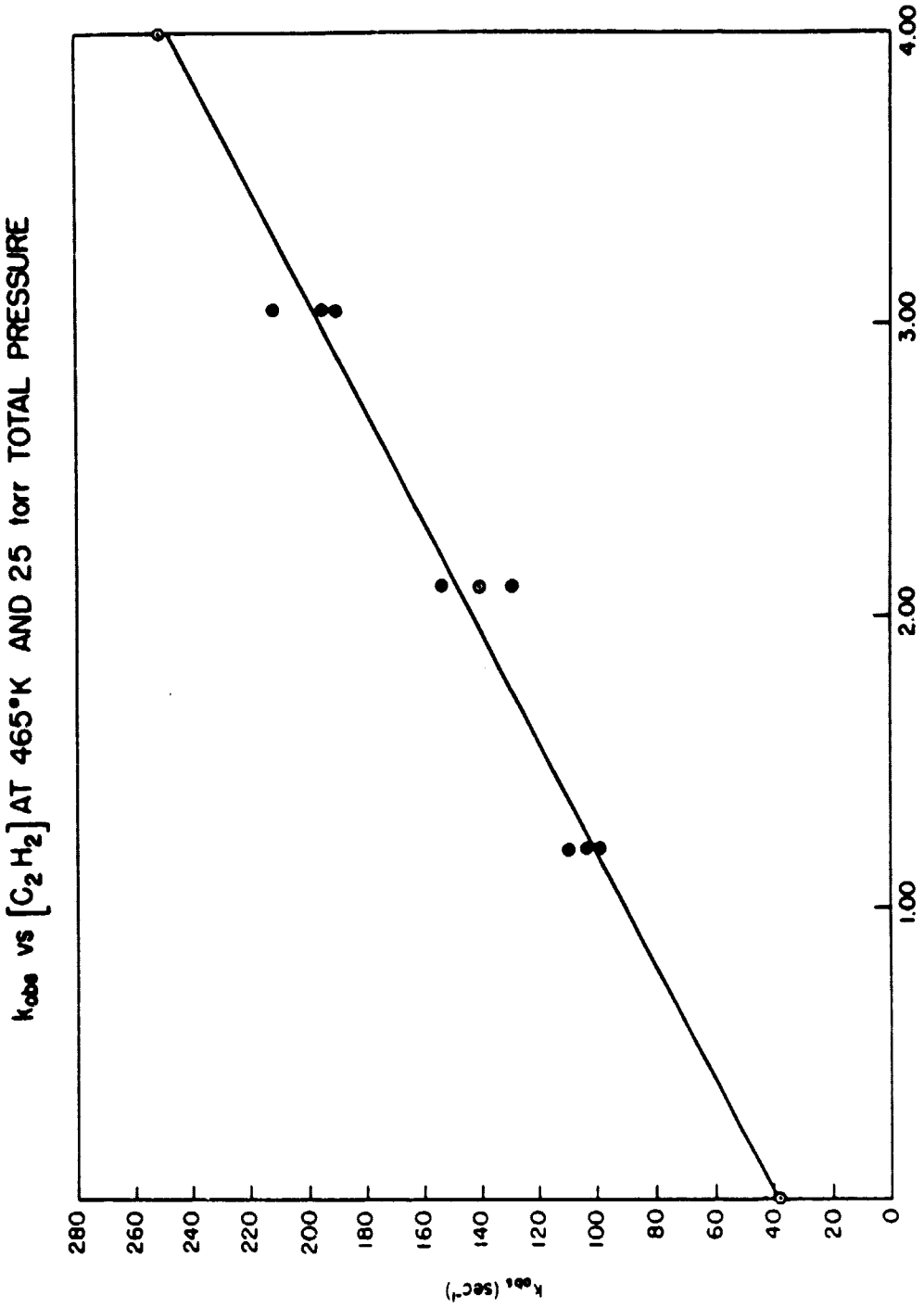

Figure 16

Figure 17

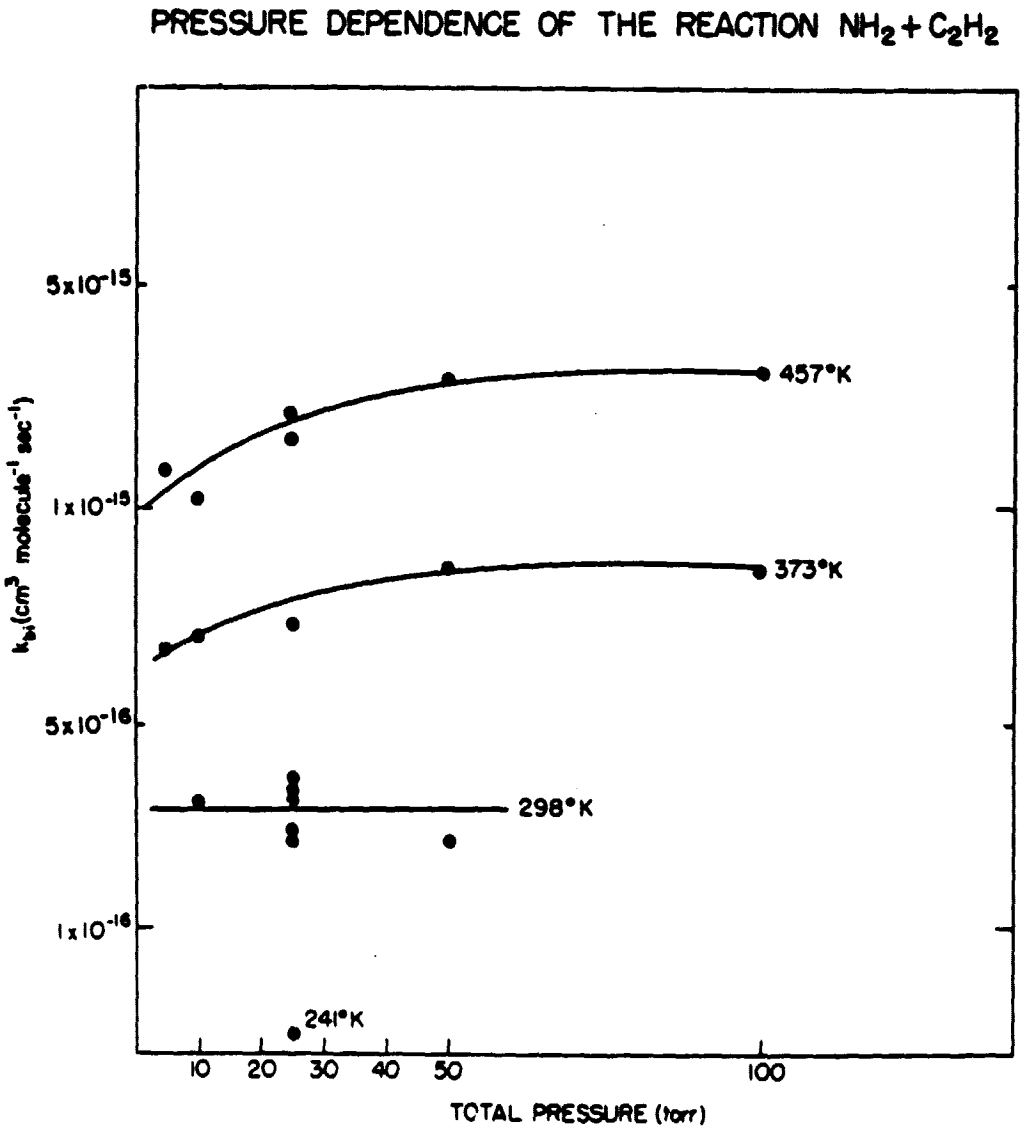

Table 8

Arrhenius Plot Data for NH_2 + Acetylene at the High Pressure Limit

Temperature (°K)	# of Experiments	k_{bi} (cm^3 $molecule^{-1}$ sec^{-1})	Pressure Range (torr)
241	17	$(5.59\pm0.71)\times10^{-17}$	25 only
298	78	$(1.96\pm0.25)\times10^{-16}$	10-50
373	19	$(7.12\pm0.06)\times10^{-16}$	50-100
459	12	$(2.08\pm0.02)\times10^{-15}$	50-100

Figure 18

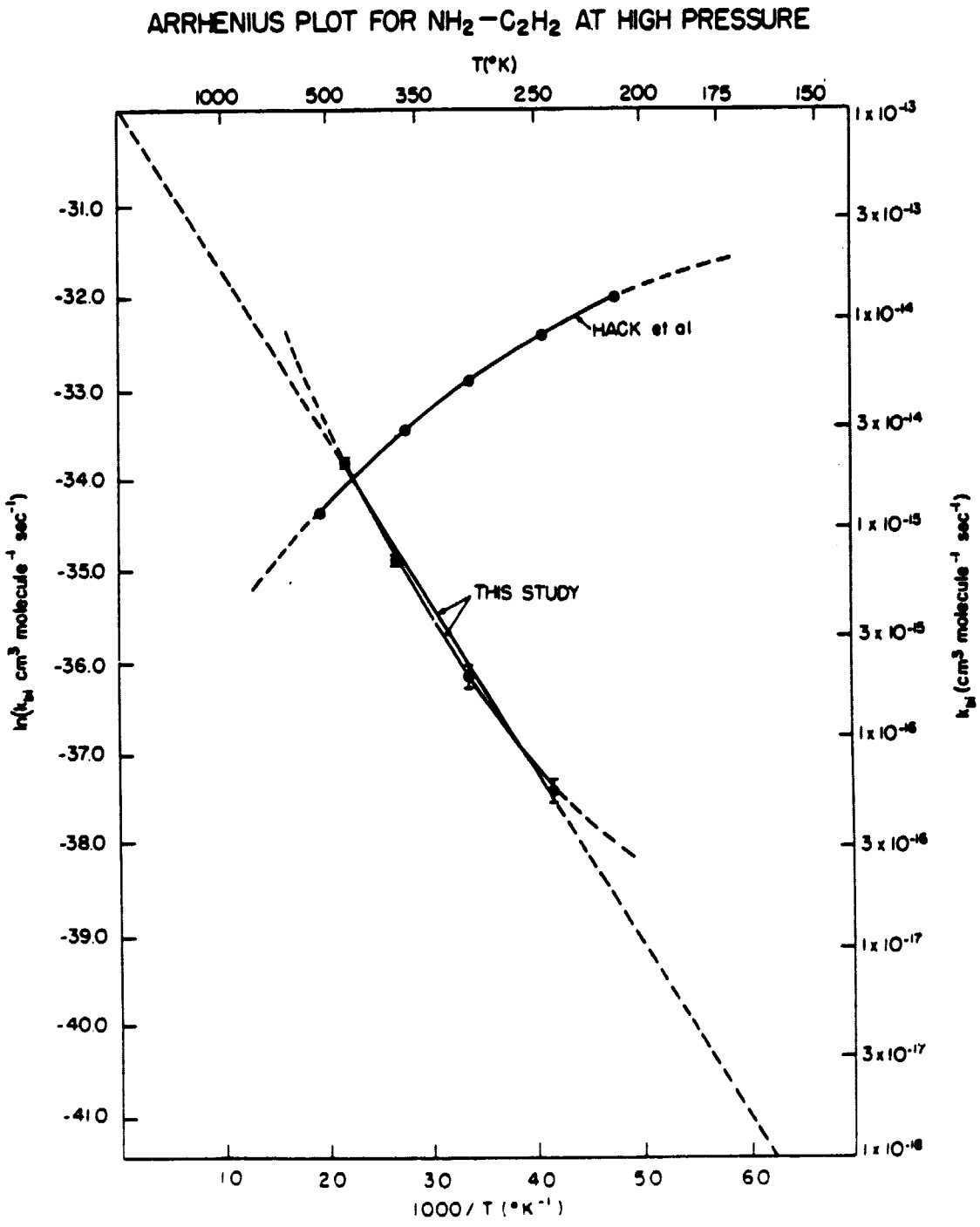

$$k_{28}^{=} = (1.11\pm0.36)\times10^{-13}\ e^{-(1852\pm100)/T}$$

3. Discussion

The only other study of the rate of reaction (28) was performed by Hack et al.[46] using the same discharge-flow system as was described previously with regards to their experiments with NH_2 and ethylene. The Hack et al data are displayed in Fig. 18. Hack et al. used the same method to generate NH_2 in their acetylene study as they did for their ethylene study. The same possible homogeneous reaction (79), that of NH_2 with O, that could have caused the difference between their results and those cited earlier in this study with regards to ethylene could also be causing the difference between their acetylene results and the acetylene results in this study. Because the method of NH_2 production used in this study is not subject to the chemical and physical complications as the Hack et al. study, the results presented herein should be regarded with a much higher level of confidence.

The experimental conditions of very low pressure (0.35 torr to 1.2 torr) used in the Hack et al. study could not be duplicated using the flash photolysis apparatus. At these pressures, k_{obs} due to diffusion should increase dramatically (at 5 torr in this study, diffusion was 106±3 sec^{-1}) while k_{obs} due to reaction (28) would drop because of insufficient acetylene (0.75 torr of acetylene would give k_{obs} of only ~4 sec^{-1} at 298°K). Measurements made under these conditions using the flash photolysis apparatus would generate an unacceptably high uncertainty and render any results so obtained meaningless.

The pressure dependence of $NH_2 + C_2H_2$ parallels the behavior of H

and OH towards reaction with C_2H_2 [89,92]. The pressure dependence in both the H and OH reactions is more pronounced indicating that it is easier to stabilize the adduct and the rates of these reactions are much higher primarily due to the larger pre-exponential factor. Thermochemical calculations based on partial bond contributions from Benson[93] indicate that adduct formation should be exothermic and a possible parallel between the mechanism suggested by Michael et al.[92] for OH and C_2H_2 and the isoelectronic NH_2 with C_2H_2 could lead to the formation of CH_2CNH, an imine. No evidence to support this suggestion is available from this study.

In comparing the rates of reactions of NH_2 with ethylene and with acetylene, it was anticipated that ethylene would reach its high pressure limit faster than acetylene because the ethylene adduct has a higher number of vibrational modes available for redistributing excess energy. The ethylene reaction was faster and it reached its high pressure limit at a lower pressure. In the ethylene reaction, however, the metathetical channel may dominate the kinetics and adduct formation may not be important until higher temperatures are reached.

The unequivocal pressure dependence in the rate of the acetylene reaction leads to the conclusion that at least there is an adduct forming channel for this reaction. If the metathetical channel is also significant, then, at the low pressure limit, k_o will have some finite value. This seems to be indicated by Fig. 17. Unfortunately, lower pressure experiments were not possible with the technique used in this study.

CHAPTER 4

THE RATE OF REACTION OF NH_2 WITH PHOSPHINE

A. Experimental Considerations

This study presents the first reported measurement of the rate of reaction of NH_2 with PH_3 by either direct or indirect methods. In studying the rate of this reaction, several experimental considerations were made including testing for possible secondary reactions, possible reactions of NH_2 with products, and reducing light scattering due to particulate formation.

Secondary processes which may be important in this system in addition to (27),

(27) $NH_2 + PH_3 \rightarrow NH_3 + PH_2$

are: (75) $NH_2 \xrightarrow{\text{diffusion}}$

(23) $NH_2 + NH_2 + M \rightarrow N_2H_4 + M$

$k_{23} = 6.1\times10^{-30}$ cm^6 molecule^{-1} sec^{-1} [50]

(83) $H + PH_3 \rightarrow H_2 + PH_2$

k_{83} (298°K) = $(3.76\pm0.32)\times10^{-12}$ cm^3 molecule^{-1} sec^{-1} [94]

(84) $NH_2 + PH_3 + M \rightarrow NH_2PH_3 + M$

$\Delta H^{\circ}_{f(298)} = 54$ kcal mole^{-1} [95]

(85) $NH_2 + PH_3 + M = NH_2PH_2 + H + M$

$\Delta H^{\circ}_{f(298)} = -23$ kcal mole-1 [95]

Reaction (27) is much faster than the corresponding reactions of NH_2 with ethylene or acetylene and other NH_2 loss processes such as (75) or (23) become relatively much less significant and do not interfere. In addition, if low total pressures are used, the effects of termolecular loss processes are minimized.

There was no evidence of reaction with products in any of the measurements conducted. Multiple fill experiments gave identical rate constants to those which were derived from single fill experiments. First order rate constants did not change when flash energy was varied by a factor of as much as 5 and therefore, detectable interference by secondary reactions was ruled out.

The effect of flash energy on reaction rate was probed further. Earlier experiments were run using a 175.0 nm filter and a LiF window in the outer chamber over the flash lamp; later experiments were performed using a suprasil window and 206.0 nm bandpass filter over the flash lamp in the outer chamber. According to Table 3, the photon flux incident on the cell was reduced by a factor of about 4 when switching from the 175.0 nm filter to the 206.0 nm filter. Identical rate constants were obtained for both filter/window combinations indicating that even with the increased NH_2 and H production when using the 175.0 nm filter, there was no increase in the rate of consumption of NH_2 radicals. Thus, any effect

due to secondary reaction was dismissed as being negligibly small.

Values of k_d measured (diffusion experiments) agreed with intercepts calculated from k_{obs} vs $[PH_3]$ plots except in a few of the high temperature (373°K and 456°K) experiments, providing additional evidence to support the position that there was no interference from secondary reactions. The few deviations that were noted at high temperatures displayed no pattern. These anomalies could have been due to small changes in the total pressure of a mix during reaction runs due to absorption of ammonia onto glass surfaces; however, this was not deemed likely since pressure changes were always less than 0.1 torr, or only a few percent of the total pressure. Further, this anomalous behavior occurred only at high temperatures where surface adsorption should be least important. No other plausible source for this anomalous behavior has been determined.

The formation of a particulate of unknown composition was a problem that made $NH_2 + PH_3$ experiments difficult and eventually limited the conditions under which experiments were conducted. Particulate formation did not appear to influence the value of the rate constants measured and could be avoided by adjusting reaction conditions. For example, when flashing a reaction mixture at total pressures above 10 torr at room temperature, the background photon count due to scattered laser light was observed to increase such that after 2 or 3 flashes, the background increased by about 3 orders of magnitude over its normal value. With such high a background, no measurement of the NH_2 fluorescence signal was possible. At lower temperatures, this phenomenon occurred at total pressures greater than 5 torr while at higher temperatures, the onset of particulate formation occurred at pressures above 20 torr. It is reasonable that any particulate should form and stabilize at low

temperatures and high pressures where excess thermal energy can be absorbed by third bodies in collision or by the vibrational modes of the molecules in the particulate. In the extreme case, at very high pressures (50–100 torr), reflected scattering of the laser beam could even be visually observed in the side arm of the reaction cell.

In order to avoid interference from scattered light due to particulates, only low total pressure conditions were examined. Low pressures did not adversely affect rate measurements, but did preclude the use of the flowing mode since it was not possible to accurately regulate low pressures using the existing apparatus. The pressure range used was later extended by introducing a Melles Griot polarizing window into the optical train just in front of the photomultiplier. The polarizer reduced reflectively scattered laser light versus fluorescent light by about an order of magnitude.

In order to eliminate any other possible source of particulates, a complete replacement or cleaning of nearly all system glassware and valves was performed; fresh, high purity tanks of reagent gases were introduced. Neither change affected the conditions under which particulate formation occurred or the extent of particulate formation.

It was thought that the particulate might be molecular phosphorus formed by the Norrish mechanism[25], but when a mixture of only phosphine in argon was flashed, no particulate formation was observed. Particulate formation was, however, directly related to phosphine concentration in a mixture.

It was also noted during experiments to elucidate the source of scattering that different gases caused the system to exhibit different degrees of light scattering as evidenced by the background photon count.

Background was noted to increase linearly with gas concentration and the amplitude of background photon count depended on the gas introduced. This phenomenon was observed independently of the particulate scattering problem and was present even when samples were not flashed.

The possibility of fluorescence due to excited PH_3 or photofragments of PH_3 was eliminated. When a PH_3 and argon mixture was flashed with the laser blocked, no fluorescence was detected. Light from the flash lamp plasma was not visible beyond the third channel of the MCA at the shortest time bases used.

B. Results

All of the experiments were carried out under pseudo- first order conditions where $[PH_3] > [NH_2]$. The phosphine initial concentration was at least 6.6×10^{14} molecules cm^{-3} whereas the initial NH_2 concentration was estimated to be about 2×10^{10} molecules cm^{-3}.

Figure 19 shows typical pseudo-first order decays for NH_2 fluorescence counts less background vs channel (converted to time in sec $\times 10^3$ for the time base used). These plots, which are linear over more than 2 reactive decay lifetimes, represent a first order process over this interval. Appendix III contains a complete compilation of values of k_{obs}. These values are calculated from the slopes of net counts vs time plots such as shown in Fig. 19 for varying conditions of temperature, total pressure, ammonia concentration, phosphine concentration, and flash energy at which the measurements were made. The value of k_{obs} for a given entry in Appendix III is the average value for that experiment under several different start and stop channel conditions.

Legend for Fig. 19

Temperature (°K)	Total Pressure (torr)	Flash Energy (J)	$[PH_3]$ (mtorr)	$[NH_3]$ (mtorr)
218	2.5	6.2	27.34	342
246	2.5	8.9	72.40	302
298	2.5	8.9	74.98	252
363	2.5	8.9	40.00	400

Figure 19

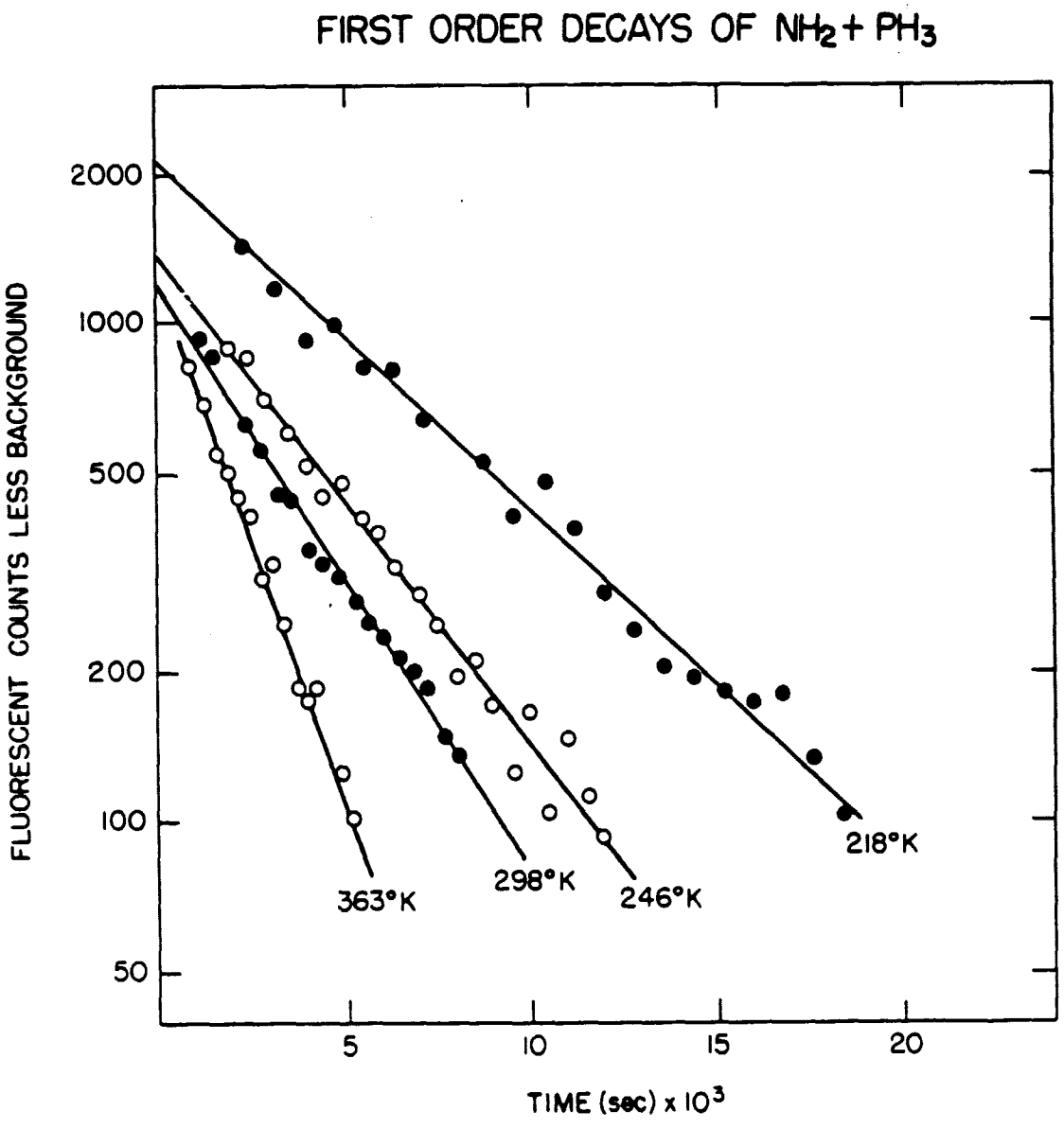

If $X = PH_3$, equation (68) becomes:

$$(86)\quad k_{obs} = k_{bi}[PH_3] + k_d$$

Equation (86) can be used to describe the bimolecular rate for the process:

$$(27)\quad NH_2 + PH_3 \rightarrow NH_3 + PH_2$$

A plot of measured values of k_{obs} vs $[PH_3]$ yields a straight line whose slope is k_{bi} and whose intercept is k_d. A typical plot for a set of k_{obs} vs $[PH_3]$ data at 298°K and 5 torr total pressure with 250 mtorr of NH_3 in each sample is presented in Figure 20. Table 9 summarizes k_{bi} values obtained from a similar graphical analysis for each set of experiments listed in Appendix III.

The average bimolecular rate constants for experiments at each temperature studied are also presented in Table 9. These values are displayed in an Arrhenius plot (Fig. 21), which is linear within the uncertainties cited, indicating a single reaction channel. The large uncertainty at low temperatures indicates that some curvature in the plot cannot unequivocally be dismissed. If such curvature did exist, it could be construed as providing some evidence for a possible second reaction channel.

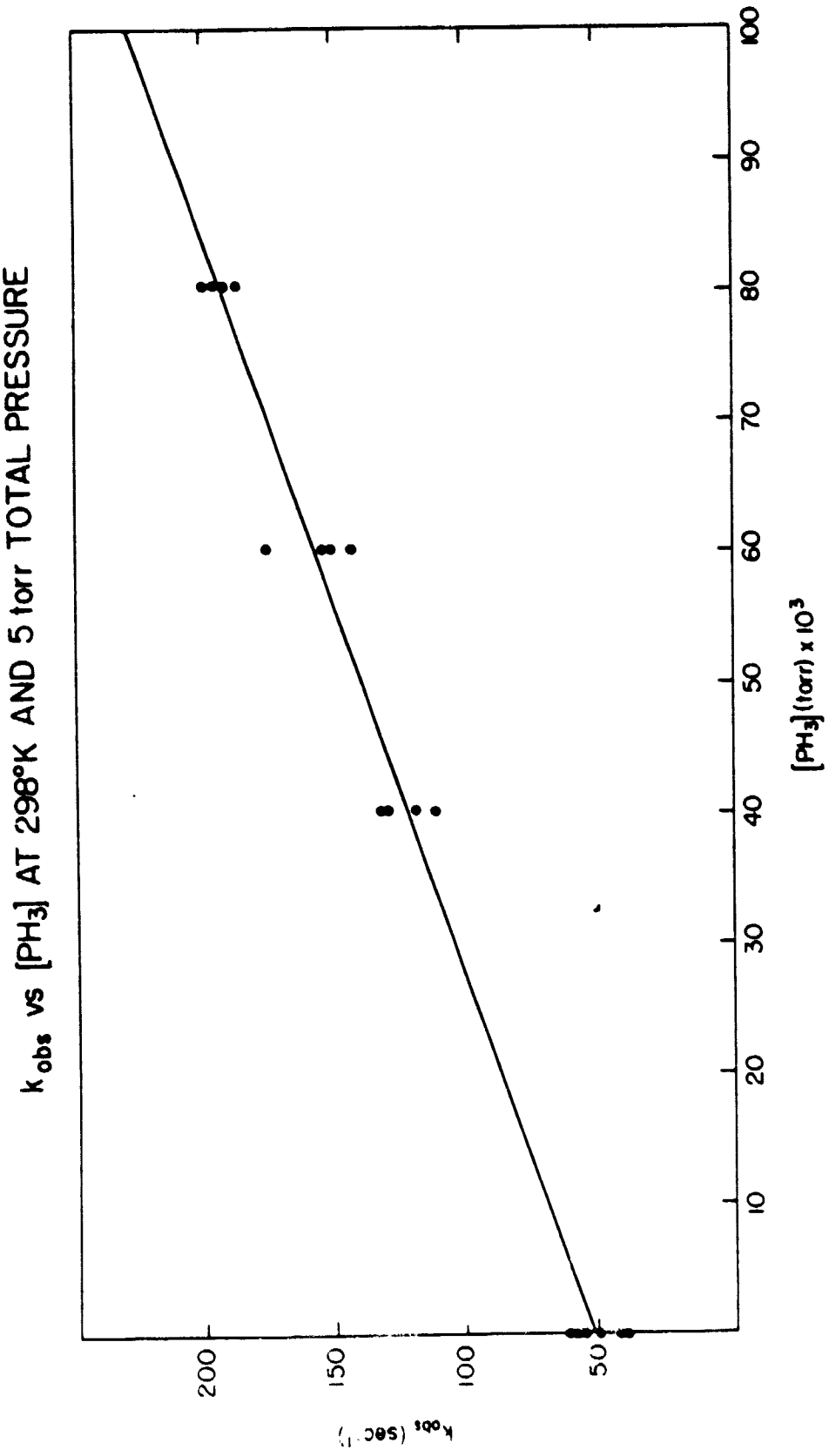

Figure 20

Table 9

k_{bi} Summary for $NH_2 + PH_3$

Temperature (°K)	P_{total} (torr)	$[NH_3]$ (mtorr)	# of Experiments	k_{bi} ($\times 10^{14}$) (cm^3 $molec^{-1}$ sec^{-1})
218	2.5	342	8	2.56±0.59
			12	2.71±0.72
	5.0	342	8	1.96±0.45
	average k_{bi} at 218°K		28	2.41±0.40
247	2.5	302	9	3.78±0.52
			16	2.39±0.12
			18	3.09±0.22
			19	3.78±0.31
	5.0	302	16	2.66±0.19
			17	3.93±0.13
	average k_{bi} at 247°K		95	3.27±0.65
298	2.5	250	20	7.12±0.30

	4.0	200	20	5.46±0.19
		280	6	5.95±0.41
	5.0	244	20	6.55±0.40
	7.5	366	16	6.39±0.22
		750	20	5.54±0.16
	10.0	208	7	5.78±0.12
	average k_{bi} at 298°K		107	6.11±0.60
363	2.5	144	13	15.0±1.1
		205	23	10.4±0.7
	5.0	205	21	12.2±0.9
		287	10	12.5±1.3
	average k_{bi} at 363°K		67	12.5±1.9
456	5.0	204	11	22.6±1.0
	10.0	400	12	20.0±0.5
	20.0	408	11	21.5±0.6
	average k_{bi} at 456°K		34	21.4±1.3

The experimentally derived bimolecular rate constant is:

$$k_{27} = (1.52\pm0.16)\times10^{-12}\ e^{-(928\pm56)/T}\ cm^3\ molecule^{-1}\ sec^{-1}$$

over the temperature range 218°K to 456°K. The activation energy for the reaction is 1.84±0.11 kcal $mole^{-1}$.

C. Discussion

The activation energy of 1.84±0.11 kcal/mole found here compares favorably with the prediction of an upper limit of 2-3 kcal/mole for reaction (27) made by Buchanan and Hanrahan[53]. They radiolyzed a mixture of ammonia and phosphine at 296°K and at total pressures of 550 torr. In a mass spectrometric analysis of the reaction products, they identified phosphorus, hydrogen, and nitrogen. While they did not perform any rate constant measurements, they did compare the scavenging of NH_2 by PH_3 with radical scavenging reactions by HBr and HI and predicted that phosphine should scavenge NH_2 radicals in reaction with PH_3 leading to the formation of PH_2 and NH_3.

The pre-exponential factor of $(1.52\pm0.16)\times10^{-12}$ cm^3 $molecule^{-1}$ sec^{-1} found in this study indicates a substantial steric factor. It is much lower than the frequency factor found for the reaction of H atoms with PH_3, $(4.52\pm0.39)\times10^{-11}$ cm^3 $molecule^{-1}$ sec^{-1} [94] and for OH with PH_3 of $(2.7\pm0.06)\times10^{-11}$ cm^3 $molecule^{-1}$ sec^{-1}.[95] This finding is consistent with the prediction of Laidler.[96] Laidler compares the reactions of atoms and radicals with various organic molecules and concludes that reactions

Figure 21

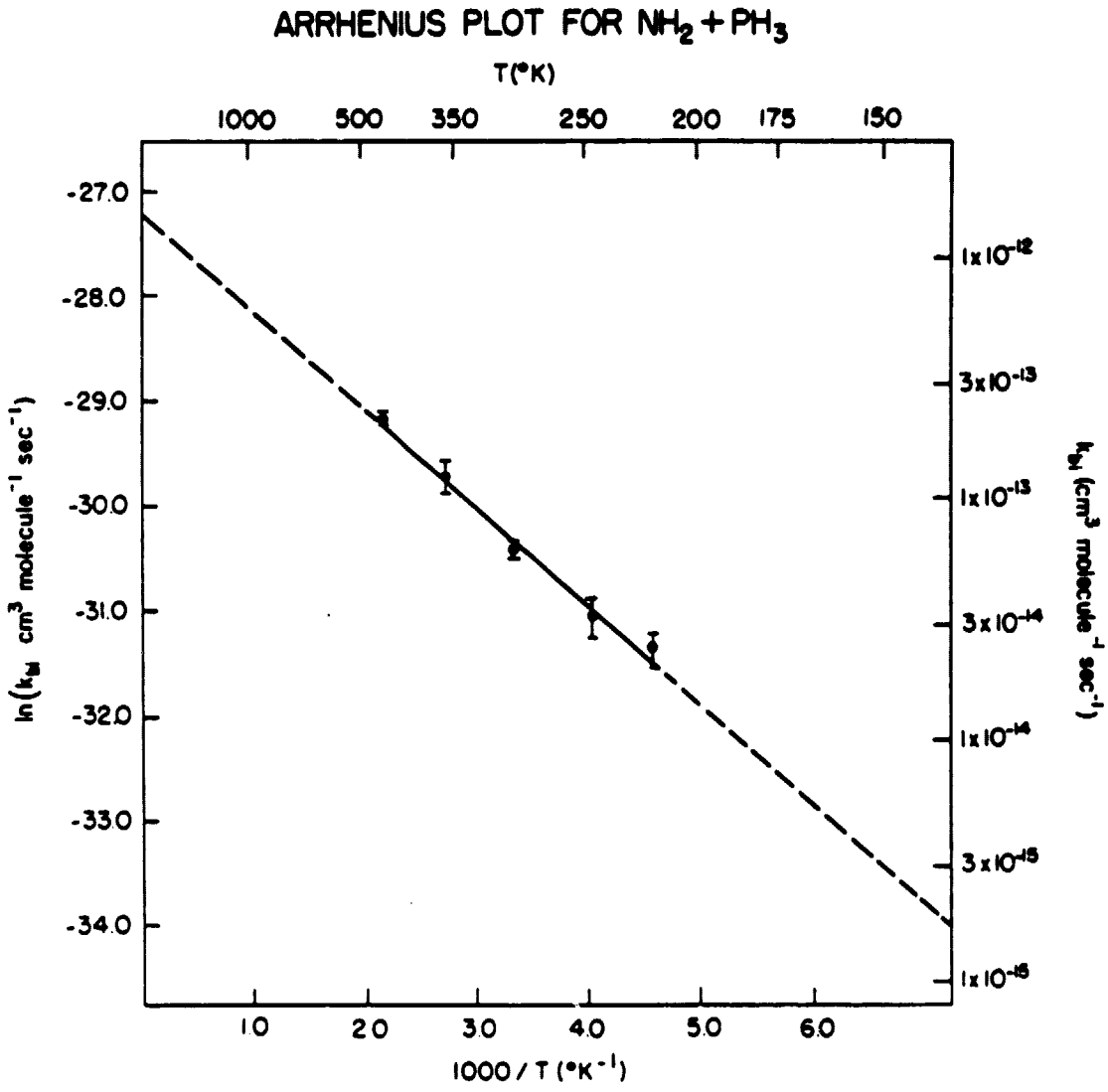

involving more complex reactants will show lower pre-exponential factors. Buchanan et al.[53] predict that reactions such as $NH_2 + PH_3$ should not have substantial steric factors and conclude that the rate constant for reaction (27) should be within one or two orders of magnitude of the rate of bimolecular collisions ($\sim 10^{-10}$ cm^3 molecule^{-1} sec^{-1}). Using this prediction and the activation energy measured in this study would lead to a pre-exponential factor in the range of 10^{-10} to 10^{-12} cm^3 molecule^{-1} sec^{-1}. The results of this study lie at the low end of their prediction. The high value pre-exponential factor prediction might more likely be found for the loose transition state associated with atom-molecule abstraction reactions.

The results presented here do not indicate any pressure dependence of the bimolecular rate constant. This supports the suggestion made here that no NH_2-PH_3 adduct forms. This finding is consistent with energetic considerations. The adduct requires the formation of an N-P bond whose bond energy should be about 54 kcal/mole, intermediate between that of the N-N bond and the P-P bond (59 and 48 kcal/mole respectively)[97]. This large an excess of energy would have to be removed by collision with a third body, M, in order to stabilize adduct formation. Such a process is termolecular and could show a pressure dependent rate constant (unless the high pressure limit is reached by 2.5 torr).

It is entirely feasible from purely energetic arguments that the adduct, NH_2PH_2, could form from $NH_2 + PH_2$. PH_2 may be produced from PH_3 by reaction (83). Then the overall process would be exothermic by an estimated 23 kcal/mole (the P-H bond energy is ~77 kcal/mole[97]). If reaction (83) occurred to a significant degree, then $NH_2 + PH_2 + M$ could contribute to the consumption of NH_2 radicals. Again, however, this

process is termolecular and if significant here should provide a pressure dependent rate constant (unless the reaction is already at the high pressure limit). Reaction (27) should then be the predominant channel for NH_2 consumption because the concentration of PH_2 radicals produced by reaction (83) is much smaller than the PH_3 concentration. Further evidence against adduct formation comes from the study of Buchanan et al.[53], who, even after radiolysis times of up to 40 hours, fail to detect any evidence of adduct formation. Since their study was conducted at 550 torr total pressure and the present study was conducted at total pressures of 20 torr or less, it is highly unlikely that (84) or (85) is of any significance here.

Bond energy-bond order, BEBO, activated complex theory, ACT, calculations were performed (Appendix IV) using two different hypothetical NH_2-PH_3 activated complex orientations. At 298°K, a linear orientation (with N-H-P colinear) gave a theoretical pre-exponential factor of 1.33×10^{-11} cm^3 $molec^{-1}$ sec^{-1}, twice as large as did the orientation with an arbitrarily selected N-H-P bent orientation, 6.68×10^{-12}. The bent orientation model, however, leads to a theoretical pre-exponential factor about a factor of four higher than that found experimentally, 1.52×10^{-12} cm^3 $molec^{-1}$ sec^{-1}. Whereas the theoretical pre-exponential factor had a 1/T factor, which arises from the ratios of the rotational partition function of the adduct and reactants and from the internal rotations, only the experimentally derived activation energy was temperature dependent. It appears that the simple hard sphere picture used in the BEBO/ACT does not accurately portray the geometry of the activated complex. With activated complex theory, molecule-molecule reactions always have a temperature dependent pre-exponential factor and show a curved Arrhenius plot. A

tighter activated complex with much smaller moments of inertia would lead to closer agreement between the A factor measured and that calculated for the NH_2-PH_3 activated complex.

It appears then, that the reaction of NH_2 with PH_3 proceeds by the metathetical channel at the temperatures and pressures studied and that PH_2 should be a product of the reaction. The abstraction reaction of H + PH_3 is faster and should be responsible for a much higher PH_2 production than is reaction (27). Finally, adduct formation is not energetically favored, nor is there any experimental evidence to support a claim for adduct formation.

Chapter 5

CONCLUSION

The purpose of this study as stated in the introduction is to provide planetary modelers with measured rate constants for the reaction of NH_2 with phosphine, ethylene, and acetylene. These rate constants could then be used in models to make predictions of the behavior of the Jovian atmosphere. The measurements made in this study were performed over as wide a temperature and pressure range as was experimentally possible. The resulting Arrhenius plots are linear within experimental error and, therefore, it is reasonable to extrapolate the results of this study to the colder temperatures of the Jovian atmosphere. The very slow rates of the NH_2-hydrocarbon reactions did not permit measurements at as low a temperature as was studied for NH_2 with phosphine; however, the linearity of the data indicates that the already very slow reacton rates would continue to decrease with decreasing temperature.

Experimental conditions precluded performing higher pressure studies on NH_2 with C_2H_2 which would have unequivocally established the high pressure limit of the rate constant. The pressure regime that was studied for the hydrocarbon reactions does, however, overlap the pressure range of interest on Jupiter. Pressures in the phosphine experiments were limited to about 20 torr due to possible particulate formation. There was no experimental evidence for any pressure effect and it appears that reaction (27) is entirely a metathetical reaction (abstraction of H by NH_2). It is therefore reasonable that the phosphine data be applied to higher pressure conditions that prevail in the Jovian regime of interest.

No further experiments for the reaction of NH_2 with phosphine appear to be either warranted or possible without major modifications to the apparatus, and then only to extend the temperature range over which the study could be done.

In order to further examine the pressure dependence of reaction of NH_2 with acetylene, higher pressure studies must be performed. A laser absorption experiment such as that performed by Lesclaux et al.[45] is the method of choice for the reasons stated in Chapter 2. On the other hand, in neither of the hydrocarbon reactions was the low pressure limit examined. To do so would require additional experiments for which the flow discharge method would be most suited. A number for the low pressure limit would be invaluable in helping to determine if there is more than one reaction channel occurring in these reactions.

The study appears to have resolved at least part of the discrepancies that existed concerning the rate of reaction of NH_2 with ethylene. The agreement of the ethylene results presented here with those of Lesclaux et al.[45] and Khe et al.[51] stands in contrast to the results of Hack et al.,[46] It is impossible to unequivocally point to the cause of disagreement, but it appears that the possibility of the reaction of NH_2 radicals with O atoms generated by the microwave discharge of oxygen, or by the heterogeneous reaction of F with the glass flow tube walls or with water adsorbed on the flow tube system walls is the most likely cause. An alternative method of NH_2 radical preparation might be achieved using a pulsed laser as a flash source for NH_2 coupled with the use of laser induced fluorescence for NH_2 radical detection. Since the system used in this study is the most sensitive method over the temperature and pressure range studied and it avoided the pitfalls of secondary reactions, reaction

with products and interfering heterogeneous reactions, it is suggested that the results presented here should merit the highest degree of confidence.

While any detailed discussion of the implications of the results presented here for Jovian models is beyond the scope of this work, some qualitative observations can be made. The results presented here lead to the conclusion that the coupling reaction between NH_2 and PH_3 is much slower than that predicted by Buchanan et al.[53]. Strobel[23] stated that the rate of reaction of NH_2 and PH_3 must be $\sim 10^{-12}$ cm^3 $molec^{-1}$ sec^{-1} in order to compete with the reaction of NH_2 with itself in the Jovian atmosphere. Since he only had available the much faster rate of Buchanan et al., he concluded that PH_3 inhibits the photochemical destruction of NH_3 by scavenging NH_2 radicals. Strobel also concluded that the coupling reaction provides some recycling of NH_3 in the Jovian atmosphere. It is suggested, based on the results presented here, that such a coupling is negligible and that the coupling reaction is too slow to be of any significance in recycling NH_3 in the Jovian atmosphere.

Likewise, the rates of the other two reactions measured appear to be too slow to be of any significance in providing an NH_3 reservoir in the Jovian atmosphere. If the formation of an adduct between NH_2 and either of the unsaturated hydrocarbons studied could lead to the ketene analog, CH_2CNH, as speculated in Chapter 3, it is possible that trace amounts of ethylamine might be detected in the Jovian atmosphere. A mass spectral analysis of the products of reactions (28) and (29) could also provide support for this conjecture.

The question of the source of the red chromophore of the Jovian atmosphere has been brought closer to solution. The coupling reaction

between NH_2 and phosphine may now be ruled out as a source of PH_2, the reaction of H with PH_3, however, still provides a viable alternative for PH_2 generation, especially if the hydrogen concentration is greater than current estimates (maximum of 1.8×10^8 molecule/cm^3 just above the tropopause)[98] It appears that the final resolution of this problem rests with observations such as might be provided by the planned Galileo Jupiter orbiting mission.

Significant work remains with regards to PH_3 kinetics. For example, the source and composition of the particulates observed formed in this study remains a mystery. In comparing experiments in which PH_3/argon mixtures were flashed with those in which ammonia, phosphine, and argon were flashed, it appears that the production of particulates in the latter, and not in the former, may possibly be explained by the degree of hydrogen atom production in the two experiments. If the absorption coefficient of NH_3 is much greater than that of PH_3 under the optical conditions used, then the higher production of H by NH_3 photolysis could lead to significant PH_2 production via reaction (83). A weak PH_3 absorption might provide insignificant PH_2 production. A simple experiment might be performed in which H atoms (for example from CH_4 photolysis) are reacted with PH_3. The appearance of detectable scattering under the same conditions of temperature, pressure and phosphine concentration as used here would help to support this hypothesis.

This study establishes the limitations of some of the possible coupling schemes that might have provided an ammonia reservoir in the Jovian atmosphere. This information should enable modelers to eliminate three of the potential coupling schemes that could have provided ammonia reservoirs in the Jovian atmosphere. It appears that the thermal

decomposition of hydrazine and the subsequent ammonia regeneration by reaction of NH_2 with abundant H_2 in the Jovian interior must take on increasing importance in any ammonia regeneration scheme.

APPENDIX I

$NH_2 + C_2H_4$ Data

Temperature (°K)	[Ar] (torr)	$[NH_3]$ (mtorr)	$[C_2H_4]$ (mtorr)	Flash Energy (J)	k_{obs} (sec^{-1})
250	10	475	0	8.9	23±2
					20±1
					25±2
				12.1	24±1
					23±1
				15.8	21±1
			554	6.2	27±1
				8.9	27±2
				12.1	29±1
					25
				15.8	26±1
			1426	8.9	35±2
					32±1
				12.1	36±1
					30±1
				15.8	35±1
					34±1
			2384	8.9	37±1
					36
				12.1	36±2
				15.8	38±2

Temperature (°K)	[Ar] (torr)	[NH_3] (mtorr)	[C_2H_4] (mtorr)	Flash Energy (J)	k_{obs} (sec^{-1})
250	25	1192	0	6.2	11±1
				8.9	11±1
				12.1	15±1
					16±3
					11±1
					13±1
				15.8	12±2
					12±1
					9±1
					12±2
					11±1
			1391	6.2	20±2
				8.9	24±2
				12.1	29±1
				15.8	29±2
					30±2
			3637	6.2	28±1
				8.9	30±1
					29±3
					33±1
				12.1	34±2
					34±3
			5960	8.9	48±3
				12.1	41±3
					41±1
					36±2
				15.8	46±1
					39±3

Temperature (°K)	[Ar] (torr)	$[NH_3]$ (mtorr)	$[C_2H_4]$ (mtorr)	Flash Energy (J)	k_{obs} (sec^{-1})
250	25	1118	0	2.2	11±1
				4.0	10
				6.2	12±1
				8.9	9±1
				12.1	10±1
					10±1
					11±1
			1207	2.2	18±1
				4.0	25±1
				6.2	20±1
				8.9	22±1
				12.1	25±2
				15.8	26±1
			2235	4.0	25±1
				6.2	27±1
				8.9	27±1
				12.1	32±1
			3353	4.0	27±2
				6.2	29±1
				8.9	30±2
				12.1	32±1
				15.8	32±2
			4470	4.0	33±2
				6.2	36±1
				8.9	34±1
				12.1	40±2
				15.8	37±1
			5588	4.0	40±1
				6.2	38±2
				8.9	42±1
				12.1	43±2
				15.8	42±1

Temperature (°K)	[Ar] (torr)	[NH_3] (mtorr)	[C_2H_4] (mtorr)	Flash Energy (J)	k_{obs} (sec^{-1})
250	50	2235	0	2.2	7
				4.0	7
				6.2	12±1
				8.9	9±1
				15.8	12±1
			2414	6.2	27±1
				8.9	25±1
				12.1	30±1
				15.8	33±1
			4470	6.2	33±1
				8.9	42±2
				12.1	42±5
					46±1
				15.8	48±2
			6705	8.9	56±5
				12.1	54±2
					51±3
				15.8	61±2
			8940	12.1	70±4
					69±3
				15.8	71±4
298	10	400	0	6.2	24±1
				8.9	25±2
					26±1
				12.1	31±3
					32±4
				15.8	29±5
			467	6.2	44±2
				8.9	35±4
					36±4
				12.1	46±4
					46±4
				15.8	36±3
			1220	6.2	49±4
				8.9	50±5
				12.1	49±4
				13.9	52±8
					53±4
				15.8	48±3
			2000	6.2	57±2
				8.9	59±1
				12.1	62±4
				13.9	62
				15.8	62±1

Temperature (°K)	[Ar] (torr)	[NH_3] (mtorr)	[C_2H_4] (mtorr)	Flash Energy (J)	k_{obs} (sec^{-1})
298	15	600	0	6.2	20±1
				10.5	26±2
					22±1
				12.1	21±2
					25±2
					18±1
					21
			700	4.0	31±2
				6.2	32±4
					32±3
				10.5	34±4
					34±3
				12.1	33±2
					38±2
			1830	8.9	55±1
				12.1	55±2
				13.9	54±4
					54±1
				15.8	55±1
			3000	12.1	65±1
					65±4
				13.9	68±1
					69±1
				15.8	71±1
					67±4

Temperature (°K)	[Ar] (torr)	[NH_3] (mtorr)	[C_2H_4] (mtorr)	Flash Energy (J)	k_{obs} (sec^{-1})
298	15	600	0	1.5	26±2
				2.2	27±1
				4.0	25±2
					26±2
				6.2	28±1
					27±1
				8.1	26±1
					28
				12.1	28±2
					28
				15.8	25±2
			515	1.5	31±2
				2.2	30±1
				4.0	30±3
				6.2	30±3
				8.9	32±2
				12.1	31±2
				15.8	31±2
			705	4.0	35±3
				6.2	37±2
				8.9	35±1
				12.1	37±2
				15.8	36±3
			1250	2.2	38±1
				4.0	42±1
				6.2	49
				8.9	44±1
				12.1	44±2
				15.8	43±2
			1825	2.2	49±4
					52±10
				4.0	51±1
					52±2
				6.2	51±1
				8.9	61±4
					56±1
				12.1	58±1
			3000	6.2	66±4
				8.9	68
				12.1	64±5
				15.8	71±1

Temperature (°K)	[Ar] (torr)	[NH_3] (mtorr)	[C_2H_4] (mtorr)	Flash Energy (J)	k_{obs} (sec^{-1})
298	25	1000	0	6.2	22±3
				8.9	22±2
				12.1	24±1
					24±3
				13.9	24±2
					26±1
				15.8	25±3
			1167	6.2	43±1
				8.9	43±1
					41±2
				12.1	44±2
				15.8	46±2
			3051	12.1	77±7
					72±6
				13.9	70±2
					69±2
				15.8	71±1
					80±5
			5000	8.9	92±7
				12.1	94±3
					96±1
				13.9	99±1
					88±2
				15.6	87±2

Temperature (°K)	[Ar] (torr)	[NH_3] (mtorr)	[C_2H_4] (mtorr)	Flash Energy (J)	k_{obs} (sec^{-1})
298	25	1463	0	6.2	16±2
					14±1
					15±1
				8.9	13±1
					17±2
					16±2
				12.1	16±1
					16±1
					16
				15.8	19±2
			781	6.2	25±1
					23±1
					23±2
				8.9	25±1
				12.1	24±1
				15.8	23±1
			1563	6.2	32±2
				8.9	29±2
					34±2
				12.1	38±2
				15.8	31±2
			2344	6.2	42±3
				8.9	42±1
					40±2
				12.1	44
				15.8	38±3

Temperature (°K)	[Ar] (torr)	[NH_3] (mtorr)	[C_2H_4] (mtorr)	Flash Energy (J)	k_{obs} (sec^{-1})
298	25	938	0	2.2	20±1
				4.0	19±1
				6.2	19
				8.9	19±1
				12.1	21±2
				15.8	21±1
			800	4.0	27±2
				6.2	29±3
					27±1
				8.9	28±2
					28±1
				12.1	27±3
				15.8	29±1
			1625	2.2	38±2
				4.0	40±1
				6.2	39±1
				8.9	40±3
				12.1	40±4
				15.8	44±2
			2572	4.0	52±3
				6.2	54±3
				8.9	57±2
				12.1	56±4
					55±4
				15.8	58±3
			3441	6.2	67±2
				8.9	70±6
					71±2
				12.1	72±2
					70±1
				15.8	72±5
			4406	6.2	79±3
				8.9	84±4
					88±2
					82±3
				12.1	81±5
				15.8	83±2

Temperature (°K)	[Ar] (torr)	$[NH_3]$ (mtorr)	$[C_2H_4]$ (mtorr)	Flash Energy (J)	k_{obs} (sec^{-1})
298	25	1000	0	12.1	15±1
					15±1
				15.8	18
					18±2
					20±1
			1167	8.9	24±1
				12.1	28±2
					27±3
				15.8	28
					32±2
			3051	8.9	38±2
				12.1	43±3
					45±1
				15.8	41±1
					45±2
			5000	13.9	59±2
				15.8	57±3
					60±2
				17.9	60±1
					61±1
298	35	1400	0	8.9	14±1
					12±1
				12.1	12±1
					11±1
					13±2
			1634	4.0	38±1
				6.2	43±2
					43±1
				8.9	47±1
					47±2
				12.1	48±2
			4271	12.1	89±2
					84±1
				13.9	81±4
					84±1
				15.8	82±3
					77±3
			7000	12.1	110±3
					111±8
				13.9	104±4
					107±2
				15.8	116±3
					120±3

Temperature (°K)	[Ar] (torr)	[NH_3] (mtorr)	[C_2H_4] (mtorr)	Flash Energy (J)	k_{obs} (sec^{-1})
298	[illegible]	1000	0	2.2	10±1
					7±1
				4.0	10±1
					10
				6.2	10
					13±2
				8.9	13
				15.8	11±1
			625	4.0	21±1
				6.2	23±1
				8.9	32±2
				12.1	28
				15.8	32±1
			1250	6.2	37±1
					35±1
				8.9	36±3
				12.1	43±2
				15.8	46±2
			2500	2.2	32±2
				4.0	39±1
					37±1
				6.2	44±3
			3750	2.2	51±2
				4.0	52±2
				5.0	50±2
			5000	2.2	57±1
				4.0	71±12
				6.1	59±5
				8.9	71±3

Temperature (°K)	[Ar] (torr)	[NH_3] (mtorr)	[C_2H_4] (mtorr)	Flash Energy (J)	k_{obs} (sec^{-1})
298	100	666	0	6.2	14±1
				8.9	16±2
				12.1	18±1
			572	6.2	18±2
				8.9	21±1
				12.1	21±2
				15.8	20±2
					22±2
			1389	6.2	30±5
				8.9	30±2
				12.1	33±2
				15.8	33±8
			3333	8.9	44±1
				12.1	48±2
				15.8	56±1
					63±4
373	5	500	0	4.0	55±4
				8.9	59±2
				15.8	52±8
			1309	4.0	95±3
				8.9	103±4
				15.8	106±4
			2397	4.0	139±4
				8.9	131±1
				15.8	136±3
			3595	4.0	174±11
				8.9	181±5
				15.8	168±1

Temperature (°K)	[Ar] (torr)	[NH_3] (mtorr)	[C_2H_4] (mtorr)	Flash Energy (J)	k_{obs} (sec^{-1})
373	10	468	0	6.2	40±2
				8.9	45±1
				12.1	41±4
				15.8	41±2
		500	250	6.2	58±1
				8.9	59±3
				12.1	62±1
				15.8	52±1
			500	6.2	61±3
				8.9	61
				12.1	57±2
					62
				15.8	60±3
			749	8.9	75±6
				12.1	64±2
					86±3
				15.8	69±4
					72±7
373	25	1169	0	6.2	19±1
				8.9	20±2
					20±3
				12.1	19±3
				15.8	18±1
		1249	624	8.9	42±1
					39±3
				12.1	39±2
					42±1
					47±1
				15.8	41±1
			1249	8.9	69±2
				12.1	59±5
					60±4
					62
				15.8	61±2
					61±3
			1873	8.9	78±2
					83±4
				12.1	74±1
					74±2
				15.8	74±2
					89±6

Temperature (°K)	[Ar] (torr)	[NH_3] (mtorr)	[C_2H_4] (mtorr)	Flash Energy (J)	k_{obs} (sec^{-1})
373	25	749	0	2.2	21±2
				4.0	23±1
				6.2	24
				8.9	26±2
				12.1	23±1
				15.8	26
			639	4.0	45±3
				6.2	49±2
				8.9	50±1
				12.1	53±2
				15.8	53±1
			1298	4.0	77±2
				6.2	83±1
				8.9	79±1
				12.1	82±1
				15.8	80±3
			2055	4.0	94±6
				6.2	96±3
				8.9	93±1
				12.1	104±4
				15.8	106±1
			2749	6.2	124±2
					131±5
				8.9	132±2
					136±4
					130±2
				12.1	137±4
					132±2
				15.8	134±2
					137±5
373	35	1118	0	13.9	18±1
				15.8	21±2
					20±2
				17.9	16±1
					16±1
			1305	15.8	66±3
					71±2
				17.9	70±5
					69±1
			3412	15.8	125±3
				17.9	114±1

Temperature (°K)	[Ar] (torr)	$[NH_3]$ (mtorr)	$[C_2H_4]$ (mtorr)	Flash Energy (J)	k_{obs} (sec^{-1})
373	25	799	0	8.9	26±1
				12.1	35±4
					29±2
				15.8	38±1
			932	15.8	59±1
					60±1
					62±2
				17.9	52±1
			2438	13.9	98±6
				15.8	94±1
				17.9	92±3
					98±4
			3995	13.9	144±6
				15.8	137±3
				17.9	152±8
					148±3
465	25	603	512	6.2	68±1
				8.9	62±4
				12.1	70±7
				15.8	69±4
			1046	6.2	98±4
				8.9	106±2
				12.1	101±6
				15.8	108±9
			1655	6.2	134±5
				8.9	152±13
				12.1	139±11
				15.8	149±3
			2215	10.5	196±1
				12.1	200±26
				13.9	192±9
				15.8	210±14
			2836	12.1	254±28
				13.9	232±8
				15.8	278±25

Temperature (°K)	[Ar] (torr)	[NH_3] (mtorr)	[C_2H_4] (mtorr)	Flash Energy (J)	k_{obs} (sec^{-1})
460	25	651	0	13.9	48±2
				15.8	41±1
					49
				17.9	41±1
					50±2
			759	15.8	96±4
					96±1
				17.9	94±3
					82±3
			1985	15.8	156±5
					145±25
				17.9	159±25
					146±8
465	25	1001	0	4.0	39±2
				6.2	38±3
				8.9	40±3
				12.1	39±1
					38±4
				15.8	45±2
			1003	6.2	88±3
				8.9	89±3
				12.1	98±2
					98±3
				15.8	95±6
			1504	6.2	121±6
				8.9	121±6
				12.1	120±12
					115±6
				15.8	123±8
			2002	6.2	154±2
				8.9	150±2
				12.1	156±3
					148±8
				15.8	159±5
			2503	8.9	189±18
				12.1	192±14
					198±6
				15.8	196±15
			3003	8.9	217±2
				12.1	236±6
				15.8	229±4

Temperature (°K)	[Ar] (torr)	[NH_3] (mtorr)	[C_2H_4] (mtorr)	Flash Energy (J)	k_{obs} (sec^{-1})
465	35	841	0	4.0	34±4
				6.2	32±2
				8.9	34±1
				12.1	36±3
				15.8	35±1
			719	6.2	73±5
				8.9	76±7
				12.1	57±4
					67±2
				15.8	77±2
			1449	8.9	109±2
				12.1	104±6
					113±12
				15.8	107±11
					113±9
			2293	8.9	173±2
				12.1	154±6
				15.8	162±8
					149±7
			3100	12.1	200±9
				13.9	190±5
				15.8	204±19
					242±2
			3962	13.9	282±19
				15.8	275±13
					266±12
460	5	327	0	4.0	99±6
				8.9	107±7
				15.8	102±6
			845	4.0	142±7
				8.9	132±8
				15.8	141±11
					135±11
			1923	4.0	178±3
				8.9	176±11
				12.1	172±3
				15.8	186±9
			2878	8.9	213±11
				12.1	215±12
				15.8	206±14

APPENDIX II

$NH_2 + C_2H_2$ Data

Temperature (°K)	[Ar] (torr)	[NH_3] (mtorr)	[C_2H_2] (mtorr)	Flash Energy (J)	k_{obs} (sec^{-1})
241	25	1005	0	4.0	9±1
				8.9	10±1
				15.8	10±1
			3091	4.0	11±1
				8.9	10±1
				15.8	13±1
			4920	4.0	12
				8.9	14±1
				15.8	17±1
			6830	8.9	21±2
					16
				12.1	24±2
				15.8	20±1
			8656	8.9	26±2
				12.1	20±2
					26±1
				15.8	26±3
298	10	500	0	4.0	28±2
				8.9	26±2
					28±4
				15.8	28±2
			1065	4.0	37±1
				8.9	37±1
					34±4
				15.8	35±1
					38±1
			2000	4.0	41±1
				8.9	42±1
				15.8	44±2
			3000	4.0	50±2
				8.9	49±3
				15.8	47±1
			4025	8.9	47±1
				12.1	56±1
					53±4
				15.8	59±2

Temperature (°K)	[Ar] (torr)	[NH_3] (mtorr)	[C_2H_2] (mtorr)	Flash Energy (J)	k_{obs} (sec^{-1})
298	25	1000	0	1.5	11±2
				4.0	11±1
				8.9	11±1
				15.8	13±2
			1296	4.0	17±1
				8.9	17±2
				15.8	19±1
			2500	4.0	27±2
				8.9	26±1
				15.8	27±1
			3750	8.9	32±2
				15.8	36±2
					39±1
			5000	4.0	46±3
				15.8	48±3
					47±3
298	25	957	0	2.2	10±2
				4.0	10±1
				6.2	13±1
				8.9	12±2
				12.1	12±1
			1000	1.5	15±1
				2.2	17±1
				4.0	20±2
				6.2	21±2
					17±1
				8.9	23±3
					19±1
			3000	2.2	26±1
				4.0	26
				6.2	26±2
				8.9	32±2
			5000	4.0	35±4
				6.2	40±2
				8.9	39±2
				12.1	45±1

Temperature (°K)	[Ar] (torr)	$[NH_3]$ (mtorr)	$[C_2H_2]$ (mtorr)	Flash Energy (J)	k_{obs} (sec^{-1})
298	25	600	0	4.0	17±1
					18±1
				8.9	20±1
					19±1
				15.8	20±2
					21±1
			1130	12.1	24±1
				15.8	27±2
			4675	8.9	52±5
				12.1	52±5
				15.8	52±4
298	25	1000	0	1.5	17±1
				4.0	15±1
				8.9	13±1
				15.8	14±1
			3000	2.2	35
				4.0	35
				8.9	36
				15.8	38
				20.0	40
298	50	800	0	4.0	6±1
				8.9	8±1
					8±1
				15.8	7±1
			1250	4.0	13±1
				8.9	15±1
				15.8	17±1
			2500	4.0	19±1
				8.9	20±2
				15.8	24±2
			3750	8.9	26±2
				12.1	26±1
				15.8	30±3

Temperature (°K)	[Ar] (torr)	[NH_3] (mtorr)	[C_2H_2] (mtorr)	Flash Energy (J)	k_{obs} (sec^{-1})
373	5	320	0	4.0	65±1
				8.9	67±3
					65±9
				15.8	65±3
					66±1
			1284	4.0	91±4
				8.9	92±9
				15.8	91±4
					88±8
			2397	4.0	100±5
				8.9	103±9
				15.8	103±6
			3250	8.9	114±4
				12.1	116±5
373	10	479	0	3.1	32±3
				8.9	25±2
					29±1
				15.8	33±2
			999	1.5	54±7
				4.0	49±2
				8.9	54±5
				15.8	51±2
			1997	4.0	59±1
				8.9	67±3
				15.8	74±4
			2996	4.0	72±2
				8.9	77±3
				15.8	80±1
			3995	4.0	94±3
				8.9	101±8
				15.8	99±6

Temperature (°K)	[Ar] (torr)	[NH_3] (mtorr)	[C_2H_2] (mtorr)	Flash Energy (J)	k_{obs} (sec^{-1})
375	25	1237	0	1.5	18±1
				4.0	14
				8.9	18±2
					18±2
				15.8	18±1
			1349	1.5	47±5
				4.0	41±4
				8.9	54±2
				15.8	53±3
			2487	4.0	64±3
				8.9	66±3
					64±1
				15.8	68±2
			3709	4.0	73
				8.9	86±4
					80±4
				15.8	91±6
			4959	8.9	92±3
				12.1	96±2
				15.8	110±5
					122±3
373	50	799	0	8.9	13±1
					14
				15.8	12±1
			799	12.1	31±1
				15.8	36±1
					30±1
			1598	12.1	51
				15.8	49±2
373	100	795	0	4.0	8±1
				8.9	8±1
				15.8	8±1
			1240	4.0	34±1
				8.9	37±1
				12.1	35±1
			2384	8.9	64±2
				12.1	58±3
				15.8	58±4
			3576	15.8	88±6
					94±5

Temperature (°K)	[Ar] (torr)	[NH_3] (mtorr)	[C_2H_2] (mtorr)	Flash Energy (J)	k_{obs} (sec^{-1})
460	5	260	0	4.0	110±6
				8.9	107±10
				15.8	102±10
			1044	4.0	135±8
				8.9	135±7
				15.8	131±1
					138±4
			1948	4.0	175
				8.9	163±7
				15.8	178±3
			2641	4.0	208±7
				8.9	220±9
				15.8	215±10
455	10	393	0	4.0	87±3
					73±3
				8.9	86±4
					82±2
				15.8	85±5
					75±2
			819	4.0	103±3
				8.9	108±4
					100±8
				15.8	104±4
					102±7
			1637	4.0	112±8
					124±2
				8.9	127±5
					118±6
				15.8	124±6
					139±3
			2456	4.0	152±12
					143±4
				8.9	158±7
					149±17
				15.8	159±7
			3275	4.0	181±10
					199±8
				8.9	204±5
					183±10
				15.8	195±9
					183±3

Temperature (°K)	[Ar] (torr)	[NH_3] (mtorr)	[C_2H_2] (mtorr)	Flash Energy (J)	k_{obs} (sec^{-1})
463	25	1004	0	4.0	38±1
				8.9	39±2
					38±3
				15.8	45±4
					38±3
					44±2
					41±2
			1091	4.0	99±5
				8.9	110±5
				15.8	104±8
			2034	4.0	140±9
				8.9	129±12
				15.8	140±5
					154±8
			3018	8.9	195±3
				15.8	212±19
			4026	12.1	257±21
				15.8	256±9
448	25	1000	0	1.5	37±1
				4.0	33±4
				8.9	30±2
					37±3
					35±3
				15.8	35±4
			1950	4.0	121±13
				8.9	112±3
					127±4
				15.8	147±5
					132±1
			3348	8.9	192±7
				15.8	199±8
					195±14

Temperature (°K)	[Ar] (torr)	[NH_3] (mtorr)	[C_2H_2] (mtorr)	Flash Energy (J)	k_{obs} (sec^{-1})
463	50	805	0	4.0	21±1
				8.9	22±2
				15.8	21±2
			1275	4.0	78±3
				8.9	90±4
				12.1	88±5
				15.8	89±3
			2575	8.9	170±19
				15.8	156±5
			3852	15.8	272±17
					259±18
			5169	15.8	372±31
					361±29
454	100	819	0	4.0	24±3
				8.9	26±1
				15.8	21±1
			910	8.9	79±13
					72±2
				12.1	81±1
				15.8	64±3
			2042	8.9	128±3
				12.1	148±5
				15.8	150±7
			3268	12.1	240±21
				15.8	250±28
			4084	15.8	355±40

Appendix III

$NH_2 + PH_3$ Data

Temperature (°K)	[Ar] (torr)	$[NH_3]$ (mtorr)	$[PH_3]$ (mtorr)	Flash Energy (J)	k_{obs} (sec^{-1})
218	2.5	342	34.17	24	85±3
				35	105±6
				47	99±5
				62	105±15
			68.34	24	123±6
				35	118±6
				47	127±7
				62	139±2
218	2.5	342	27.34	24	146±12
				35	149±2
				47	154±11
				62	149±8
			54.68	24	138±10
				35	145±17
				47	131±12
			82.02	35	190±11
				47	186±12
					180±3
				62	208±10
					214±24
218	5.0	342	23.24	35	63±5
					57±9
				47	62±6
				62	60±3
			46.48	35	75±3
				47	84±2
					70±3
				62	72±7
247	2.5	302	60.32	35	110±6
				47	125±12
					130±6
				62	124±14
					130±17
			90.48	47	165±7
					161±6
				62	151±8

Temperature (°K)	[Ar] (torr)	[NH_3] (mtorr)	[PH_3] (mtorr)	Flash Energy (J)	k_{obs} (sec^{-1})
247	2.5	302	0	16	115±19
				24	114±16
				35	116±25
				47	102±16
			24.1	16	133±10
				24	135±6
				35	130±19
				47	129±9
			48.3	16	156±8
				24	146±6
				35	149±24
				47	148±14
			72.4	16	162±2
				24	170±13
				35	171±11
				47	169±23
247	2.5	302	0	16	102±10
				24	96±14
				35	100±18
				47	104±16
			30.16	9	117±8
				16	122±7
				24	127±11
				35	120±9
			60.32	4	131±7
				16	155
				24	130±12
				35	152±7
				47	146±23
				62	158±12
			90.48	24	199±16
				35	192±14
				47	183±3
				62	199±46

Temperature (°K)	[Ar] (torr)	[NH_3] (mtorr)	[PH_3] (mtorr)	Flash Energy (J)	k_{obs} (sec^{-1})
247	2.5	302	0	16	127±9
				24	108±11
				35	144±5
				47	118±7
			24.1	16	151±5
				24	153±7
					155±8
				35	170±2
				47	152±10
			48.3	16	189±5
				24	187±18
					180±6
				35	216±28
				47	184±13
			72.4	16	212±1
				24	217±9
				35	219±4
					201±1
				47	209±8
247	5.0	302	0	16	62±16
				24	64±6
				35	62±3
				47	73±10
			24.1	24	93±22
				35	77±10
				47	90±7
				62	95±6
			48.3	24	105±5
				35	104±11
				47	116±22
				62	109±9
			72.4	24	138
				35	127±4
				47	129±2
				62	118±6

Temperature (°K)	[Ar] (torr)	[NH_3] (mtorr)	[PH_3] (mtorr)	Flash Energy (J)	k_{obs} (sec^{-1})
247	5.0	302	0	35	34±2
					36±6
				47	36±3
					39±2
					41±4
				62	36±5
			20.51	35	66±6
					66±7
				47	63±4
				62	55±3
			41.02	35	88±16
					83±3
				47	84±5
				62	92±9
			61.53	35	114±5
				47	121±10
				62	115±11
298	2.5	249.5	0	11.2	75±4
				16	89±5
				35	89±5
				47	79±4
			50.00	9	207±6
				16	196±8
				24	196±12
				35	206±22
				47	209±19
		251.8	74.98	15	262±6
				24	253±10
					289±12
				35	270±7
					276±21
				47	284±8
		250.0	100.0	9	289±10
				16	292±12
				24	308±13
				35	334±7
				47	315±10

Temperature (°K)	[Ar] (torr)	$[NH_3]$ (mtorr)	$[PH_3]$ (mtorr)	Flash Energy (J)	k_{obs} (sec^{-1})
298	4.0	200	0	35	58±4
				47	51±4
					42±5
					40±2
					55±5
					58±5
					61±8
				62	52±9
			40	35	112±6
				47	119±8
					133±4
				62	131±9
			60	35	177
					152±16
				47	155±17
				62	144±7
			80	35	196±10
					193±7
				47	200±20
				62	188±8
298	4.0	280	0	37	120±2
			48	24	195±22
				37	197±13
			72	24	263±17
				37	256±19
			96	37	298±6
298	7.5	365.63	0	9	30±2
				16	38±5
					40±9
				24	39±2
				35	34±2
				47	33±3
			45.20	16	141±8
				35	132±13
				47	119±11
			68.06	16	173±24
				24	152±18
				35	179±7
				55	166±23
			90.0	24	239±21
				35	227±36
				47	220±25

Temperature (°K)	[Ar] (torr)	[NH_3] (mtorr)	[PH_3] (mtorr)	Flash Energy (J)	k_{obs} (sec^{-1})
298	5.0	243.75	0	37	73±12
				56	82±3
				81	80±7
				110	80±2
			30.13	9	132±5
				16	137±10
				24	160±2
					178±12
				35	142±8
				47	141±8
			45.38	9	174±9
				16	167±7
				24	180±9
				35	200±9
				47	174±5
			60.00	9	215±16
				16	194±14
				24	205±16
				35	215±16
				47	201±6
298	7.5	750	0	16	59±4
				24	61±6
				35	54±2
				47	56±2
				62	60±6
			39.38	16	133±8
				24	131±1
				35	137±9
				47	147±7
				62	146±15
			80.81	16	205±5
				24	198±14
				35	212±12
				47	197±14
				62	213±7
			120.0	16	265±22
				24	288±4
				35	263±16
				47	266±13
				62	300±37

Temperature (°K)	[Ar] (torr)	[NH_3] (mtorr)	[PH_3] (mtorr)	Flash Energy (J)	k_{obs} (sec^{-1})
298	10.0	208.3	0	9	30±3
				16	28±1
			25	9	79±4
				16	80±7
			50	9	121±1
				16	121±1
			75	16	172±1
363	2.5	143.7	0	47	210±11
			24.63	47	301
				55	299
				62	330
			36.94	47	36
				55	352
				62	348
			49.26	47	439
					433
				55	433
					461
				62	417
					454
363	2.5	205	0	24	164±9
				35	110±6
				47	135±4
					136±18
				62	139±7
			41.0	24	303±12
				35	330±12
					375±27
				47	380±21
					349±11
				62	415±11
			82.0	24	451±11
				35	430±9
					450±41
				47	419±21
					490±16
				62	422±10
			120.0	24	543±123
				35	584±53
					505±14
				47	561±15
					574±26
				62	618±12

Temperature (°K)	[Ar] (torr)	[NH_3] (mtorr)	[PH_3] (mtorr)	Flash Energy (J)	k_{obs} (sec^{-1})
363	5.0	205	0	24	192±1
					158±35
				35	171±18
					196±3
				47	216±44
			41.0	35	283±8
				47	300±14
					304±11
				62	295±6
			61.6	35	386±8
					373±15
				47	398±44
					353±9
					401±22
				62	392±13
					381±7
			82.1	35	434±56
				47	556±21
					537±6
				62	546±36
					566±21
363	5.0	287.3	0	47	191±3
					197±8
			49.26	47	311±26
					327±26
				62	327±6
			73.89	47	504±11
					398±15
				62	412±35
			110.84	47	630±39
				62	663±30
456	5.0	204	0	4	110±2
				9	104±2
				16	103±5
			20.5	9	225±14
				12	215±12
				16	211±15
			40.8	9	383±9
				12	385±5
				16	383±7
			61.1	16	522±27
					583±23

Temperature (°K)	[Ar] (torr)	[NH_3] (mtorr)	[PH_3] (mtorr)	Flash Energy (J)	k_{obs} (sec^{-1})
456	10.0	400	0	4	68±8
				9	69±3
				16	72±2
			41.0	4	309±18
				9	307±16
				16	321±20
			81.9	4	563±25
				9	577±10
				16	538±14
			122.4	4	863±57
				9	839±12
				16	910±24
457	20.0	408	0	4	62±4
				9	59±2
				16	64±4
			33	4	269±4
				9	285±5
				16	333±7
			65	4	485±9
				9	508±46
				16	516±29
			97	16	730±41
					763±6

Appendix IV

Theoretical Calculation of the Frequency Factor for $NH_2 + PH_3$

A modified bond energy-bond order (BEBO) - activated complex theory (ACT) calculation was performed to provide a theoretically determined value for the frequency factor for the metathetical channel of reaction (27) in order to compare theory with experiment. The BEBO calculation was performed to provide the equilibrium bond distances, R_{PH} and R_{NH}, for the activated complex, NH_2PH_3, which were used in the ACT calculation.

The Pauling relation:[99]

$$(87)\quad R = R_s - 0.26 \ln n$$

was used to determine the bond distance, R, between two atoms given the order, n, of the bond whose length is to be determined if the length of a single bond, R_s, between the two atoms is known. For the present problem, $R_s = 1.421\times10^{-8}$ cm and 1.01×10^{-8} cm for the P-H and N-H single bonds, respectively.[100]

The bond orders, n and m, for the N-H and P-H bonds in the activated complex formed in the metathetical reaction between NH_2 and PH_3 will be calculated using (8d) and assuming that the total bond order for the N-H and P-H bonds formed is equal to the bond order in the P-H bond broken, namely, one:[101]

$$(88)\quad V = E_{1s} - E_{1s}n^p - E_{2s}m^q + E_{3s}(1/2\, e^{-\beta r_1})(1 + 1/2\, e^{-\beta r_1})$$

Rearranging, (88) becomes:

$$(89)\quad V = E_{1s}(1 - n^{p}) - E_{2s}(1 - n)^{q} + E_{3s}B(n - n^{2})^{\gamma}[1 + B(n + n^{2})^{\gamma}]$$

In (88) and (89), 1 and 2 are the indices corresponding to the P-H and N-H bonds and 3 refers to the N-H-P intermediate in H_2P-H-NH_2. p and q are the empirical bond energy indices for PH_3 and NH_2, respectively. If the relationship between single order bonds and Lennard-Jones molecules is assumed to be linear, then p (and q) may be calculated from (90) [102]:

$$(90)\quad p = \frac{0.26\ \ln(E_s/E_x)}{(R_x - R_s)}$$

where R_s and E_s are the single bond length and single bond energy for P-H in PH_3 (or N-H in NH_2) and R_x and E_x are the bond length and bond energy for the noble gas analog of P-H (or N-H).[103] β_3 is the Morse parameter for the complex and can be calculated from (91) [104].

$$(91)\quad \beta_3 = (F/2De)^{1/2}$$

where F = 545 dynes/cm[105] and De, the dissociation energy for N-H-P was obtained from the geometric mean of the N-N and P-P values[106] of a bond energy-bond distance plot. $\gamma = 0.26\beta_3$ and B in (89) is calculated from (92) [101]:

$$(92)\quad B = 1/2\ e^{-(\beta\Delta R_s)}$$

for $\Delta R_s = R_{1s} + R_{2s} - R_{3s}$ [101]. E_s may be calculated from (93):

$$(93)\quad E_s = D_o + 1/2\ h\nu \quad [107]$$

using the appropriate zero point energies, D_o [108], and frequency, ν, values.[40]

Taking $\partial V/\partial n = 0$ and solving for n gives a minimum on the potential energy surface for reaction (27). With n calculated to be 0.4645 and $m = 1 - n$, equation (87) gives $R_{PH} = 1.620$ Å and $R_{NH} = 1.172$ Å.

Using activated complex theory, the frequency factor, A, of the rate constant for a reaction such as (27) may be expressed as a ratio of the partition functions of the complex formed by an intermediate when the when the two reacting species come together divided by the product of the partition functions of the individual reactants:[109]

$$(94)\quad A = \frac{\kappa T}{h} \frac{q^{\ddagger}_{NH_2PH_3}}{q_{NH_2} q_{PH_3}}$$

where q‡ is the total partition function for the intermediate given by:[110]

$$(95)\quad q^{\ddagger} = g^{\ddagger} \frac{(2\pi m^{\ddagger} KT)^{3/2}}{h^3}\ q_e^{\ddagger}\ q_v^{\ddagger}\ q_r^{\ddagger}$$

and for NH_2 and PH_3 the total partition functions are:

$$(96)\quad q(NH_2) = g(NH_2) \frac{(2\pi m_{(NH_2)} KT)^{3/2}}{h^3}\ q_e(NH_2)\ q_v(NH_2)\ q_r(NH_2)$$

and $$(97)\quad q(PH_3) = g(PH_3)\frac{(2\pi m_{(PH_3)}KT)^{3/2}}{h^3}\, q_e(PH_3)\, q_v(PH_3)\, q_r(PH_3)$$

g is the degeneracy of the electronic state and q_e, q_v, and q_r are the electronic, vibrational, and rotational partition functions. Substituting for the constant terms, with $g^{\ddagger} = 2$, $g(NH_2) = 2$, and $g(PH_3) = 1$, and with all the electronic partition functions equal to unity since all species are in their ground electronic states, reduces (94) to:

$$(98)\quad A = \frac{3.0902\times10^{-12}}{T^{1/2}} Q_V Q_R \text{ cm}^3 \text{ molec}^{-1}\text{sec}^{-1}\text{deg}^{1/2}$$

where the rotational and vibrational partition functions are consolidated using: $Q = q^{\ddagger}/q(NH_2)q(PH_3)$.

The combined rotational partition function may be evaluated using:[111]

$$(99)\quad Q_R = \pi^{-1/2}\frac{(\sigma_{PH_3}\sigma_{NH_2})(h^3)}{\sigma^{\ddagger}\,(8\pi^2KT)^{3/2}}\,\frac{(I_1I_2I_3)^{\ddagger 1/2}}{(I_1I_2I_3)^{1/2}_{NH_2}(I_1I_2I_3)^{1/2}_{PH_3}}$$

where σ represents the number of discrete positions a molecule can assume about its principle symmetry axis and I_1, I_2, and I_3 are the principle moments of inertia. I_1, I_2 and I_3 can be evaluated using:[112]

$$(100)\quad I_1I_2I_3 = \begin{vmatrix} I_{11} & -I_{12} & -I_{13} \\ -I_{21} & I_{22} & -I_{23} \\ -I_{31} & -I_{32} & I_{33} \end{vmatrix}$$

where the larger subscripts refer to a coordinate system whose origin is

at the center of mass of the molecule and the smaller subscripts on the moments and products of inertia refer to any general set of coordinates. The principle moments (diagonals) can be evaluated using:

$$(101)\quad I_{11} = \sum_i m_i (z_i'^2 + y_i'^2)$$

$$(102)\quad I_{22} = \sum_i m_i (x_i'^2 + z_i'^2)$$

$$(103)\quad I_{33} = \sum_i m_i (x_i'^2 + y_i'^2)$$

and the off-diagonal terms are the products of inertia:

$$(104)\quad I_{12} = I_{21} = \sum_i m_i' x_i' y_i'$$

$$(105)\quad I_{13} = I_{31} = \sum_i m_i' x_i' y_i'$$

$$(106)\quad I_{23} = I_{32} = \sum_i m_i' x_i' y_i'$$

The coordinates of the four atoms of PH_3 are evaluated using Fig. 22.a.,(all bond distances are in Å) the P-H calculated bond distance of 1.421 Å, and the H-P-H bond angle of 93.3°. The coordinates are first evaluated using an arbitrary coordinate system with P at the origin. Then, the center of mass (x, y, z) coordinates are determined and are:

Figure 22

NH_2 and PH_3 GEOMETRIES

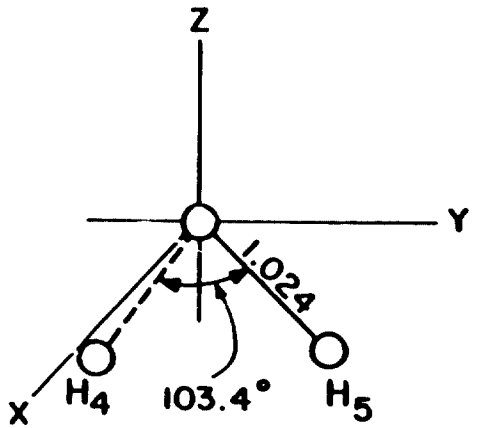

b. NH_2 GEOMETRY

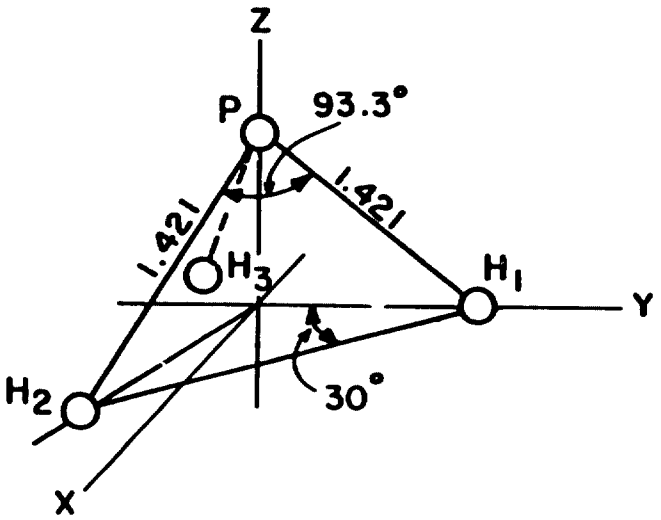

a. PH_3 GEOMETRY

$$H_1 = (\quad 0,\ \ 1.1932,\ -0.7442)$$

$$H_2 = (\ 1.0333,\ -0.5966,\ -0.7442)$$

$$H_3 = (-1.0333,\ -0.5996,\ -0.7442)$$

$$P = (\quad 0,\quad\ \ 0,\ \ 0.0720)$$

Using equations (101)-(106) where, incidentally in this case (104)-(106) are zero, the principle moments are evaluated and

$$I_1 = 7.0923\times10^{-40}\ \text{g cm}^2\ \text{molec}^{-1}$$

$$I_2 = 6.5719\times10^{-40}\ \text{g cm}^2\ \text{molec}^{-1}$$

$$I_3 = 6.5722\times10^{-40}\ \text{g cm}^2\ \text{molec}^{-1}$$

and $(I_1I_2I_3)^{1/2}$ for $PH_3 = 1.7502\times10^{-59}\ \text{g}^{3/2}\ \text{cm}^3\ \text{molec}^{-3/2}$.

In a similar fashion, $(I_1I_2I_3)^{1/2}$ for NH_2 may be evaluated using Fig. 22.b. The NH_2 center of mass coordinates are:

$$N = (0,\quad\ \ 0,\ \ 0.0793)$$

$$H_4 = (0,\ \ 0.8036,\ -0.5554)$$

$$H_5 = (0,\ -0.8036,\ -0.5554)$$

and $(I_1I_2I_3)^{1/2}$ for $NH_2 = 2.8852\times10^{-60}\ \text{g}^{3/2}\ \text{cm}^3\ \text{molec}^{-3/2}$.

The evaluation of $(I_1I_2I_3)^{1/2}$ for the complex requires a somewhat more difficult calculation using Fig. 23.a (all distances in Å). The complex is first assumed to form with N, P, and H_1 colinear. A new set of

Figure 23

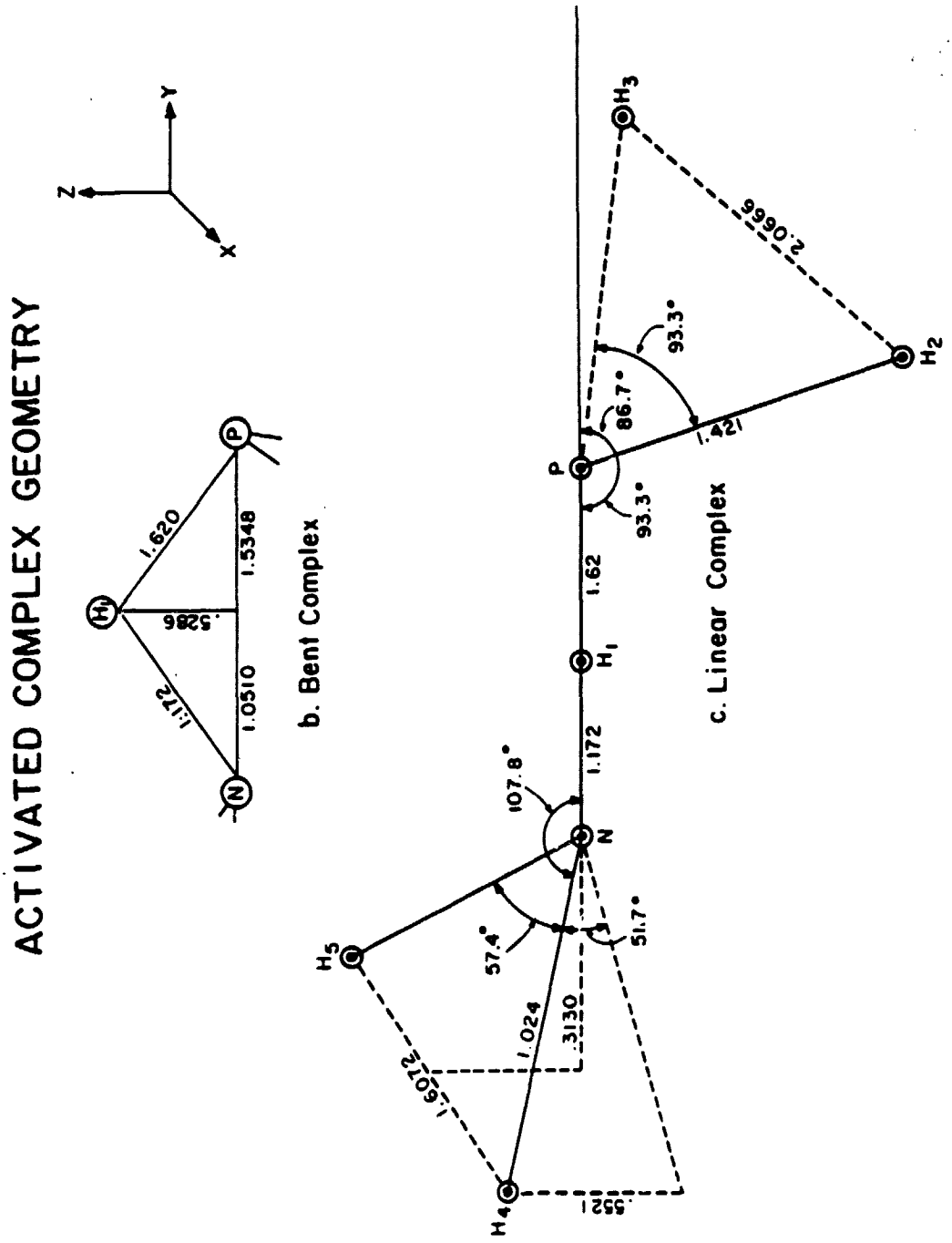

center of mass coordinates must be evaluated for each of the atoms. These are:

$$H_1 = (\quad 0, -0.6849, \quad 0.0168)$$
$$P \quad = (\quad 0, \quad 0.9351, \quad 0.0168)$$
$$N \quad = (\quad 0, -1.8569, \quad 0.0168)$$
$$H_2 = (\ 1.0333, \quad 1.0169, -0.9552)$$
$$H_3 = (-1.0333, \quad 1.0169, -0.9552)$$
$$H_4 = (\ 0.8036, -2.1699, \quad 0.5689)$$
$$H_5 = (-0.8036, -2.1699, \quad 0.5689)$$

The moments are calculated using (101)-(106) and I_1, I_2 and I_3 are evaluated using (100) to give:

$$(I_1 I_2 I_3)^{*1/2} = 4.6133 \times 10^{-58}\ g^{3/2}\ cm^3\ molec^{-3/2}.$$

Q_R can now be determined using the quantities calculated to give:

$$Q_R = 7905.54\ T^{-3/2}\ {}^{\circ}K^{3/2}$$

Two of the vibrations of the complex are internal rotations and the partition functions for each may be evaluated using:

$$(107)\quad Q_f = \frac{(8\pi^3 I_{red}\ KT)}{h}$$

following the approximation method described by Johnston[113] where I_{red} may be evaluated using:

$$(108)\ I_{NH_3\text{-}PH_2} = \frac{I_{yy}^{NH_3}\, I_{yy}^{PH_2}}{I_{yy}^{NH_3} + I_{yy}^{PH_2}}$$

A similar calculation may be performed for the analog, $I_{NH_2\text{-}PH_3}$.

I_{yy} for NH_2 and PH_3 have already been evaluated and I_{yy} for NH_3 and PH_2 are evaluated using analogous figures to Figs. 22.a. and 22.b. to determine the values:

$I_{yy}^{NH} = 2.8266\times10^{-40}$ g cm^{2}molec^{-1} and $I_{yy}^{PH} = 6.5121\times10^{-40}$ g cm^{2}molec^{-1}.

Inserting these values into equations (108) and (107) in turn gives:

$Q_f(NH_2\text{-}PH_3) = .3921\ T^{1/2}$ and $Q_f(NH_3\text{-}PH_2) = .4146\ T^{1/2}$.

These values may be incorporated into (98) to give:

$$(109)\ A = 3.9715\times10^{-9}\ T^{-1}\ Q_v^*$$

where Q_v^* contains the vibrational modes not accounted for by internal rotations.

In the preceding treatment, the partition functions for the linear complex were evaluated. A second calculation was performed in which H_1 was displaced in the z direction so that the complex was tighter (Fig 23.b.). In effect, the NH_3 and PH_2 were rotated so that a closer approach would be achieved. An identical calculation to the preceding ACT was carried out and A for the bent complex was determined to be:

$$(110)\quad A = 1.9953\times10^{-9}\ T^{-1}\ Q_v^*$$

Q_v^* could not be evaluated because no spectroscopic data were available for the complex, however the partition function for each vibration should be close to 1.

References

(1) G. Abell, "Exploration of the Universe," Holt, Reinhart & Winston, New York, 1964, p. 247.

(2) D. Morrison and J. Samz, "Voyage to Jupiter," NASA SP-439, NASA Scientific and Technical Branch, National Aeronautics and Space Administration, Washington, D. C., 1980, p. 117.

(3) G. Abell, "Exploration of the Universe," Holt, Reinhart & Winston, New York, 1964, p. 264.

(4) D. Morrison and J. Samz, "Voyage to Jupiter," NASA SP-439, NASA Scientific and Technical Branch, National Aeronautics and Space Administration, Washington, D. C., 1980, p. 17.

(5) T. Gehrels, Editor, "Jupiter," University of Arizona Press, Tucson, Arizona, 1976, p. 354.

(6) ibid., p. 23.

(7) ibid., p. 326.

(8) D. Morrison and J. Samz, "Voyage to Jupiter," NASA SP-439, NASA Scientific and Technical Branch, National Aeronautics and Space Administration, Washington, D. C., 1980, p. 129.

(9) T. Gehrels, Editor, "Jupiter," University of Arizona Press, Tucson, Arizona, 1976, p. 322.

(10) G. Abell, "Exploration of the Universe," Holt, Reinhart & Winston, New York, 1964, p. 244.

(11) H. Okabe, "Photochemistry of Small Molecules," John Wiley & Sons, New York, 1978, p. 354.

(12) D. R. Stull and H. Prophet, Project Directors, "JANAF Thermochemical Tables," NSRDS - NBS 37, 2nd edition, 1971.

(13) D. Morrison and J. Samz, "Voyage to Jupiter," NASA SP-439, NASA Scientific and Technical Branch, National Aeronautics and Space Administration, Washington, D. C., 1980, p. 15.

(14) ibid., p. 70.

(15) H. Okabe, "Photochemistry of Small Molecules," John Wiley & Sons, New York, 1978, p. 345.

(16) T. Gehrels, Editor, "Jupiter," University of Arizona Press, Tucson, Arizona, 1976, p. 30.

(17) H. Okabe, "Photochemistry of Small Molecules," John Wiley & Sons, New York, 1978, p. 25.

(18) ibid., p. 341.

(19) K. J. Laidler, "Chemical Kinetics," McGraw Hill Book Co. Inc., New York, 1965, pp. 4, 49.

(20) H. Okabe, "Photochemistry of Small Molecules," John Wiley & Sons, New York, 1978, p. 360.

(21) S. K. Atreya and T. M. Donahue, Rev. Geophys. and Space Phys., 17, 2 (1979).

(22) D. F. Strobel, J. Atmos. Sci., 30, 1205 (1973).

(23) D. F. Strobel, Astrophys. J., 214, L97 (1977).

(24) H. Okabe, "Photochemistry of Small Molecules," John Wiley & Sons, New York, 1978, pp. 377-379.

(25) R. Norrish and G. Oldershaw, Proc. Roy. Soc. (Lond.), 261, 1 (1961).

(26) R. G. Prinn and J. S. Lewis, Science, 190, 274 (1975).

(27) H. G. Ruiz and F. S. Rowland, Geophys. Res Lett., 5, 407 (1978).

(28) U. Schurath, P. Tiedemann, R. N. Schindler, J Phys. Chem., 73, 2, 456 (1969).

(29) G. Herzberg, "Electronic Spectra and Electronic Structure of Polyatomic Molecules," D. Van Nostrand Co., Inc., Princeton, New Jersey, 1967, p. 609.

(30) K. Watanabe, J. Chem. Phys., 22, 1564 (1954).

(31) G. Herzberg, "Electronic Spectra and Electronic Structure of Polyatomic Molecules," D. Van Nostrand Co., Inc., Princeton, New Jersey, 1967, p. 458.

(32) H. Okabe, "Photochemistry of Small Molecules," John Wiley & Sons, New York, 1978, p. 269.

(33) J. R. McNesby and H. Okabe, in "Advances in Photochemistry," Vol III, W. A. Noyes Jr, G. S. Hammond, J. N. Pitts, Editors, John Wiley & Sons, Inc., New York, 1964, pp. 195-203.

(34) H. Okabe, and M. Lenzi, J. Chem. Phys., 47, 12, 5241 (1967).

(35) W. E. Groth, U. Schurath, R. N. Schindler, J. Phys. Chem., 72, 3914 (1968).

(36) H. Okabe, "Photochemistry of Small Molecules," John Wiley & Sons, New York, 1978, pp. 269-272.

(37) ibid., p. 270.

(38) G. Herzberg, "Electronic Spectra and Electronic Structure of Polyatomic Molecules," D. Van Nostrand Co., Inc., Princeton, New Jersey, 1967, p. 504.

(39) J. Manaset, J. Fournier, C. Vermeil, Can. J. Chem., 51, 17, 2948 (1973).

(40) G. Herzberg, G., "Electronic Spectra and Electronic Structure of Polyatomic Molecules," D. Van Nostrand Co., Inc., Princeton, New Jersey, 1967, p. 584.

(41) K. Dressler and D. A. Ramsay, Phil. Trans. R. Soc., A251, 553 (1959).

(42) M. Lenzi and J. R. McNesby, A. Mele, C. N. Xuan, J. Chem. Phys., 57, 1, 329 (1972).

(43) M. Kroll, J. Chem. Phys., 63, 1, 320 (1975).

(44) G. Hancock, W. Lange, M. Lenzi, K. H. Welge, Chem. Phys. Lett., 33, 1, 168 (1975).

(45) R. Lesclaux and P. Van Khe, 12th Informal Conf. on Photochemistry, p. 3-1 (1976).

(46) W. Hack, H. Schacke, M. Schröter, H. Gg. Wagner, 17th Symposium on Combustion, p. 505 (1979).

(47) L. J. Stief, D. F. Nava, W. D. Brobst, R. P. Borkowski, J. V. Michael, Trans. Far. Soc. II, (in press) (1982).

(48) a. M. H. Hanes and E. J. Bair, J. Chem. Phys., 38, 672 (1963).

b. R. W. Diesen, J. Chem. Phys., 39, 2121 (1963).

c. J. D. Salzmann and E. J. Bair Jr, J. Chem. Phys., 41, 3654 (1964).

d. K. A. Mantei and E. J. Bair Jr, J. Chem. Phys., 49, 3248 (1968).

e. M. Gehring, K. Hoyermann, H. Gg. Wagner, J. Wolfrum, Ber. Bunsenges Phys. Chem., 75, 1278 (1971).

(49) S. Gordon, W. Mulac, P. Nangia, J. Phys. Chem., 75, 2087 (1971).

(50) P. Van Khe, J. C. Soulignac, R. Lesclaux, J. Chem. Phys., 81, 3, 210 (1977).

(51) P. Van Khe, R. Lesclaux, J. Chem. Phys., 83, 9 (1979).

(52) M. Demissey, "Etude de la Reactivite du Radical NH_2 avec les Alcanes et les Radicaux Alkyles," (Ph.D. Dissertation, Univ. of Bordeaux, 1979) p. 80.

(53) J. W. Buchanan and R. J. Hanranan, Rad. Res, 44, 296 (1970).

(54) S. Benson, "The Foundations of Chemical Kinetics", McGraw Hill Book Co., Inc., New York, 1960, p. 67.

(55) J. J. Hood, Phil. Mag., 6, 371 (1878).

(56) J. H. van't Hoff, "Etudes de Dynamic Chimique", F. Müller & Co., Amsterdam (1884).

(57) S. Arrhenius, Z. Physik. Chem., 4, 226 (1889).

(58) S. Glasstone, "Textbook of Physical Chemistry", D. Van Nostrand Co., Inc., Princeton, New Jersey, 1940, p. 194.

(59) R. E. Huie and J. T. Herron, Progress in Reaction Kinectics, Vol. 8, Edited by K. R. Jennings and R. B. Cundall, Pergammon Press, New York, 1978, p. 1.

(60) C. J. Howard, J. Phys. Chem., 83, 1, 3 (1979).

(61) J. V. Michael and J. H. Lee, J. Phys. Chem., 83, 1, 11 (1979).

(62) R. G. W. Norrish and G. Porter, Nature, 164, 658 (1949).

G. Porter, Proc. R. Roy. Soc. (Lond.), A200, 284 (1950).

(63) D. N. Bailey and D. M. Hercules, J. Chem. Ed., 42, 2 (1965).

(64) R. B. Klemm and L. J. Stief, J. Chem. Phys., 61, 11, 4900 (1974).

(65) a. K. H. Kley and K. H. Welge, Z. Naturforsch., 20a., 124 (1965).

b. K. Watanabe, J. Chem. Phys., 22, 1564 (1954).

c. K. Watanabe, J. Chem. Phys., 40, 558 (1964).

(66) H. Okabe., "Photochemistry of Small Molecules," John Wiley & Sons, New York, 1978, p. 271.

(67) G. H. Atkinson, J. Chem. Phys., 59, 1, 350 (1973).

(68) M. Kroll, J. Chem. Phys., 63, 1, 320 (1975).

(69) G. M. Barrow, "Introduction to Molecular Spectroscopy", McGraw Hill Book Co., Inc., New York, 1962, p. 70.

(70) H. Okabe, "Photochemistry of Small Molecules," John Wiley & Sons, New York, 1978, pp. 108, 117.

(71) Spectra-Physics Instruction Manual, Issue A/375, Spectra Physics Inc., Mountain View, California, 1975, p. 13.

(72) ibid. p. 25.

(73) J. B. Halpern, G. Hancock, M. Lenzi, and K. H. Welge, J. Chem. Phys., 63, 11, 4808 (1975).

(74) W. J. Youden, "Statistical Methods for Chemists", John Wiley & Sons, New York, 1951, pp. 42-44.

(75) D. R. Stull, Industrial and Engineering Chem., 39, 517 (1947).

(76) "Matheson Gas Data Handbook", 5th Ed., W. Braker and A. L. Mossman, Editors, Matheson Gas Products Co., E. Rutherford, New Jersey, 1971, p. 17.

(77) ibid. p. 477.

(78) ibid. p. 1.

(79) J. G. Calvert and J. N. Pitts Jr, "Photochemistry", John Wiley and Sons, Inc., New York, 1966, p. 720.

(80) H. Okabe, "Photochemistry of Small Molecules," John Wiley & Sons, New York, 1978, p. 120.

(81) J. H. Lee, J. V. Michael, W. A. Payne, and L. J. Stief, J. Chem. Phys., 68, 4, 1317 (1978).

(82) M. Demissey, "Etude de la Reactivite du Radical NH_2 avec les Alcanes et les Radicaux Alkyles," (Ph. D. Dissertation, Univ. of Bordeaux, 1979) p. 61.

(83) H. Adachi, N. Basco, and D. G. L. James, Int. J. Chem. Kin., XI, 995 (1979).

(84) S. Benson, "Thermochemical Kinetics," John Wiley and Sons, Inc., New York, 1968, p. 104.

(85) S. Shih, R. J. Buenker, S. D. Peyerimhoff, and C. J. Michejda, J. Am. Chem. Soc., 94, 22, 7620 (1972).

(86) S. Benson, "Thermochemical Kinetics," John Wiley and Sons, Inc., New York, 1968, p. 106.

(87) ibid. p. 103.

(88) R. Foon and M. Kaufman, Progress in Reaction Kinetics, Vol. 8, Edited by K. R. Jennings and R. B. Cundall, Pergammon Press, New York, 1978, p. 81.

(89) W. A. Payne and L. J. Stief, J. Chem. Phys., 64, 3, 1150 (1976).

(90) S. Benson, "Thermochemical Kinetics," John Wiley and Sons, Inc., New York, 1968, pp. 195-204.

(91) ibid. p. 22.

(92) J. V. Michael, D. F. Nava, R. P. Borkowski, W. A. Payne, and L. J. Stief, J. Chem. Phys., 73, 12, 6108 (1980).

(93) S. Benson, "Thermochemical Kinetics," John Wiley and Sons, Inc., New York, 1968, p. 22.

(94) J. H. Lee, J. V. Michael, W. A. Payne, D. A. Whytock, and L. J. Stief, J. Chem. Phys., 65, 8, 3280 (1976).

(95) B. Fritz, K. Lorenz, W. Steinert, and R Zellner, 2nd Eur. Symp. of Physico-Chem. Beh. of Atmos. Pollutants (1981).

(96) K. J. Laidler, "Theories of Chemical Reaction Rates", McGraw Hill, New York, 1969, p. 83.

(97) J. E. Huheey, "Inorganic Chemistry, Principles of Structure and Reactivity", 2nd Ed., Harper and Row, New York, 1978, pp. 842-850.

(98) D. F. Strobel, private communication.

(99) L. Pauling, J. Am. Chem. Soc., 69, 542 (1947).

(100) G. Herzberg, "Electronic Spectra and Electronic Structure of Polyatomic Molecules," D. Van Nostrand Co., Inc., Princeton, New Jersey, 1967, p. 610.

C-3

(101) H. S. Johnston, "Gas Phase Reaction Rate Theory", Ronald Press Co., New York, 1966, pp. 339-340.

(102) ibid. p. 82.

(103) ibid. p. 81.

(104) ibid. p. 59.

(105) ibid. p. 74.

(106) ibid. p. 28.

(107) J. E. Huheey, "Inorganic Chemistry, Principles of Structure and Reactivity", 2nd Ed., Harper and Row, New York, 1978, p. 839.

(108) ibid. Appendix F.

(109) H. S. Johnston, "Gas Phase Reaction Rate Theory", Ronald Press Co., New York, 1966, p. 125.

(110) S. Benson, "The Foundations of Chemical Kinetics," McGraw Hill Book Co., New York, 1960, p. 202.

(111) ibid. p. 204.

(112) ibid. p. 205.

(113) H. S. Johnston, "Gas Phase Reaction Rate Theory", Ronald Press Co., New York, 1966, pp. 226-228.